Research sponsored by the Air Force Office of Scientific Research, Office of Aerospace Research, United States Air Force.

SHOCK WAVE PROPAGATION IN A DISSIPATING LATTICE MODEL

Ramachandra N. R. Manvi

Department of Mechanical Engineering

WSU SDL 68-04
Grant No. AF-AFOSR-1088-66
Project No. 9763-01

June, 1968

This report is derived from a thesis submitted in partial fulfillment of the requirements for the Ph.D. degree in Engineering Science, Washington State University.

ABSTRACT

We have investigated the phenomenon of shock wave propagation in a nonlinear, one-dimensional, semi-infinite lattice. The lattice model for the study consists of a chain of mass points with nonlinear nearest-neighbor interaction. The nonlinear force law for springs connecting mass points is of parabolic and Morse type.

Viscosity is introduced for dissipation by means of a mechanical dashpot in parallel with the spring. The resulting differential-difference equation is numerically integrated by an iterative scheme on the IBM 360/67 computer. It is found that viscosity as introduced in the model plays an important role in the structure and propagation mode of the shock wave. In the absence of dissipation, the shock profile is oscillatory as reported by Tsai and Beckett for a cubic lattice. The amplitude of the oscillations decreases from the front to the rear of the shock profile, resulting in an essentially uniform region.

The explicit shock solution for a linear lattice, when extended to the nonlinear lattice, shows that the decay in amplitude of oscillations is due to the dynamics of the lattice. The numerical results show oscillatory particle paths. We find particle paths for two neighboring mass points to be similar.

A characteristic recurrence relationship is deduced from this similarity. In the present study, the shock front also

propagates along an oscillatory path. However, the average shock speed is constant and when this value is used in jump conditions to obtain steady state values of stress and dilatation, the agreement between these values and those obtained numerically in the essentially uniform region is satisfactory. The error is 1 to 5%, showing that the average shock speed in the lattice is always higher than that required by jump conditions.

The effect of dissipation is to reduce oscillations in the particle paths and shock front path. The recurrence relationship for particle paths obtained with no dissipation transforms to an expression for steady state when damping is critical or greater. It is possible to use this relation to obtain an approximate analytic solution for the shock profile in the lattice model. For a particular constitutive relation, we find an equivalence between our lattice model and the continuum for shock wave propagation. This equivalence provides a procedure to relate continuum constants with the constants of a lattice model.

TABLE OF CONTENTS

LIST OF TABLES

LIST OF ILLUSTRATIONS

CHAPTER I

INTRODUCTION

In recent years the availability of high speed computing machines has stimulated research in the area of finite amplitude wave propagation in solids. It is possible to obtain numerical solutions to the governing nonlinear differential equations of motion with an arbitrary constitutive relation [1].[1] The equations of fluid dynamics successfully describe the motion in solids if material rigidity is neglected. This is acceptable when pressures occurring are far in excess of shear yield stress [2].

Shock waves are formed as a result of the tendency of finite amplitude waves to "shock up" into a steep front due to the nonlinear (convective) terms in the equations of motion [3,4,5,6]. Riemann [7] demonstrated this for plane waves in the absence of dissipation. The existence of a mathematical discontinuity in the solution of quasilinear equations of fluid dynamics, even for sufficiently smooth initial data, has become a well-known fact [8].

In real physical systems shocks represented as mathematical discontinuities do not occur. Qualitatively, a shock wave in such systems may be described as a finite amplitude stress wave consisting of regions of essentially stable discontinuous or nearly discontinuous stress change across a front adjacent to regions of uniform flow [1]. The zone through which material properties change will have a finite structure controlled by important irreversible dissipative effects such as thermal diffusion, phonon scattering,

---

[1] Numbers in brackets refer to Literature Cited at the end of the text.

and viscosity [6,9,10]. For fluids the expressions for viscosity and thermal conduction can be easily written down, and experimental values are readily available. Lighthill [6], Hirschfelder [11], and others have discussed such effects and this influence on the shock structure in ideal gases. The dissipation behavior of solids is quite complex and varies considerably with the nature of the solid [12]. There is at present no satisfactory theory to arrive at suitable expressions analogous to those for fluids. However, thermal conduction in solids is thought to be unimportant for the times available for shock transition [2]. The actual shock structure in solids remains an open question. The non-availability of a general constitutive relation for solids further imposes restrictions on the discussion of shock structure.

In the continuum theory of fluids, the feeling has persisted that the Navier-Stokes equations predict values for shock thickness which are unrealistically small, and that these equations are basically inadequate to deal with the shock problem [13]. This feeling developed from the results of Becker's fundamental paper [14] in which it was observed that in gases the shock thickness is of the order of one mean free path. Continuum concepts may not have much meaning when dealing with such small dimensions.

This motivated a number of people, chiefly Grad [15] and Mott-Smith [16], to use kinetic theory to attack shock problems. Gilbarg and Paolucci [13] have discussed this controversy in detail. Taking thermal and viscous diffusion effects into account, they demonstrated that continuum equations of fluid dynamics are quite capable of accurately predicting steady shock structures. They also concluded that rejection of continuum methods in shock profile calculations on "a priori" grounds seems unjustified. It is not clear at this stage whether arguments developed for fluids are true for solids, too.

The atomic nature of a crystal lattice introduces spatial discretization. If shock thickness is of the order of lattice dimensions, then the solution of shock profile problems may require methods of lattice dynamics. The lattice dynamical approach for calculating shock profile in solids is of recent vintage [17,18].

The purpose of this thesis is to investigate the phenomenon of shock wave propagation in a nonlinear, one-dimensional, semi-infinite lattice. This will be carried out with and without dissipation. It is well known that linear lattices have frequency dispersional properties associated with them [19]. In a nonlinear lattice, we will have both frequency and amplitude dispersion [20]. In this study an attempt is made to investigate the effects of such dispersion combined with dissipation on shock wave propagation in the nonlinear lattice model. Numerical solutions will be compared with approximate analytic solutions. Before proceeding to do this, let us briefly review the current state of knowledge of the subject.

Tsai and Beckett [17] used a cubic lattice model for a solid. They studied the propagation of a strong, one-dimensional shock wave in a semi-infinite cubic lattice. All the lattice points were assumed to be constrained to move only in the direction of longitudinal wave propagation in order to simplify computation. This was justified on the basis of an exact balance of the transverse components of the forces from the neighboring lattice points due to the symmetry of the lattice model. Therefore, their semi-infinite lattice model was equivalent to the semi-infinite chain of lattice points.

For different types of interactions, ranging from Hooke's law forces to forces corresponding to Morse-type potential functions and various neighbor interactions, they reported that wave structure was unsteady in time. They concluded that this was due to the dispersive nature of the lattice.

Moreover, the computed stresses behind the shock front were different from those obtained by employing the Rankine-Hugoniot jump conditions valid for steady shocks.

Tsai and Beckett [17] did not use any dissipative mechanism in their model. The typical shock stress profile reported in this study consisted of a steady shock front propagating at a steady speed, a uniformly compressed region of uniform stress and particle velocity trailing far behind the shock front, and an oscillatory region joining the shock front and the uniformly compressed region. The oscillatory region increased in extent as the shock propagated into the lattice. It was also observed that this oscillatory region consisted of high amplitude, low frequency oscillations near the front and low amplitude, high frequency waves close to the essentially uniform region far behind. Because of this oscillatory wave structure, it was concluded that the shock wave structure was unsteady in time.

Certain questions arise. Does the damping out of the oscillations in the oscillatory region in the Tsai and Beckett study [17], resulting in a uniform compressed region, represent a property of the undamped lattice? Does the integration scheme employed in this study have a built-in diffusion term? If present, how much does this term contribute to the observed phenomenon? Why do the Rankine-Hugoniot jump conditions not hold for their model? How will a small dissipation alter the behavior? The present study tries to provide insight into these questions.

Anderson [18] obtained a steady shock profile in a one-dimensional lattice with dissipation. His nonlinear model was a simple case involving a double spring coupling between nearest neighbors. His object was to seek analogy with a continuum for shock propagation. To obtain a steady, stable shock profile, he employed large damping. He did not investigate the problem

in the absence of dissipation or for small damping.

In the present study, we shall deal with two separate kinds of nonlinearity different from Anderson's model [18] and investigate both the transient and steady state behavior. If we consider realistic interatomic forces, then it should be possible to compute the approximate amount of damping necessary to obtain steady state shock profiles. An effort is made to arrive at a numerical value of viscosity for aluminum under shock.

A better understanding of the shock wave propagation problem in a nonlinear lattice is also important when it is realized that the nonlinear problems of wave propagation in a continuum are numerically solved by finite difference methods. Such techniques [21] introduce spatial and temporal discretization. Concepts applicable to a continuum, i.e., pressure, density, and sound speed, are retained in the computations. Von Neumann [22] and Von Mises [23] suggested particle models in shock problems in which fluid mass is distributed at a finite number of mass points. The fluid properties are considered constant in the spatial interval at any time. The motion of each small mass element is then traced with time subsequent to prescribed initial data and boundary conditions. In effect, we are dealing in these methods with a form of lattice.

The results obtained by such models may show behavior similar to the nonlinear lattice. A good understanding of the lattice problem should therefore help interpret the results more realistically. The object is then to provide an insight into the question: How do the results obtained from a lattice dynamical approach to the shock problem in solids require modification when considered from a continuum point of view? An answer to this question should better reveal the validity of concepts of continuum mechanics when applied to shock processes in solids.

In the next chapter, we shall review the fundamental theory of one-dimensional shock wave propagation in a continuum. This will be followed by a description and study of the model under consideration. Succeeding chapters deal with the numerical integration and approximate analytic solution of the equations of the model, followed by conclusions and recommendations.

CHAPTER II

FUNDAMENTAL LAWS AND EQUATIONS OF SHOCK PROPAGATION

The Flow Equations

When solids are subjected to stresses much greater than their shear strength, it is often assumed that the stress system is isotropic and equivalent to hydrostatic pressure [2]. In the present study, we are concerned only with the problem of one-dimensional, plane, time-dependent flow. The flow is described by the conservation equations, i.e., the continuity equation, the momentum equation, and the energy equation. By application of Newton's laws of motion and the conservation laws, the required equations are obtained. In addition, we need a constitutive relation between stress, strain, and the internal energy to solve for four independent variables (P, V, u, E).

The equations in Lagrangian coordinates are [24,25]:

Equation of Motion

$$\rho o \left(\partial u/\partial t\right)_L + \partial P_x^*/\partial h = 0 \ , \tag{2.1}$$

Equation of Continuity

$$(\rho o/\rho^2) \left(\partial \rho/\partial t\right)_L + \partial u/\partial h = 0 \ , \tag{2.2}$$

Conservation of Energy

$$\left(\partial E/\partial t\right)_L = \left(\partial Q/\partial t\right)_L - (1/\rho o) \, P_x^* \left(\partial u/\partial h\right) \ . \tag{2.3}$$

Constitutive Relations

When rate dependent processes are involved, the constitutive relations will depend on the time derivatives of the stress and strain as well as the functions themselves;

$$f\ (P_x,\ \partial P_x/\partial t,\ ---,\ e_x,\ \partial e_x/\partial t,\ - -,\ E) = 0\ . \qquad (2.4)$$

The variables in equations (2.1) to (2.4) are defined as follows: h = Lagrangian position coordinate = x(o, h), t = time, ρ = density, u = particle velocity, P = hydrostatic pressure, P_x = compressive stress in the flow direction, P_x^* = the sum of P_x and any viscous stresses, E = internal energy per unit mass, Q = heat per unit mass added to the mass element by conduction and/or radiation, e_x = total strain in the flow direction, and V = specific volume = $1/\rho$.

Strain e_x is defined in several ways. In our work we shall define it as $e_x = \partial S_x/\partial x$, where S_x is the component of displacement in the flow direction x. It is also a widespread practice to use the natural strain defined as $e_x = \mathrm{Ln}\ (\rho/\rho o)$, ρo being the density of undisturbed material.

Equations (2.1) to (2.4) can also be expressed in Eulerian coordinates x and t. Here, t is again the time and x is the Eulerian position coordinate fixed in space. As Lagrangian derivative $(\partial/\partial t)_L$ is equivalent to the convective derivative d/dt, it follows that

$$(\partial/\partial t)_L = d/dt = (\partial/\partial t)_x + u(\partial/\partial x)_t\ . \qquad (2.5)$$

From the conservation of mass relation, we have

$$V/V_0 = (\partial x/\partial h)_t\ . \qquad (2.6)$$

Differentiating the above equation with respect to t holding h constant,

$$(1/V_0)\ (\partial V/\partial t)_h = \partial^2 x/\partial h \partial t = (\partial/\partial h)\ (\partial x/\partial t) = (\partial u/\partial h)_t \ . \qquad (2.7)$$

If we regard P_x^*, h, and u as functions of (x, t),

$$(\partial u/\partial h)_t = (\partial u/\partial x)_t\ (\partial x/\partial h)_t = (V/V_0)\ (\partial u/\partial x)_t \ ,$$

therefore

$$(\partial/\partial h)_t = (V/V_0)\ (\partial/\partial x)_t = (\rho_o/\rho)\ (\partial/\partial x)_t \ . \qquad (2.8)$$

Next, using relations (2.5 to (2.8) in equations (2.1) to (2.4), we obtain

$$\rho \cdot du/dt + \partial P_x^*/\partial x = 0 \ , \qquad (2.9)$$

$$(1/\rho)\ d\rho/dt + \partial u/\partial x = 0 \ , \qquad (2.10)$$

$$dE/dt = dQ/dt - (1/\rho)\ P_x^*\ (\partial u/\partial x), \qquad (2.11)$$

$$f(P_x,\ dP_x/dt,\ ---,\ e_x,\ de_x/dt,\ ---,\ E) = 0 \ . \qquad (2.12)$$

For one-dimensional flow, Lagrange equations are sometimes preferable to Euler's equations because the path of a mass element in the h, t plane is a straight line parallel to the t axis. Values of the Eulerian coordinates are given implicitly in the Lagrange scheme; if the complete history of u(h, t) in a solid is known, then the Euler coordinate x is given by

$$x(h,\ t) = h + \int_o^t u(h,\ y)\ dy \ , \qquad (2.13)$$

where x(h, 0) = h, and hence all quantitites as functions of x and t are obtained. Using the identity of equation (2.5), we easily rewrite the equations (2.9) to (2.12) in the more familiar Eulerian form.

Equation of Motion

$$\rho \cdot \partial u/\partial t + \rho u \partial u/\partial x + \partial P_x^*/\partial x = 0 . \qquad (2.14)$$

Equation of Continuity

$$\partial \rho/\partial t + (\partial/\partial x)(\rho u) = 0 . \qquad (2.15)$$

Equation of Energy

$$\partial E/\partial t + u \partial E/\partial x = \partial Q/\partial t + u \partial Q/\partial x - (1/\rho) P_x^* (\partial u/\partial x) . \qquad (2.16)$$

Constitutive Relations

$$f(P_x, dP_x/dt, \text{----------}, E) = 0 . \qquad (2.12)$$

When waves of finite amplitude propagate into matter, motions are possible in which discontinuities in the distribution of hydrodynamic quantities, i.e., pressure, velocity, density, etc., occur on some surfaces moving in space [7,8,23,26]. These discontinuities are usually called shock waves. On the surface of the shock discontinuity, the conditions of continuity of matter, energy, and momentum (Hugoniot's conditions) must be fulfilled. Let us derive these conditions next.

Multiplying equation (2.15) by u and adding to (2.14), we get

$$(\partial/\partial t)(\rho u) = -(\partial/\partial x)(\rho u^2 + P_x^*) . \qquad (2.17)$$

Neglecting heat transfer, the energy equation (2.16) can be transformed with some rearranging as

$$(\partial/\partial t)(\rho E + \tfrac{1}{2} \rho u^2) = -(\partial/\partial x)(\rho u E + u P_x^* + \rho u \cdot u^2/2) . \qquad (2.18)$$

Now if we assume that the shock profile has reached a steady state and that the shock is travelling with a constant velocity U in a coordinate system moving with the shock wave, the particle velocities are denoted by

$$v = (U - u) \ . \tag{2.19}$$

All partial time derivatives, $(\partial/\partial t)_x$, vanish in this coordinate system because of steady state assumptions. Hence, equations (2.15), (2.17), and (2.18) for this coordinate system give

$$\rho v = \rho(U - u) = \text{constant} \ , \tag{2.20}$$

$$\rho v^2 + P_x^* = \rho (U - u)^2 + P_x^* = \text{constant} \ , \tag{2.21}$$

$$\rho v(E + P_x^*/\rho + v^2/2) = \text{constant} \ . \tag{2.22}$$

We denote values of quantities far ahead of the shock by subscript o and those far behind by 1. We assume also that thermal and mechanical equilibrium have been established in each region so that all viscous pressures vanish. Then P_x^* becomes the ordinary longitudinal component of stress P_x, and equations (2.20) to (2.22) yield the familiar Rankine-Hugoniot jump conditions of shock propagation [27] as

$$(U - u_o)^2 = V_o^2 \ (P_{x1} - P_{xo})/(V_o - V_1) \ , \tag{2.23}$$

$$(u_1 - u_o)^2 = (P_{x1} - P_{xo}) \ (V_o - V_1) \ , \tag{2.24}$$

$$(E_1 - E_o) = (1/2) \ (P_{x1} + P_{xo}) \ (V_o - V_1) \ . \tag{2.25}$$

The above relations find frequent applications in the theory of shock wave propagation. They are useful even for cases where the conditions required

for their derivation are not fully satisfied. These relations could also be easily derived by considering a discontinuous jump of hydrodynamic quantities at the shock front and applying the conservation of mass, momentum, and energy directly [5]. If thermal conduction is taken into account, then jump conditions will hold provided the temperature gradients vanish ahead of and behind the shock front [26].

Viscous Dissipation in Solids

Several mechanisms, which are not very well understood, act to produce internal friction in solids. The ultimate result is the degradation of mechanical energy to heat. In spite of the variety of mechanisms and types of material systems, internal friction or damping phenomena can, in general, be classified under two major categories [12]: (1) rate dependent and (2) rate independent. The first group of losses correspond to viscosity type of losses in fluids, and the second to thermal diffusion losses. A considerable amount of work has been done in the area of internal friction of solids [12,28]. We briefly discuss the ideas appropriate for the present study.

If the stress-strain curve for a single cycle is in the form of a hysteresis loop, the area enclosed by this loop represents mechanical energy dissipated. To represent various forms of internal friction or damping in solids, workers in solid mechanics attach importance to the shape of the hysteresis loop [28]. Generally, rate-dependent damping is exhibited by materials showing loops with rounded ends, and rate-independent damping by those showing loops with sharp ends. For metals, examples of micro- and macro-mechanisms dissipating energy and included in the rate-dependent damping category are anelasticity, point defects, and pinned dislocations.

The anelasticity of solids may be regarded as a particular type of stress-strain-time behavior [29]. Anelastic materials, therefore, often exhibit mechanical behavior which depends on the rate of straining. Losses in such materials are associated with velocity gradients and the forces producing losses are of a viscous nature.

Mechanical models of Maxwell, Voigt, and others distinguish various types of viscous loss in solids [12]. This is a formal way of studying anelasticity. The phenomena may also be interpreted in terms of micro-mechanisms which produce them, i.e., anelastic relaxation processes [30]. Examples are point defect relaxations, displacement of dislocation segments, and presence of viscous grain boundaries.

For metals, examples of micro- and macro-mechanisms dissipating energy and included in the rate-independent damping category are unpinned dislocation motions, plastic slip, slip, and slide between micro- and macro-constituents [31].

Zener [32] has discussed losses due to thermal diffusion, arising chiefly in metals by various mechanisms. Changes in volume of a solid will be accompanied by changes in temperature. If the motion takes place very slowly, the heat transfer takes place isothermally, i.e., reversibly, so that there is no net loss or gain; on the other hand, if motion occurs at a very rapid rate so that heat has no time to flow across the medium, the conditions will be essentially adiabatic. Neither is a loss in this case. It is in the ranges intermediate to these that heat diffusion becomes important. In a shock process it is sometimes assumed that the mechanical wave is generated and propagated away from the heated region before appreciable heat conduction modifies the temperature field [33].

Experimental and theoretical studies thus far conclusively demonstrate that all solid materials dissipate mechanical energy by some complicated mechanism; to keep the mathematics simple it is reasonable to assume a linear damping mechanism.

In a shock, we do not need to specify the behavior of material under decreasing negative stress in order to obtain steady state profiles. Hence, questions of permanent deformation and hysteresis do not arise and need not be specified. In the present work, it is assumed that energy dissipation takes place by viscous losses only. In Appendix B a reasonable value for viscosity coefficient of aluminum is obtained. Physical constants of aluminum are used in the constitutive relations of the present study.

Shock Structure in a Solid

The steady profile of shock in a solid is determined by the equations of motion with appropriate constitutive relations, including suitable expressions for time dependence of stress. A simple form of constitutive equation for a compressible solid which exhibits second-order convective and dissipative effects was considered by Bland [34]. His mathematical treatment for arriving at the shock structure is analogous to that of Lighthill [6], developed for fluids, and is briefly outlined below. This theory is essentially developed for weak shocks, i.e., shocks in which entropy changes are small.

We express the stress-strain relation, including a small dissipative term, by

$$P_x^* = -\sigma = -A e + C e^2 - R \partial e/\partial t \cdot (A, C, R > 0) . \qquad (2.26)$$

The mechanical model for the above equation is shown in Fig. 1. This constitutive equation approximates the behavior of a strain-rate-dependent, work

hardening, elasto-plastic solid if the loading is monotonic. $R\partial e/\partial t$ represents internal friction in the solid, including viscous and thermal dissipation, and P_x^* is the negative stress.

$$e = \partial S/\partial h = \text{longitudinal strain} . \tag{2.27}$$

$S = S(h, t)$ = displacement in the direction of propagation expressed as a function time and original Lagrangian coordinate h .

The first-order behavior of a solid represented by equation (2.26) is given by $P_x^* = - Ae$; A is the modulus $\lambda + 2\mu$, where λ and μ are Lame's constants. Only terms up to and including second order in e are retained in further work with equation (2.26). The entropy changes are also neglected and hence, the theory is good for weak shocks only. Below, we demonstrate that $R\partial e/\partial t$ is equivalent, correct to order of (e^2), to the more usual form of viscous term, i.e., $R\partial u/\partial x$ for fluids, R denoting in this case the viscosity coefficient.

We have $u = \frac{\partial s}{\partial t}$, and $x = h + s$. Therefore,

$$\frac{\partial u}{\partial x} = \frac{\partial h}{\partial x} \cdot \frac{\partial}{\partial h} \frac{\partial s}{\partial t} = (1 + e)^{-1} \cdot \frac{\partial e}{\partial t}$$

and

$$R \frac{\partial u}{\partial x} = R \cdot \frac{\partial e}{\partial t} + \text{order of } (e^3) . \tag{2.28}$$

We obtain from equation (2.1) the equation of motion for this particular solid as

$$\rho o \left(\frac{\partial u}{\partial t}\right)_h = - \frac{\partial P_x^*}{\partial h} = \frac{\partial \sigma}{\partial h} .$$

or

$$\frac{\partial \sigma}{\partial h} = \rho o \cdot \frac{\partial^2 S}{\partial t^2} . \tag{2.29}$$

If equations (2.26) to (2.29) are to represent a wave travelling with a constant velocity U without distortion and attenuation, any dependent variable f must be a function of a particular combination of the independent variables h and t, namely h - Ut [6,35].

By putting $\xi = h - Ut$, we have

$$\frac{\partial f}{\partial h} = \frac{df}{d\xi} \text{ and } \frac{\partial f}{\partial t} = - U \cdot \frac{df}{d\xi} . \tag{2.30}$$

Equations (2.27), (2.26), and (2.28) become

$$e = \frac{ds}{d\xi} , \tag{2.31a}$$

$$- \sigma = - Ae + Ce^2 + RU \frac{de}{d\xi} , \tag{2.31b}$$

and

$$\frac{d\sigma}{d\xi} = \rho o \, U^2 \frac{d^2 S}{d\xi^2} . \tag{2.31c}$$

Eliminating $\frac{dS}{d\xi}$ from equations (2.31a) and (2.31c) and integrating once, we get

$$\sigma = \rho o \, U^2 e + b , \tag{2.32}$$

where b is a constant of integration.

Substituting for σ from above into equation (2.31b), we have, after some rearranging

$$RU \frac{de}{d\xi} = - b + (A - \rho_o U^2) e - Ce^2 . \qquad (2.33)$$

Equation (2.32) has two arbitrary constants, U and b. Let us look for a wave profile which connects two uniform conditions at large distances ahead of and behind a central region in which the strain e varies monotonically. If the uniform strains ahead of and behind the wave are e_0 and e_1 respectively, we require that $de/d\xi = 0$ when $e = e_0$ and $e = e_1$. These requirements fix U and b. If the wave is progressing into an unstrained medium, $e_0 = 0$; and therefore, we have

$$de/d\xi = 0 \text{ when } e = e_0 = 0 \text{ and } e = e_1 . \qquad (2.34)$$

Substitution of (2.34) into (2.33) gives b = 0 and

$$\rho_o U^2 = A - Ce_1 . \qquad (2.35)$$

For a wave travelling in the positive sense, taking positive root only,

$$U = \sqrt{\frac{(A - Ce_1)}{\rho_o}} \cong \sqrt{\frac{A}{\rho_o}} \cdot \left(1 - \frac{Ce_1}{2A}\right) + \text{order of } (e_1^2) . \qquad (2.36)$$

Sound velocity in the unstrained medium is

$$D_o = \sqrt{\frac{A}{\rho_o}} = \sqrt{\frac{(\lambda + 2\mu)}{\rho_o}} .$$

In a shock the strain is compressive and is taken as negative; therefore, the shock velocity U in equation (2.36) exceeds the sound velocity by

approximately $D_o \cdot \frac{Ce_1}{2A}$.

With b = 0, equation (2.33) becomes

$$RU \frac{de}{d\xi} = (A - \rho o U^2)\, e - Ce^2 . \qquad (2.37)$$

As $u = \frac{\partial S}{\partial t}$ and from (2.30), $\frac{\partial S}{\partial t} = - U \frac{dS}{d\xi} = - Ue$, hence,

$$u = - Ue = - U(\rho o/\rho - 1) = U(1 - \rho o/\rho) . \qquad (2.38)$$

Integrating equation (2.37) using equation (2.35) for $(A - \rho o U^2)$, we get the strain shock profile as

$$e = e_1 \left[1 + \exp \{\frac{-Ce_1}{RU} (\xi - b')\} \right]^{-1} . \qquad (2.39)$$

In the above equation, b' is an integration constant which represents the arbitrary shift in the zero of ξ, and may be taken to be zero. It is to be noted that C and R are positive, whereas e_1 is negative in compression. For a wave travelling in the positive direction, e goes to zero with ξ approaching $+ \infty$, and e goes to e_1 as ξ approaches $- \infty$. These requirements are met by equation (2.39). We may also write (2.39) alternatively with b' = o, as

$$e = e_1 \cdot \left[1 + \exp \{\frac{-Ce_1}{RU} (h - Ut)\} \right]^{-1} . \qquad (2.40)$$

or

$$e = \frac{e_1}{2} \cdot \left[1 - \tan h \{\frac{-Ce_1}{2RU} (h - Ut)\} \right] . \qquad (2.41)$$

The velocity shock profile is obtained by using equation (2.38) in equation (2.40) or (2.41). We get

$$u = u_1 \left[1 + \exp\left\{\frac{Cu_1}{RU^2}(h - Ut)\right\}\right]^{-1} , \tag{2.42}$$

or

$$u = \frac{u_1}{2} \cdot \left[1 - \tan h \left\{\frac{Cu_1}{2RU^2}(h - Ut)\right\}\right] . \tag{2.43}$$

The solution (2.41) or (2.43) in compressible fluid dynamics is called a "Taylor shock" [35]. The thickness of the shock profile is strongly dependent on the damping coefficient R. The shock structure is a result of balance between convection and dissipation in the nonlinear medium [34]. Any monotonic wave form ultimately adopts the profile of equation (2.41) for strain, and of equation (2.42) for particle velocity, as it propagates into material with a constitutive relation given by equation (2.26) [34].

Equation (2.42) is illustrated in Fig. 1 for a fixed time and different amounts of damping. At large distances behind the wave front, u equals u_1 and all the derivatives of u vanish. From equation (2.35) we obtain [using equation (2.38)]:

$$\rho o U^2 = A - Ce_1 = A + C\frac{u_1}{U} , \tag{2.44}$$

or, rearranging terms,

$$\begin{aligned}(A - \rho o \cdot U^2) + C \cdot u_1/U &= 0 \\ = \rho o \cdot D_o^2 (1 - U^2/D_o^2) + C \cdot (u_1/D_o) \cdot (D_o/U) &= 0 .\end{aligned} \tag{2.45}$$

Call the nondimensional quantities

$$U/D_o = U_s,\ 1/U_s = \theta,\ u_1/D_o = u_p,\ C/\rho o \cdot D_o^2 = A_p . \tag{2.46}$$

Substituting the above relations in equation (2.45), we get

$$(1 - U_s^2) + A_p \cdot u_p/U_s = 0$$

or

$$\theta^2 (1 + A_p \cdot u_p \cdot \theta) = 1 . \qquad (2.47)$$

The shock velocity is uniquely determined from the above equation in terms of the final particle velocity. Equation (2.47) will be discussed in detail in Chapter VI in connection with the model under study. For a steady shock in a dissipating nonlinear lattice with parabolic inter-particle force interaction, we arrive at an analogous relation to determine the shock velocity.

Equation (2.44) could also have been obtained easily by substituting the stress-strain relation of equation (2.26) directly into the jump conditions of mass and motion, i.e., equations (2.23) and (2.24). The final state being an equilibrium state, the viscous forces vanish; hence, the dissipative term $R \frac{\partial e}{\partial t} = 0$ at $e = e_1$ and from (2.26)

$$P_{x1}(e_1) = - Ae_1 + Ce_1^2 . \qquad (2.48)$$

Mechanical Model for $P_x^* = - A \cdot e + C \cdot e^2 + R \cdot \partial e/\partial t$, eqn. (2.26)

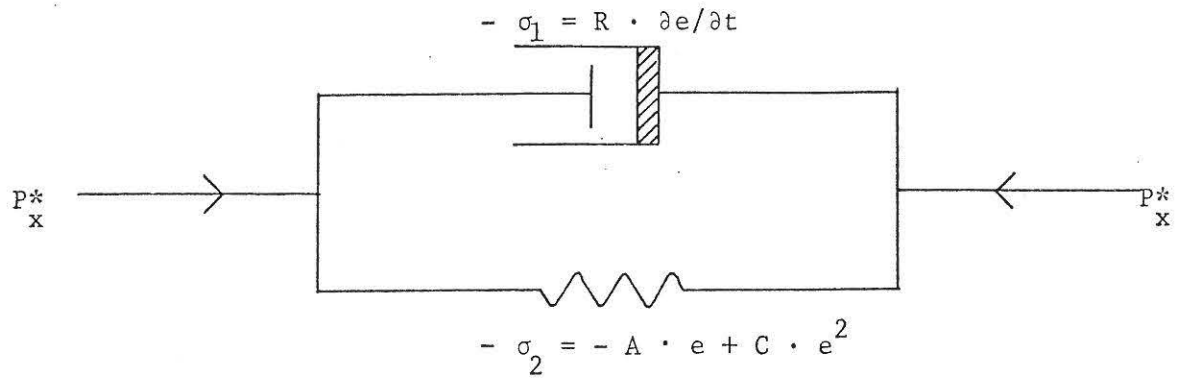

Steady Shock Profile, Velocity against Space, eqn. (2.42), at a Fixed Time

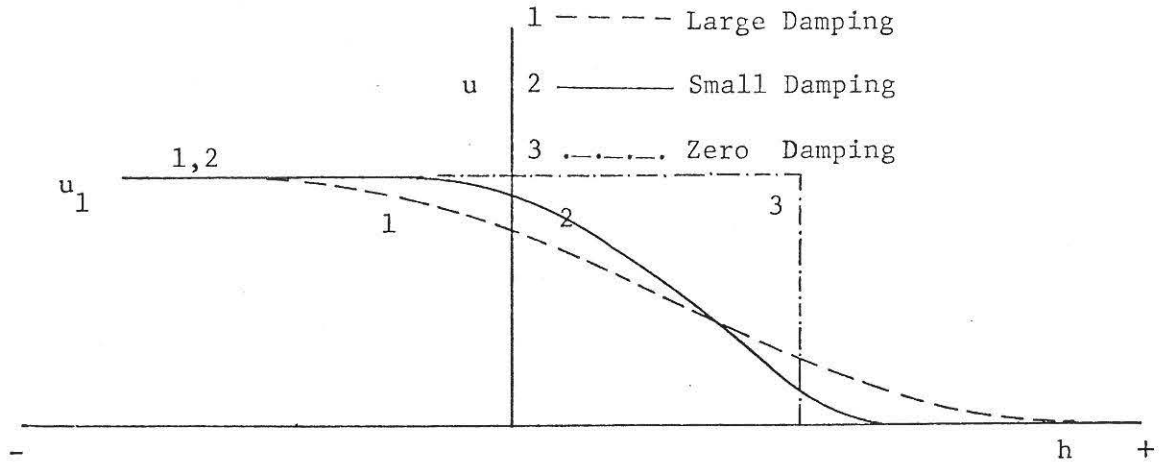

Fig. 1.--A Particular Solid Model and Shock Profile, Eqn. (2.42)

Mechanical Model for $P^*_x = - A \cdot e + C \cdot e^2 + R \cdot \partial e/\partial t$, eqn. (2.26)

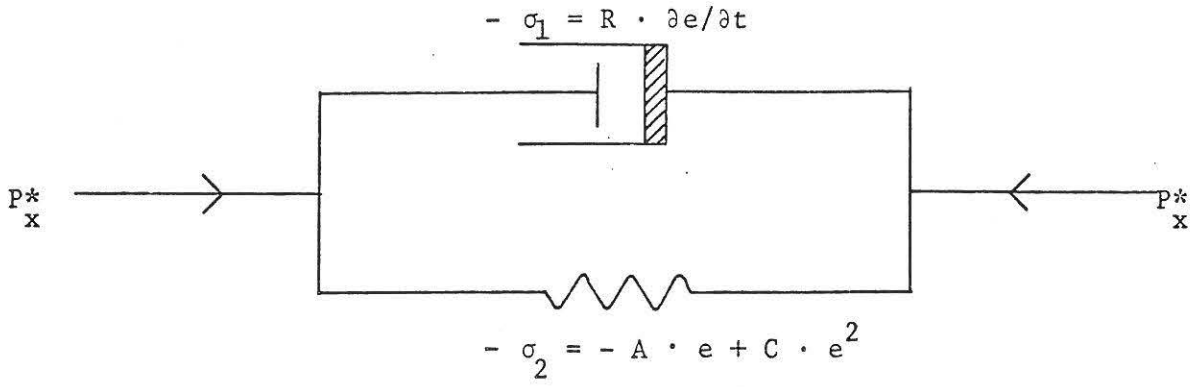

Steady Shock Profile, Velocity against Space, eqn. (2.42), at a Fixed Time

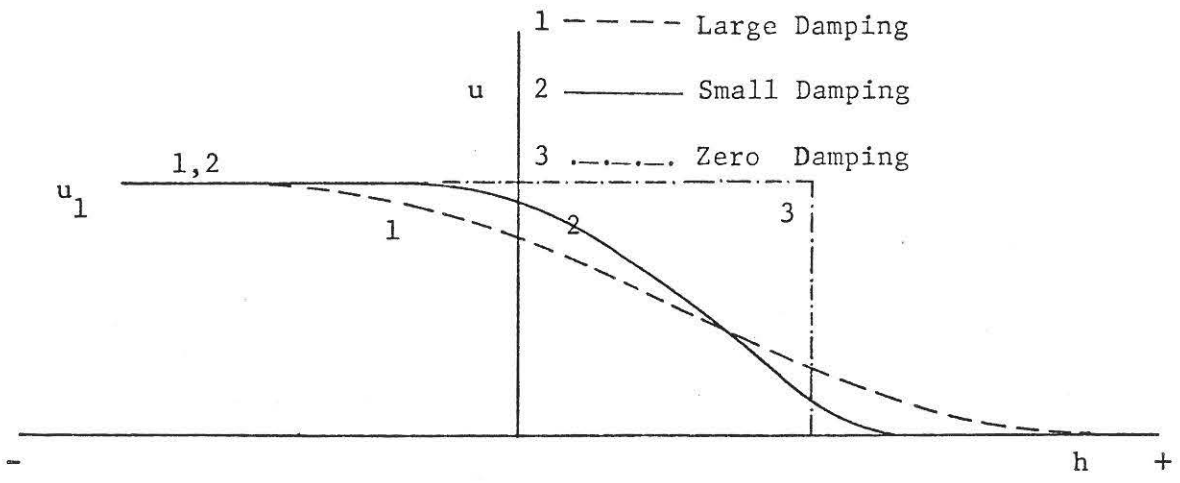

Fig. 1.--A Particular Solid Model and Shock Profile, Eqn. (2.42)

CHAPTER III

MODEL UNDER STUDY

Description of the Model

In Chapter II, we discussed the fundamental laws and equations of shock propagation in a continuum. We saw that the balance between the convective (nonlinear) terms in the equations of motion and the dissipative mechanisms resulted in the form of the shock profile. Our aim in the present study is to investigate shock wave propagation in a particular lattice model. Later we are interested in studying the analogy between the lattice model and continuum. To achieve this purpose, it is therefore necessary to include dissipation and nonlinearity in the lattice model.

The model under study is illustrated in Fig. 2. It is a one-dimensional, semi-infinite lattice located on the positive side of the x axis in cartesian coordinates. The semi-infinite chain of mass points has a mechanical dashpot in parallel with the nonlinear springs. The dashpot is a linear viscous damper. This accounts for the dissipation of mechanical energy. The lattice is assumed to be perfect and monatomic, having only one kind of atom or mass point, in this case at each lattice point. The free surface is located at the first mass point, i.e., N = 1. This initially is at x = 0.

The solution for the shock profile in the continuum is given as the pressure, density, or material velocity as a function of x, an Eulerian variable. In the present discrete model, it is more appropriate to seek a solution for the position of each particle $x_N(t)$ in Lagrangian variables. Here, $x_N(t)$

denotes the position, in cartesian coordinates, of the mass point N at any time t.

All the lattice points are assumed to be constrained to move only in the x direction. This corresponds to uniaxial strain in the continuum. With the assumed constraint, questions of transverse waves do not arise. It is believed that stable lattices have a very high theoretical strength and therefore should be relatively free from plastic yield phenomena [19]. Hence, for the present model we need concern ourselves with longitudinal elastic waves only.

For initial conditions, we assume that all mass points are at rest in their equilibrium positions, i.e., at time t = 0, the displacement from equilibrium position, velocity, and acceleration of every lattice point equals zero.

There are two simple ways in which a shock could be produced in the lattice model. One way is to apply a constant force pulse at the free surface at time t = 0+. The second way is to give the first mass point, i.e., N = 1, a constant velocity u_1 in the positive x direction at time $t = 0^+$ and maintain this velocity for this mass point at all times. This operation is simple to treat mathematically and will, therefore, be employed in the present investigation. Physically, this condition is artificial. The case corresponds perhaps to the impact of the stationary lattice model at time $t = 0^+$ with another identical lattice moving toward it from the negative x direction. The velocity of the impacting lattice is $2u_1$ before the impact. The impact may be assumed to occur when the mass points in the free surfaces of the two lattices are one lattice spacing apart. The contact surface, after such an impact, would move with a velocity u_1 relative to the stationary lattice.

In the absence of dissipation, the mass points in the free surfaces of the two chains are going to oscillate with a mean velocity u_1 [36]. Questions of multiple collisions between the two surface mass points will complicate the mathematics. We need to specify the surface interaction separately. For simplicity, we can imagine that dissipative mechanisms are present in this interaction which rapidly diminish the oscillations; therefore, the first mass point in the stationary chain attains a constant velocity u_1 instantaneously at time $t = 0^+$.

Choice of Nonlinear Interaction

We have to specify the nonlinearity in the inter-particle interaction. It is a widespread practice to use central pairwise potentials in the description of the solid state [37]. The potential is the energy of interaction. If $\Phi(r)$ is the energy of interaction of two atoms a distance r apart, then in order that $\Phi(r)$ represent the interaction potential of two atoms in a stable crystal, it must satisfy the following conditions [38]:

1. The force $- d\Phi/dr$ must be attractive at large r and repulsive at small r; therefore, $\Phi(r)$ must have a minimum at some point $r = r_0$.
2. The magnitude of Φ must decrease more rapidly with r than r^{-3}.
3. All elastic constants are positive.

Conditions 1 and 2 are results of simply physical considerations. The first arises from the existence of condensed phases, and the second is equivalent to requiring that the cohesive energy be finite. The two conditions taken together guarantee that the crystal will be stable with respect to infinitesimal homogeneous expansions and contractions.

Born [39] and his colleagues have studied the stability of different types of crystal lattices under uniaxial stress and strain with small

deformations. For finite strains, the situation is not clear. The present model does not belong to any particular crystal structure. Here we have an entirely one-dimensional, semi-infinite chain. Born [39] found that the model of a linear chain of identical particles is stable for small deformations if the second derivative of the interaction potential is positive between the nearest neighbors and negative between all other neighbors.

Stability of all lattice waves follows from the stability against homogeneous deformations. The stability conditions for small deformations dictate the choice of the interaction potential. In the lattice model under study, the mass points correspond to the atoms in the regular lattice of a crystal. We assume in this study that the nonlinear lattice model is stable for finite strains for an interaction potential which satisfies the above-mentioned stability conditions valid for small deformations. The computer results will verify this assumption.

A frequently used interaction potential in solid state is the Morse function [37]. This is given as

$$\Phi(r) = D \cdot [\exp\{-2a\,(r - r_o)\} - 2\exp\{-a(r - r_o)\}], \qquad (3.1)$$

where a and D are constants with dimensions of reciprocal distance and energy respectively, and r_o is the equilibrium separation. Since $\Phi(r_o) = -D$, D is the association energy. Girifalco and Weizer [38] considered the above interaction potential for cubic lattices and demonstrated that the stability conditions are satisfied. We will employ in our study a similar type of potential for one particular case. Equation (3.1) and its negative derivative $-d\Phi/dr$, which is the force of interaction, are shown in Fig. 3.

If we consider the Einstein model of a solid [37], in which a solid of N atoms behaves as a system of 3N coupled oscillators, equation (3.1)

represents the potential energy function of each of these oscillators. All oscillators have the same frequency of oscillation, ν. Slater [37] obtained, using such a solid model, the relation

$$\Gamma_o = \frac{ar_o}{2} + 1/3 \ . \tag{3.2}$$

The constant a and equilibrium separation r_o appearing in the above equation are the same as in equation (3.1). The term on the left-hand side of equation (3.2) is the Gruneisen parameter Γ defined as

$$\Gamma = \frac{-d \ln \nu}{d \ln V} \ . \tag{3.3}$$

The Gruneisen parameter Γ is a function of interatomic distance, hence, of volume V [40]. However, the experimental results on shock wave propagation in solids indicate that the percentage change of Γ upon changing the volume is about the same as the percentage volume change itself [41]. In view of the weakness of volume dependence of Γ, it is possible in the first approximation to regard it as a constant given by equation (3.2). There is considerable disagreement among workers on the numerical value of this constant for aluminum [40]. Our interest in this brief discussion is to indicate that the constants appearing in equation (3.1) are directly related to quantities which can be experimentally evaluated.

In our present study of a one-dimensional chain of mass points, we will consider only nearest-neighbor interaction for a choice of interaction potential analogous to equation (3.1);

$$\Phi(z) = F[\exp(-2bz) - 2 \exp(-bz)] \ . \tag{3.4}$$

In the above equation, B and b are arbitrary constants. By suitable choice of these constants, it is possible to obtain various kinds of interactions. This statement will be made clear later. In equation (3.4) we have for z

$$z = x_{N+1} - x_N - d_1 \ . \tag{3.5}$$

The initial equilibrium spacing at time t = 0 is d_1, and x_{N+1} and x_N denote the position coordinates of mass points N + 1 and N at any time t. Hence, z = 0 at t = 0.

The interaction force between the two neighboring mass points is the negative derivative of the potential and is given by

$$\text{Interaction force} = F(z) = 2bB\,[\exp(-2bz) - \exp(-bz)] \ . \tag{3.6}$$

If z is a very small quantity, not very much different from zero, we can expand the potential in equation (3.4) as

$$\Phi(z) \cong \text{constant} + B\,[b^2z^2 - b^3z^3 + \text{----}] \ . \tag{3.7}$$

Here we have neglected terms of higher than third order. Calling $B \cdot b = \alpha$ and $b = \beta$ in equation (3.7), we obtain

$$\Phi(z) \cong \text{constant} + \alpha\beta\, z^2 - \alpha\beta^2 z^3 + \text{----} \ . \tag{3.8}$$

Let us for the moment consider that we are free to choose the value of constants α and β in the above equation. If we keep $\alpha\beta$ finite and take the limit $\beta \to 0$ as $\alpha \to \infty$, we obtain the harmonic case. On the other hand, if we choose α and β so that for $z \geq 0$, α is finite, $\beta \to 0$ and for $z < 0$, α is finite, $\beta \to \infty$, we get the limit of hard sphere interaction. Hence, the interaction potential of equation (3.4) has wide applicability.

To get a reasonable nonlinear interaction between these two special cases, we arbitrarily fix the constants $\alpha\beta = K/2$ and $\alpha\beta^2 = \frac{K'}{3d_1}$ and later relate these constants to material properties. With these relations, equation (3.8) is rewritten as

$$\Phi_p(z) = \text{constant} + \frac{K}{2} z^2 - \frac{K'}{3d_1} z^3 . \tag{3.9}$$

The interaction force is obtained from the above as

$$F_p(z) = - \frac{d\Phi}{dz} = - Kz + \frac{K'}{d_1} z^2 . \tag{3.10}$$

Equation (3.10) shows that the interaction force is a quadratic function of z, i.e., parabolic. Hence, the subscript p in equations (3.9) and (3.10).

We will use equation (3.10) as the parabolic interaction between two neighboring mass points in future chapters, without restricting z to be a very small quantity. The potential energy is given by equation (3.9).

The second interaction studied is the original Morse potential given by equations (3.4) for the energy and (3.6) for force. We list them below with B = D and b = a as

$$\Phi_M(z) = D\,[\exp(-2az) - 2\exp(-az)] , \tag{3.11}$$

and

$$F_M(z) = 2aD\,[\exp(-2az) - \exp(-az)] . \tag{3.12}$$

In these equations the subscript M denotes the Morse law interaction.

Equations of Motion

It is simple to write down the equation of motion for any mass point N by using Newton's second law. Let us derive the general relation for the acceleration of the N-th mass point in terms of the total force acting upon it. Substituting the appropriate nonlinear interaction, the required equations of motion are obtained. For convenience, we define the following nondimensional quantities,

$$x_N/d_1 = X_N \ , \tag{3.13}$$

$$\omega_1 \cdot t = T \ , \tag{3.14}$$

where ω_1 is the appropriate constant frequency defined as

$$\omega_1 = \sqrt{K/m} \text{ for parabolic interaction} \tag{3.15}$$

and

$$\omega_1 = \sqrt{\frac{2a^2D}{m}} \text{ for Morse law interaction .} \tag{3.16}$$

From equations (3.13) and (3.14), we obtain

$$X_N' = \frac{dX_N}{dT} = u_{NP} = \frac{1}{\omega_1}\frac{dX_N}{dt} = \frac{1}{\omega_1 d_1} \cdot \frac{dx_N}{dt} = \frac{\dot{x}_N}{\omega_1 d_1} \ . \tag{3.17}$$

Differentiating once more with respect to T, the above gives

$$X_N'' = \frac{d^2X_N}{dT^2} = u_{NP}' = \frac{1}{\omega_1^2 d_1} \cdot \frac{d^2x_N}{dt^2} = \frac{1}{\omega_1^2} \cdot \frac{d^2X_N}{dt^2} \ . \tag{3.18}$$

In equations (3.17) and (3.18) a prime denotes differentiation with respect to nondimensional time T, and a dot represents differentiation with respect to time t.

The origin of the cartesian coordinate system in the present investigation is taken to be at the free surface in the undisturbed position, i.e., $x = 0$ at the equilibrium position of $N = 1$ at time $t = 0$. Let us take arbitrarily $d_1 = 1$ cm for mathematical convenience. All distances are nondimensionalized with respect to this unit from equation (3.13). Time t is in seconds, ω being second^{-1} so that T is nondimensional.

With the assumed value for $d_1 = 1$ cm, the equilibrium positions for all mass points are given by

$$X_N(0) = N - 1, \text{ at } T = 0, \text{ for } N = 1, 2, 3, \text{------} . \tag{3.19}$$

From Fig. 2 we see that four forces act on a mass point at any time. Considering the particle N, these are:

1. $F_{N, N+1}$, acting in the negative x direction and tending to decelerate the mass point N.
2. $F_{N-1, N}$, acting in the positive x direction and tending to accelerate the mass point N.
3. $G_{N, N+1}$, acting in the negative x direction and tending to decelerate the mass point N.
4. $G_{N-1, N}$, acting in the positive x direction and tending to accelerate the mass point N.

Therefore, the net spring force accelerating the mass point is

$$F_N^{Net}(T) = F_{N-1, N} - F_{N, N+1} . \tag{3.20}$$

Similarly, the net viscous force accelerating the particle is given by

$$G_N^{Net}(T) = G_{N-1, N} - G_{N, N+1} . \tag{3.21}$$

The total force tending to accelerate the mass point N is given by the sum of equations (3.20) and (3.21) as

$$F(N, T) = F_N^{Net}(T) + G_N^{Net}(T)$$

$$= F_{N-1, N} - F_{N, N+1} + G_{N-1, N} - G_{N, N+1} \cdot \qquad (3.22)$$

From Newton's second law of motion, if m is the mass of (every) particle, using equation (3.13) and (3.22) we get

$$m\ddot{x}_N = m \cdot d_1 \cdot (\ddot{x}_N/d_1) = m \cdot d_1 \cdot \ddot{X}_N = F(N, T) \ . \qquad (3.23)$$

Let us next derive the equation of motion for each of the two cases of parabolic and Morse type interaction.

Parabolic Case

From equations (3.10) and (3.5), we get

$$F_{N, N+1} = F_P(z) = -K \cdot (x_{N+1} - x_N - d_1)$$

$$+ (K'/d_1)(x_{N+1} - x_N - d_1)^2 \ . \qquad (3.24)$$

Using equation (3.13) in (3.24), we get

$$F_{N, N+1} = -K \cdot d_1 \cdot (X_{N+1} - X_N - 1) + K' \cdot d_1 \cdot (X_{N+1} - X_N - 1)^2 \qquad (3.25)$$

$$= -K \cdot d_1 \cdot [(X_{N+1} - X_N - 1)\{1 - A_P \cdot (X_{N+1} - X_N - 1)\}] \ ,$$

where we define

$$A_P = (K'/K) \ . \qquad (3.26)$$

Similarly,

$$F_{N-1,N} = - K \cdot d_1 \cdot [(X_N - X_{N-1} - 1)\{1 - A_P \cdot (X_N - X_{N-1} - 1)\}] \quad . \quad (3.27)$$

Therefore, from equation (3.20)

$$F_N^{Net}(T) = K \cdot d_1 \cdot [(X_{N+1} - X_N - 1)\{1 - A_P \cdot (X_{N+1} - X_N - 1)\} -$$

$$(X_N - X_{N-1} - 1)\{1 - A_P \cdot (X_N - X_{N-1} - 1)\}] \quad . \quad (3.28)$$

Simplifying the above equation, we get

$$F_N^{Net}(T) = K \cdot d_1 \cdot [(X_{N+1} - 2 \cdot X_N + X_{N-1})\{1 - A_P \cdot (X_{N+1} - X_{N-1} - 2)\}] \quad . \quad (3.29)$$

For both cases under study we assume a linear damping mechanism. If R is the viscosity coefficient of the dashpot in Fig. 2, then

$$G_{N,N+1} = - R \cdot (\dot{x}_{N+1} - \dot{x}_N), \text{ and } G_{N-1,N} = - R (\dot{x}_N - \dot{x}_{N-1}) \quad . \quad (3.30)$$

Employing equations (3.21) and (3.13), the net viscous force is

$$G_N^{Net}(T) = - R \cdot d_1 (\dot{X}_N - \dot{X}_{N-1}) + R \cdot d_1 (\dot{X}_{N+1} - \dot{X}_N)$$

$$= R \cdot d_1 \cdot (\dot{X}_{N+1} - 2 \cdot \dot{X}_N + \dot{X}_{N-1}) \quad . \quad (3.31)$$

From equations (3.22), (3.23), (3.29), and (3.31) we get

$$m d_1 \cdot \ddot{X}_N = K \cdot d_1 \cdot [(X_{N+1} - 2X_N + X_{N-1})\{1 - A_P \cdot (X_{N+1} - X_{N-1} - 2)\}]$$

$$+ R d_1 (\dot{X}_{N+1} - 2 \cdot \dot{X}_N + \dot{X}_{N-1}) \quad . \quad (3.32)$$

Using equations (3.15), (3.17), and (3.18), the above equation transforms to

$$X_N''(T) = [(X_{N+1} - 2X_N + X_{N-1})\{1 - A_P(X_{N+1} - X_{N-1} - 2)\}]$$

$$+ \eta\,(X'_{N+1} - 2X'_N + X'_{N-1}) \,, \tag{3.33}$$

where we have introduced the nondimensional quantity of

$$\eta = \frac{R}{m\omega_1} \,, \tag{3.34}$$

Defining the nondimensional displacement from initial equilibrium position by $S_N(T)$, we have from equation (3.19)

$$S_N(T) = X_N(T) - X_N(0) = X_N(T) - (N - 1) \,. \tag{3.35}$$

Substituting the above relation in equation (3.33), we get

$$S_N''(T) = [(S_{N+1} - 2S_N + S_{N-1})\{1 - A_P \cdot (S_{N+1} - S_{N-1})\}]$$

$$+ \eta \cdot (S'_{N+1} - 2S'_N + S'_{N-1}) \,. \tag{3.36}$$

A_P in equations (3.33) and (3.36) represents the nonlinearity of the chain. If A_P and η are zero, the equations become the equations of motion of the harmonic chain.

The concept of stress in terms of intermolecular forces is discussed at some length by Love [42]. In the present study we introduce the notion of stress in a different way. We imagine that our one-dimensional chain is but one of many acting in parallel and with identical displacements at every time T and index N; and that there is one such chain per unit of area normal to the length of chain. The force between the adjacent particles under these

conditions is the magnitude of the stress acting in the direction of the chain. We define the stress between each pair of particles as

$$\sigma_S\ (N,\ T) = F_{N,\ N+1}/\text{unit area [using equation (3.25)]}$$
$$= \frac{-\ Kd_1}{\text{unit area}} [(X_{N+1} - X_N - 1)\ \{1 - A_P(X_{N+1} - X_N - 1)\}] \ . \tag{3.37}$$

We have $K = \omega_1^{\ 2} \cdot m$ from equation (3.15); substituting this into the above, we get

$$\sigma_S\ (N,\ T) = \frac{\omega_1^{\ 2} \cdot md_1}{\text{unit area}} [-(X_{N+1} - X_N - 1)\ \{1 - A_P(X_{N+1} - X_N - 1)\}]. \tag{3.38}$$

But for the chain under the conditions discussed above, we can write

$$\frac{m}{\text{unit area} \cdot d_1} = \rho o, \text{ as the initial density} \ . \tag{3.39}$$

Using equation (3.39) in (3.38) and rearranging, we get

$$P_S\ (N,\ T) = \frac{\sigma_S(N,\ T)}{\rho o \omega_1^{\ 2} d_1^{\ 2}}$$
$$= -\ [(X_{N+1} - X_N - 1)\ \{1 - A_P(X_{N+1} - X_N - 1)\}] \ . \tag{3.40}$$

$P_S\ (N,\ T)$ is the nondimensional stress due to spring forces. The subscript S refers to the contribution of spring forces to the net stress at any mass point. Next we will calculate the viscous contribution. The net stress is the sum of spring stresses and viscous stresses.

Adopting the same concept of stress as stated above, the viscous stress between each pair of particles is

$$\sigma_V\ (N,\ T) = \frac{G_{N,\ N+1}}{\text{unit area}} \text{ [using equations (3.30) and (3.17)]}$$

$$= \frac{-R\omega_1 d_1\ (X'_{N+1} - X'_N)}{\text{unit area}} \quad . \tag{3.41}$$

Using equations (3.34) and (3.39), the above equation is transformed to

$$P_V\ (N,\ T) = \frac{\sigma_V\ (N,\ T)}{\rho o \cdot \omega_1^{\ 2} d_1^{\ 2}} = -\ \eta\ (X'_{N+1} - X'_N) \quad . \tag{3.42}$$

Hence, the total nondimensional stress acting between each pair of particles (N, N+1) is

$$P(N,\ T) = P_S\ (N,\ T) + P_V\ (N,\ T) \quad . \tag{3.43}$$

Morse Function Force Law

From equations (3.12), (3.5), and (3.13), we obtain

$$F_{N,\ N+1} = F_M(z) = 2aD\ [\exp\ \{-2ad_1\ (X_{N+1} - X_N - 1)\} -$$

$$\exp\ \{-ad_1\ (X_{N+1} - X_N - 1)\}] \quad . \tag{3.44}$$

We substitute d_1 for r_o is equation (3.2) and rearranging, we get

$$A_M = ad_1 = 2\ (\Gamma_o - 1/3) \quad . \tag{3.45}$$

Combining the above with equation (3.44), we get

$$F_{N,\ N+1} = 2aD\ [\exp\ \{-2A_M(X_{N+1} - X_N - 1)\} -$$

$$\exp\ \{-A_M(X_{N+1} - X_N - 1)\}] \quad . \tag{3.46}$$

Similarly,

$$F_{N-1,\,N} = 2aD\,[\exp\{-2A_M\,(X_N - X_{N-1} - 1)\} -$$

$$\exp\{-A_M(X_N - X_{N-1} - 1)\}] \,. \tag{3.47}$$

Therefore, from equation (3.20) we get

$$F_N^{Net}\,(T) = 2aD \cdot [Y(N,\,T)] \,, \tag{3.48}$$

where

$$Y(N,\,T) = \exp\{-2A_M(X_N - X_{N-1} - 1)\} - \exp\{-A_M(X_N - X_{N-1} - 1)\}$$

$$- \exp\{-2A_M(X_{N+1} - X_N - 1)\} + \exp\{-A_M(X_{N+1} - X_N - 1)\}] \,. \tag{3.49}$$

We assume for this case also a linear damping mechanism. Then the viscous force is the same as that obtained for the parabolic case, equation (3.31);

$$G_N^{Net}\,(T) = Rd_1\,(\dot{X}_{N+1} - 2\dot{X}_N + \dot{X}_{N-1}) \,. \tag{3.31}$$

The equation of motion for the case is obtained by combining equations (3.48), (3.31), (3.22), and (3.23) as

$$md_1\ddot{X}_N = 2aD\,[Y(N,\,T)] + Rd_1\,(\dot{X}_{N+1} - 2\dot{X}_N + \dot{X}_{N-1}) \,. \tag{3.50}$$

By use of equations (3.16), (3.17), (3.18), and (3.34), the above equation is transformed as

$$X_N''\,(T) = \frac{1}{A_M} \cdot [Y(N,\,T)] + \eta \cdot (X'_{N+1} - 2X'_N + X'_{N-1}) \,. \tag{3.51}$$

In terms of $S_N(T)$, the displacement from initial equilibrium position, the above equation with equation (3.35) gives

$$S''_N(T) = \frac{1}{A_M} \cdot [\exp\{-2A_M(S_N - S_{N-1})\} - \exp\{-A_M(S_N - S_{N-1})\} -$$

$$\exp\{-2A_M(S_{N+1} - S_N)\} + \exp\{-A_M(S_{N+1} - S_N)\}] +$$

$$\eta \cdot (S'_{N+1} - 2S'_N + S'_{N-1}) \ . \qquad (3.52)$$

The procedure for calculating the nondimensional stresses at the mass point N is identical to that for the parabolic case. For completeness sake we list below the appropriate equations;

$$P_S(N, T) = \frac{F_{N, N+1}}{\text{unit area}} \cdot \frac{1}{\rho o \omega_1^2 d_1^2}$$

$$= \frac{1}{A_M} \cdot [\exp\{-2A_M(X_{N+1} - X_N - 1)\} - \exp\{-A_M(X_{N+1} - X_N - 1)\}] \ , \qquad (3.53)$$

$$P_V(N, T) = -\eta (X'_{N+1} - X'_N) \ , \qquad (3.42)$$

$$P(N, T) = P_S(N, T) + P_V(N, T) \ . \qquad (3.43)$$

The constants used here are appropriate to the Morse case.

In the next chapter we describe the procedure for numerical integration of the nonlinear differential-difference equations of motion of this chapter.

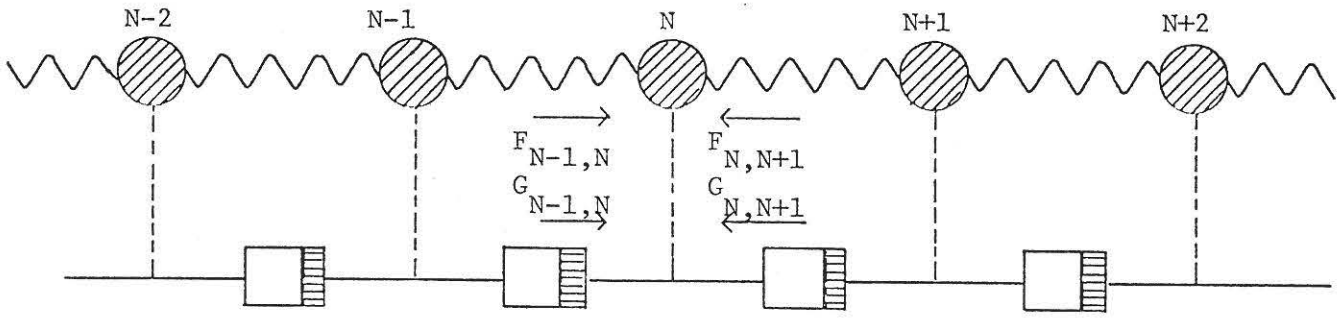

Fig. 2.--Dissipating Lattice Model

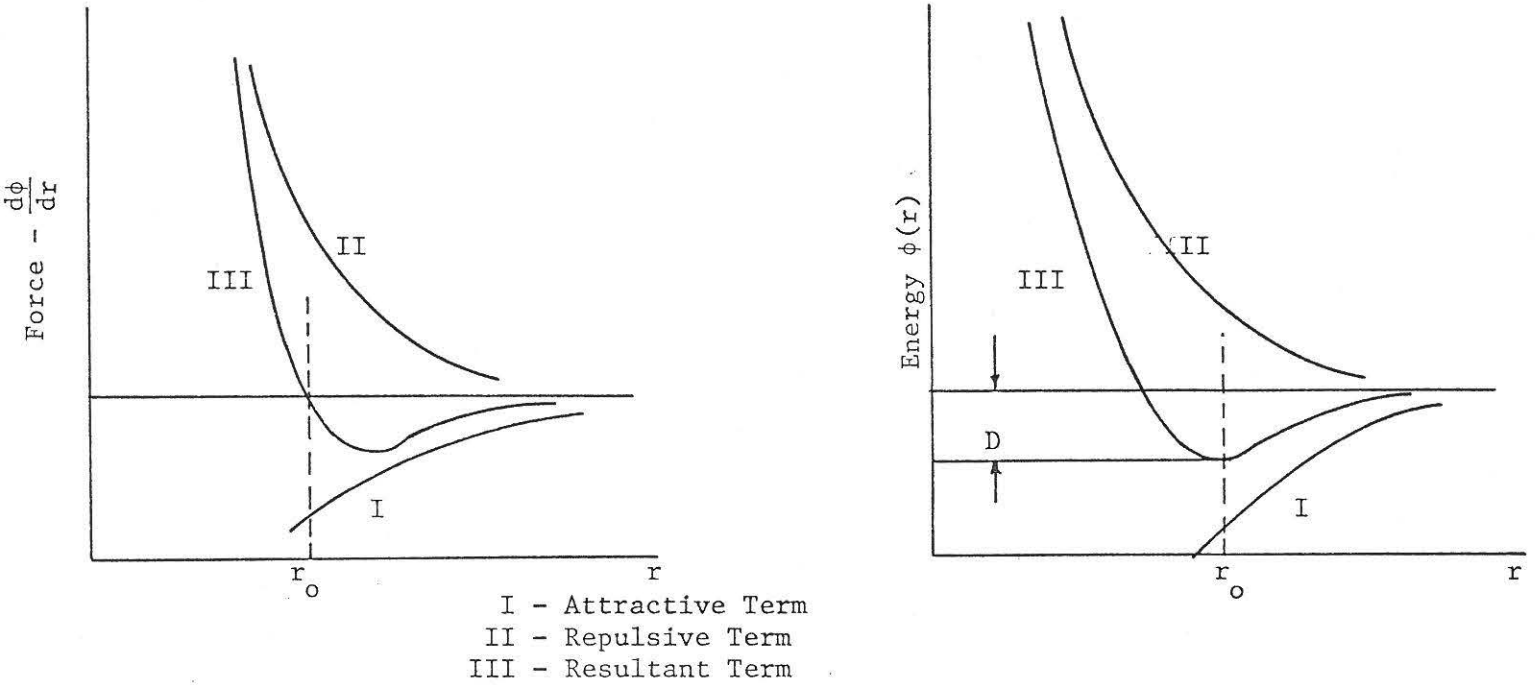

I - Attractive Term
II - Repulsive Term
III - Resultant Term

Fig. 3.--Morse Law

CHAPTER IV

NUMERICAL INTEGRATION OF EQUATIONS OF MOTION

In the preceding chapter we derived the equations of motion of the model under study. It is to be remembered that equations (3.33) and (3.51) are completely nondimensional. Our aim in this chapter is to integrate these nonlinear equations numerically on the IBM 360/67 computer under the following initial and boundary conditions.

Initial Conditions

$$\begin{aligned} X_N(0) &= (N-1) \quad \text{for } N \geq 1 \ . \\ X_N'(0) &= 0 \quad \text{for } N > 1 \ . \\ X_N''(0) &= 0 \quad \text{for } N > 1 \ . \end{aligned} \tag{4.1}$$

All the higher derivatives $X_N'''(0)$, $X_N''''(0)$, etc., are zero.

Boundary Condition

$$X_1(T) = u_1 \cdot T, \text{ for } T \geq 0 \ .$$

and

$$X_1'(T) = u_1 = \text{constant, for } T \geq 0 \ . \tag{4.2}$$

Method of Integration

The numerical integration method employed in the present study is the same in all essential aspects as that described by Tsai and Beckett [17]. We outline below the procedure briefly.

Let us consider the typical case of calculations at two successive steps 1 and 2. Figure 4 illustrates the procedure. For Step 1--i.e., at the time T_1--the position, velocity, and acceleration of lattice points 1, 2, 3, etc., are known either from previous calculations or from the prescribed initial conditions. Step 2 follows Step 1 at a time ΔT later. The conditions for the lattice point N = 1 for any time T are given by the boundary conditions of equation (4.2).

Our problem is to determine the values of position, velocity, and acceleration for mass points N = 2, 3, ---- for Step 2--i.e., at time $T = T_2 = T_1 + \Delta T$. This is accomplished by obtaining values of X_N, X'_N, and X''_N for the new time step by an iteration process in which the first estimate of the new position is the final position arrived at for the previous time step. This estimate is then improved by the procedure described below.

In the computer programs we employ the following notation:

$$\begin{aligned} X(N, I, J) &= \text{position of N-th mass point} , \\ DX(N, I, J) &= \text{velocity of N-th mass point} , \\ DDX(N, I, J) &= \text{acceleration of N-th mass point} . \end{aligned} \tag{4.3}$$

Here the first index refers to the lattice mass point, the second to the time step, and the third to the latest iteration number. The new time step corresponds to I = 2 and the old to I = 1. For achieving computational economy, the maximum number of iterations was limited; i.e., $J_{Max} \leq 10$. This

was quite satisfactory for most of the cases studied. For small time steps ($\Delta T = 0.2$) the convergence was rapid; and at the most, five to six iterations sufficed for a value to converge under prescribed tolerances. This point will be discussed in greater detail in a later section. To indicate that iterations are complete for a particular time step, we put J = 10. To explain the notation: X(N, 2, 10) = final value of the position of N-th mass point at the new time step. The same notation is employed for velocity and acceleration.

As a first approximation, we assume (see Fig. 4) for the first iterates

$$\begin{aligned} X(N, 2, 1) &= X(N, 1, 10) \\ DX(N, 2, 1) &= DX(N, 1, 10) \qquad N = 2, 3, \text{---} \\ DDX(N, 2, 1) &= DDX(N, 1, 10) \end{aligned} \tag{4.4}$$

For the mass point N = 1 we know the position and velocity correctly all the time; hence, all the iterates for this particle are set equal.

$$\begin{aligned} X(1, 2, J) &= X(1, 2, J + 1) \\ DX(1, 2, J) &= DX(1, 2, J + 1) \end{aligned} \qquad J = 1, 2, \text{---- } 9 \tag{4.5}$$

The need for doing this will become clear as we proceed further. We illustrate the integration procedure for the simple case of a linear lattice obtained by setting $A_P = 0$ in equation (3.33). We get

$$X''_N(T) = (X_{N+1} - 2X_N + X_{N-1}) + \eta\,(X'_{N+1} - 2X'_N + X'_{N-1}) \,. \tag{4.6}$$

Here the first group of terms on the right-hand side represent the contribution of spring forces, and the second group the contribution of viscous dampers. In the computer program (see Appendix C), we denote the first

group of terms by FORCE 1 and the second by FORCE 2. Considering the mass point N = 2 in Fig. 4, we have from equations (4.6), (4.4), and (4.5)

$$\text{FORCE 1} = X(3, 2, 1) - 2X(2, 2, 1) + X(1, 2, 10) \ . \qquad (4.7)$$

Similarly,

$$\text{FORCE 2} = DX(3, 2, 1) - 2DX(2, 2, 1) + DX(1, 2, 10) \ . \qquad (4.8)$$

From the equation of motion (4.6), we obtain the improved second iterated acceleration by equating

$$DDX(2, 2, 2) = \text{FORCE 1} + \text{FORCE 2} \ . \qquad (4.9)$$

The second iterates for velocity and position are then obtained from equation (4.9) as

$$DX(2, 2, 2) = DX(2, 1, 10) + 1/2 \cdot \Delta T \cdot [DDX(2, 1, 10) + DDX(2, 2, 2)] \ ,$$

and

$$X(2, 2, 2) = X(2, 1, 10) + 1/2 \cdot \Delta T \cdot [DX(2, 1, 10) + DX(2, 2, 2)] \ . \qquad (4.10)$$

By repeated applications of equations (4.7) to (4.10) to successive points N = 3, 4, 5, ----, etc. using the newest iterated values of the preceding point, we easily obtain the second iterates for points N = 3, 4, etc. N is incremented until some mass point, say N = NN, does not move appreciably from its previous equilibrium position [19]. The test for this condition is

$$\left|[\{X(N, 2, 2) - X(N, 1, 10)\}/X(N, 1, 10)]\right| \leq QC \ . \qquad (4.11)$$

Here QC is a small number, usually taken to be 10^{-7}. The third and higher iterates are obtained in a similar manner. The computation for Time Step 2 is terminated when the maximum change in value between iterates J, J + 1 is less than some preset value;

$$|[\{X(N, 2, J+1) - X(N, 2, J)\}]| \leq QD, \text{ for all } N , \qquad (4.12)$$

where QD is again a small number, usually taken to be 10^{-5}. This test is made for N = 2, 3, --- NN.

As mentioned earlier, we have limited the maximum number of iterations to 10. If more than 10 iterations are required for values to converge for a particular time step, then the prescribed value of QD is increased by a small amount (say 10^{-5}) and a message is printed prior to the next iteration. The number of such increments is limited in the program to three or four.

The procedure outlined above for the linear lattice is also valid for the nonlinear lattice with parabolic and Morse-law interactions. The only difference is in the expressions for FORCE 1, i.e., equation (4.7). The flow chart and the Fortran program in Appendix C explain the computing procedure in greater detail.

Tsai and Beckett [17] do not mention any particular error-checking devices in their integrating scheme. In the present study we have included a scheme for checking conservation of momentum and energy.

Momentum and Energy Check

Momentum and energy checks are provided in the computer program to permit checking for errors or to halt calculation if error becomes serious. These are described below.

Momentum Check

In the present study we have assumed that the mass point N = 1 acquires a uniform velocity instantaneously at t = 0. Let the external force acting on N = 1 be denoted by F. Figure 5 shows the forces acting on N = 1. If the mass point is required to move at a constant velocity, then the external force F must equal the sum of spring and viscous forces acting between N = 1 and N = 2. Further, if the last mass point which shows any appreciable motion is denoted by N = NN, we have for the conservation of momentum the following relation:

$$\int_0^t F(t)dt = \sum_{N=1}^{N=NN} m \dot{x}_N \, . \tag{4.13}$$

Differentiating the above with respect to time t, we get

$$F(t) = \sum_{N=1}^{N=NN} m \ddot{x}_N \, . \tag{4.14}$$

Next we derive the explicit relations for the parabolic and Morse-law interactions. For convenience we denote

$$(X_{N+1} - X_N - 1) = Z_N, \; N = 1, 2, 3 \text{ ----} \tag{4.15}$$

and

$$(X_{N+1} - X_N) = C_N, \; N = 1, 2, 3 \text{ ---- } . \tag{4.16}$$

Parabolic Law

We have

$$F(t) = F_{21} + G_{21} \, . \tag{4.17}$$

Substituting from equations (3.25) and (3.30) using (4.15) and (4.16) in equation (4.17), finally from (4.14) we get

$$F(t) = - Kd_1 [Z_1(1 - A_P Z_1)] - Rd_1(\dot{C}_1) = \sum_{N=1}^{NN} md_1 \cdot \ddot{X}_N . \qquad (4.18)$$

A dot represents differentiation with respect to time t, whereas a prime will denote differentiation with respect to nondimensional time $T = \omega_1 t$.

With techniques similar to those of Chapter III for nondimensionalizing the quantities and using equations (3.15), (3.17), (3.18), and (3.34) for this purpose, equation (4.18) can be transformed and rewritten as

$$\sum_{N=1}^{N=NN} X_N''(T) = - [Z_1(1 - A_P Z_1) + \eta C_1'] . \qquad (4.19)$$

To verify this conservation relation, in the computer program we call the left-hand side of the equation by H TOTAL and the right-hand side by H INPUT; i.e.,

$$\text{H INPUT} = - [Z_1(1 - A_P Z_1) + \eta C_1'] , \qquad (4.20)$$

and

$$\text{H TOTAL} = \sum_{N=1}^{N=NN} X_N''(T) . \qquad (4.21)$$

Morse Law

Substituting from equations (3.46) and (3.30) using (4.15) and (4.16) in equation (4.17), finally from (4.14) we get

$$F(t) = 2aD\,[\exp(-2A_M Z_1) - \exp(-A_M Z_1)] - Rd_1(\dot{C}_1)$$

$$= \sum_{N=1}^{NN} md_1 \ddot{X}_N \,. \tag{4.22}$$

With the use of equations (3.16), (3.17), (3.18), and (3.34), the above equation can be transformed and rewritten as

$$\sum_{N=1}^{N=NN} X_N''(T) = 1/A_M\,[\exp(-2A_M Z_1) - \exp(-A_M Z_1)] - \eta C_1' \,. \tag{4.23}$$

As in the parabolic case the left-hand side of the above equation is called H TOTAL in the computer program and is given by equation (4.21). The right-hand side, i.e., H INPUT, is given for the Morse case by

$$\text{H INPUT} = 1/A_M\,[\exp(-2A_M Z_1) - \exp(-A_M Z_1)] - \eta\, C_1' \,. \tag{4.24}$$

In the integration we check for the ratio

$$\text{H CHECK} = (\text{H INPUT} - \text{H TOTAL})/\text{H INPUT} \,. \tag{4.25}$$

If the ratio is less than the prescribed error, computations are continued; otherwise a message is printed and calculation halts. In the present study H CHECK was observed to be less than 10^{-3} always. This low error gives us confidence in the integration scheme.

Energy Check

For calculating the total energy of the system, we have to take into account the potential energy stored in springs, the kinetic energy of the mass points, and when viscosity is present, the dissipation energy of the dampers. We denote

T_N = kinetic energy of mass point N

$= 1/2\ m\ \dot{x}_N^2 = 1/2 \cdot m d_1^2 \dot{X}_N^2$ [from equation (3.13)] ,

ϕ_N = potential energy of the spring connecting the mass points N, N+1 ,

D_N = dissipation rate of energy due to damper connecting the mass points N, N+1 $= R(\dot{x}_{N+1} - \dot{x}_N)^2 = R d_1^2 \cdot \dot{C}_N^2$. (4.26)

The external work done on the system should equal the total energy of the system. If $\dot{x}_1(t)$ = constant represents the velocity of the mass point N = 1, then we have

$$\int_0^t F(t)\ \dot{x}_1(t)dt = \text{total energy of the system} . \tag{4.27}$$

Differentiating the above with respect to time t, we obtain

$$F(t) \cdot \dot{x}_1(t) = \frac{d}{dt} [\text{total energy})$$

$$= \frac{d}{dt}\left[\sum_{N=1}^{NN} \{T_N + \phi_N + D_N\} \right] . \tag{4.28}$$

NN is the last mass point which shows any appreciable motion.

Parabolic Law

With the constant appearing in equation (3.9) taken as zero, and using equations (3.5), (3.13), and (4.15), we get

$$\phi_N = \frac{K d_1^2}{2} \cdot Z_N^2 - \frac{K' d_1^2}{3} \cdot Z_N^3 . \tag{4.29}$$

Combining equations (4.26), (4.29), and (4.28), we arrive at

$$F(t) \cdot \dot{x}_1(t) = \frac{d}{dt}\left[\sum_{N=1}^{NN} \{1/2\ m d_1^2\ \dot{X}_N^2 + K/2\ d_1^2 \cdot Z_N^2 - \frac{K' d_1^2}{3} \cdot Z_N^3 + R d_1^2 \cdot \dot{C}_N^2\}\right] . \quad (4.30)$$

Substituting for F(t) for the parabolic case from equation (4.18) and using equations (3.13) to (3.15), (3.17), (3.18), (3.26), and (3.34), equation (4.30) can be transformed and rewritten as

$$\text{H INPUT} \cdot u_1 = \text{SUM 1} + \text{SUM 2} + \text{SUM 3} , \quad (4.30a)$$

where H INPUT = equation (4.20).

$$\text{SUM 1} = \sum_{N=1}^{NN} X_N' X_N'' . \quad (4.31)$$

$$u_1 = \dot{x}_1/(\omega_1 d_1) . \quad (4.32)$$

$$\text{SUM 2} = \sum_{N=1}^{NN} \{Z_N \cdot C_N' \cdot (1 - A_P Z_N)\} . \quad (4.33)$$

$$\text{SUM 3} = \eta \cdot \sum_{N=1}^{NN} (C_N')^2 . \quad (4.34)$$

In the Fortran program we denote

$$\text{H INPUT} \cdot u_1 = \text{E INPUT} \quad (4.35)$$

and

$$\text{SUM 1} + \text{SUM 2} + \text{SUM 3} = \text{E TOTAL} \ . \tag{4.36}$$

Morse Law

From equations (3.11), (3.13), (3.5), and (4.15), we obtain

$$\phi_N = D\,[\exp\{-2A_M \cdot Z_N\} - \exp\{-A_M Z_N\}] \ . \tag{4.37}$$

Proceeding in a manner similar to that used for the parabolic law, we get from combining equations (4.26), (4.37), and (4.28):

$$F(t)\,\dot{x}_1(t) = \frac{d}{dt}\left[\sum_{N=1}^{NN} \{1/2\ m d_1^{\,2}\,\dot{X}_N^{\,2} + D(\exp\{-2A_M Z_N\} - \exp\{-A_M Z_N\}) + R d_1^{\,2} \cdot C_N^{\,2}\}\right]. \tag{4.38}$$

Substituting for F(t), the Morse law interaction from equation (4.22) and using equations (3.16) to (3.18), (3.5), and (3.34), the above equation is transformed and rewritten as

$$\text{H INPUT} \cdot u_1 = \text{SUM 1} + \text{SUM 2} + \text{SUM 3} \ , \tag{4.39}$$

where H INPUT = equation (4.24)

u_1 = equation (4.32)

SUM 1 = equation (4.31)

$$\text{SUM 2} = -1/A_M \sum_{N=1}^{NN} [\{\exp(-2A_M Z_N) - \exp(-A_M Z_N)\} \cdot C_n'] \tag{4.40}$$

SUM 3 = equation (4.34).

In the computer program, E INPUT and E TOTAL are given by equations (4.35) and (4.36) respectively. During the integration on the machine, we check for the ratio

$$\text{E CHECK} = (\text{E INPUT} - \text{E TOTAL})/\text{E INPUT} \ . \qquad (4.41)$$

If the ratio is less than the prescribed error, computations are continued; otherwise a message is printed and calculation halts. We observed in the present study that E CHECK was always less than 10^{-3}. The momentum and energy checks suggest that the integration procedure is satisfactory and that no spurious errors are introduced in the computations.

Convergence and Stability

Tsai and Beckett [17] chose the size of the time step (ΔT) by trial and error by comparing numerical results with known analytic solutions of the harmonic lattice. Convergence and stability of a numerical integration scheme govern the choice of time interval (ΔT). These provide two different criteria which are to be defined with reference to the present study.

By convergence we mean that the absolute difference between two successive iterations at a time step diminishes as the number of iterations increases, whereas by stability we mean that the numerical solution remains finite for large times. It is a difficult task to derive rigorous convergence and stability tests with the equations of motion of Chapter III. We outline below an approximate analysis of the requirements and discuss these terms separately.

The integration procedure described in an earlier section consisted of (1) computing an improved iterated value for acceleration of a mass point by using in the equation of motion the newest iterated values of the preceding point, (2) computing the velocity and position of each mass point from equations of the type (4.10), and (3) terminating iterations by a convergence test of equation (4.12).

Next, let us consider once more the simple harmonic lattice, but this time without dissipation. From equation (4.6), with $\eta = 0$, we get

$$\ddot{X}_N = X_{N+1} - 2X_N + X_{N-1} \ . \tag{4.42}$$

For convenience in this section let us denote

$X^K_{N,J}$ = position of N-th mass point at time $T = K \cdot \Delta T$

$DX^K_{N,J}$ = velocity of N-th mass point at time $T = K \cdot \Delta T$

$DDX^K_{N,J}$ = acceleration of N-th mass point at time $T = K \cdot \Delta T$. (4.43)

The second subscript in the above notation refers to the iteration number. The integration procedure of that section is then summarized for equation (4.42) as

$$DDX^K_{N,J+1} = X^K_{N+1,J} - 2X^K_{N,J} + X^K_{N-1,J+1} \ , \tag{4.44}$$

$$DX^K_{N,J+1} = DX^K_{N,1} + 1/2 \cdot \Delta T \cdot [DDX^{K-1}_N + DDX^K_{N,J+1}] \ , \tag{4.45}$$

$$X^K_{N,J+1} = X^K_{N,1} + 1/2 \cdot \Delta T \cdot [DX^{K-1}_N + DX^K_{N,J+1}] \ . \tag{4.46}$$

In the equations above, dropping of the iteration subscript means that it is the final value for that particular time. Combining equations (4.45) and (4.46) and noting that the first iterates are the final values of the previous time step (see integration section), we get

$$X^K_{N,J+1} = X^K_{N,1} + (\Delta T) \cdot DX^K_{N,1} + 1/4 \cdot (\Delta T)^2 [DDX^K_{N,1} + DDX^K_{N,J+1}]. \tag{4.47}$$

Similarly,

$$X^K_{N,J} = X^K_{N,1} + (\Delta T) \cdot DX^K_{N,1} + (1/4) \cdot (\Delta T)^2 \, [DDX^K_{N,1} + DDX^K_{N,J}] \, . \qquad (4.48)$$

Subtracting equation (4.48) from (4.47), we get

$$X^K_{N,J+1} - X^K_{N,J} = (1/4) \cdot (\Delta T)^2 \, [DDX^K_{N,J+1} - DDX^K_{N,J}] \, . \qquad (4.49)$$

Substituting from equation (4.44) for $DDX^K_{N,J+1}$ and $DDX^K_{N,J}$ in the above and rearranging, we get, dropping the superscript K for convenience, the expression

$$X_{N,J+1} - X_{N,J} = (1/4) \cdot (\Delta T)^2 \, [(X_{N+1,J} - X_{N+1,J-1}) - 2(X_{N,J} - X_{N,J-1}) + (X_{N-1,J+1} - X_{N-1,J})] \, . \qquad (4.50)$$

Next, we assume that the difference between successive iterates for all mass points is the same, i.e.,

$$X_{N+1,J} - X_{N+1,J-1} = X_{N,J} - X_{N,J-1} \equiv \varepsilon_J, \text{ etc.} \qquad (4.51)$$

From equation (4.50) we obtain

$$\varepsilon_{J+1} = (1/4) (\Delta T)^2 \, [-\varepsilon_J + \varepsilon_{J+1}] \, . \qquad (4.52)$$

or

$$\left| \frac{\varepsilon_{J+1}}{\varepsilon_J} \right| = \left| \frac{-(1/4) (\Delta T)^2}{1 - (1/4) (\Delta T)^2} \right| = \text{convergence rate } \gamma \qquad (4.53)$$

If the integration procedure is to converge rapidly, in the above equation we require that $\gamma << 1$. We can find the maximum value of ΔT for convergence as $(\Delta T)_{max} < \sqrt{2}$ from equation (4.53) when γ is slightly less than unity. When

γ is close to 1, the convergence is very poor and a large number of iterations are required. A very small value of ΔT assures rapid convergence. Let us assume that $\left|\frac{\varepsilon_{J+1}}{\varepsilon_J}\right|$ becomes 10^{-5} in five iterations. Then $\gamma = 0.1$ and $\Delta T \simeq 0.6$. In the present study, it was observed that time steps of smaller size than this converged rapidly in five to six iterations.

Stability of the integration scheme is assured by using a value of $\Delta T << 1$. If we imagine that equation (4.42) approximates a linear string [43], then the Courant-Friedrichs-Lewy condition [21] for stability of difference scheme is that $\Delta T < 1$.

We are interested here in studying the problem of nonlinear coupled oscillators. It is known from lattice dynamics of a chain of particles that there is a limit to the highest frequency that can be propagated in the lattice [19]. This is known as the cutoff frequency. This also influences the choice of time step ΔT, which must be much less than the period of the cutoff frequency if the computed displacements are to include all frequency components.

Most of our runs are with a time step $\Delta T = 0.2$ and $\Delta T = 0.1$. With such time steps we did not have any stability or convergence difficulties in our numerical integration.

Built-in Diffusion of the Integration Scheme

Often numerical integration schemes introduce extraneous diffusion terms in the equations of motion [21]. Such terms are sometimes related to the size of the time step ΔT. Tsai and Beckett [17] do not report on the effect of size of ΔT on their observations. We therefore seek to determine whether any diffusion type of term is present in the integration scheme in

order to answer the question of what computational effects are related to the size of the time step. We investigate this in the following paragraph for a simple case.

When there is no viscous dissipation in the lattice, the equation of motion can be written

$$Y''^{K}_{N} = F(Y^{K}_{N+1}, Y^{K}_{N}, Y^{K}_{N-1}) = F^{K}_{N}(Y) \quad . \tag{4.54}$$

Here Y^{K}_{N} is the true position of the N-th mass point at time $T = K \cdot \Delta T$, and Y'^{K}_{N}, Y''^{K}_{N}, etc. represent its derivatives. The expression on the right-hand side of the above equation denotes the force acting on the mass point, a function of Y_{N+1}, Y_{N}, Y_{N-1}. Let X^{K}_{N} denote the position of the N-th mass point at time $T = K \cdot \Delta T$ for the same lattice obtained as a solution of equation (4.54) by numerical integration. On the machine we solve

$$X''^{K}_{N} = F(X^{K}_{N+1}, X^{K}_{N}, X^{K}_{N-1}) = F^{K}_{N}(\bar{X}) \quad . \tag{4.55}$$

Assuming that our iteration scheme converges, the scheme of the integration section of this chapter is

$$\begin{aligned} X''^{K+1}_{N} &= F^{K+1}_{N}(\bar{X}) \quad , \\ X'^{K+1}_{N} &= X'^{K}_{N} + 1/2 \cdot \Delta T(X''^{K}_{N} + X''^{K+1}_{N}) \quad , \\ X^{K+1}_{N} &= X^{K}_{N} + 1/2 \cdot \Delta T(X'^{K}_{N} + X'^{K+1}_{N}) \quad . \end{aligned} \tag{4.56}$$

The above equations can be combined to give

$$X_N^{K+1} = X_N^K + hX_N^{'K} + 1/4\ h^2[F_N^K(\bar{X}) + F_N^{K+1}(\bar{X})] \ , \tag{4.57}$$

where $h = \Delta T$.

From Taylor series expansion of Y_N^{K+1}, we get

$$Y_N^{K+1} = Y_N^K + hY_N^{'K} + \frac{h^2}{2} Y_N^{''K} + \frac{h^3}{6} Y_N^{'''K} + \text{.. higher order terms.} \tag{4.58}$$

Using equation (4.54) in the above, we obtain

$$Y_N^{K+1} = Y_N^K + hY_N^{'K} + \frac{h^2}{2} F_N^K(\bar{Y})$$

$$+ \frac{h^3}{6} \frac{d}{dT} \cdot \{F_N^K(\bar{Y})\} + \text{higher order terms.} \tag{4.59}$$

Assuming that at time T, Y_N^K and its derivatives are equal to X_N^K and its derivatives (might be the same initial data), we get from equations (4.57) and (4.59)

$$X_N^{K+1} = Y_N^{K+1} + 1/4\ h^2\ [F_N^{K+1}(\bar{X}) - F_N^K(\bar{X})]$$

$$- 1/6\ h^3 \frac{d}{dT} \{F_N^K(\bar{X})\} + \text{.. higher order terms.} \tag{4.60}$$

To the first approximation,

$$F_N^{K+1}(\bar{X}) - F_N^K(\bar{X}) \simeq h \cdot \frac{d}{dT} \{F_N^K(\bar{X})\} \ ,$$

hence, from above

$$X_N^{K+1} \simeq Y_N^{K+1} + 1/12\ h^3 \cdot \frac{d}{dT} F_N^K(\bar{X}) \ . \tag{4.61}$$

In a single degree of freedom system, the error in a single step of integration for position is given by

$$1/12\ h^3 \cdot \frac{d}{dT}\{F_N^K(\bar{X})\} \text{ at time } (K+1) \cdot h \ . \tag{4.62}$$

Next let us consider a simple harmonic lattice of equation (4.42). We have

$$F_N^K(\bar{X}) = \text{force at mass point } N = X_{N+1}^K - 2X_N^K + X_{N-1}^K \ . \tag{4.63}$$

Using equation (4.61) on the right-hand side of the above equation, we get

$$F_N^K(\bar{X}) = F_N^K(\bar{Y}) + 1/12\ h^3 \cdot \left[\frac{d}{dT}\{F_{N+1}^{K-1} - 2F_N^{K-1} + F_{N-1}^{K-1}\}\right] \ . \tag{4.64}$$

By substitution of relation (4.63) at time $T = (K-1) \cdot h$ on the right-hand side of the above equation, we see that

$$F_N^K(\bar{X}) - F_N^K(\bar{Y}) = h^3/12 \cdot [(X'_{N+2} - 2X'_{N+1} + X'_N) - 2(X'_{N+1} - 2X'_N + X'_{N-1})$$

$$+ (X'_N - 2X'_{N-1} + X'_{N-2})]^{K-1} \ . \tag{4.65}$$

This equation shows that the force at the mass point N, as determined by the numerical integration, differs from that in the true case by the expression on the right-hand side. As this pseudo force is proportional to velocity gradient, it represents a form of viscous force. Hence, the term $(h^3/12)$ acts like a pseudo viscosity responsible for introducing extraneous viscous forces into the computations. When dissipation exists in the system, the additional effect of this pseudo viscosity can be made negligible by the choice of a very small $h = \Delta T$. However, in the lattice without dissipation, the derivatives X'_N, etc. may become large and choice of $h = \Delta T$ becomes very important in keeping the pseudo forces, and thus the error, small.

We observed in our study that two different values of time step ΔT gave significantly different shock wave profiles for the same lattice under identical initial and boundary conditions. The effect of larger time step was to make the front less steep, suggesting a diffusive effect.

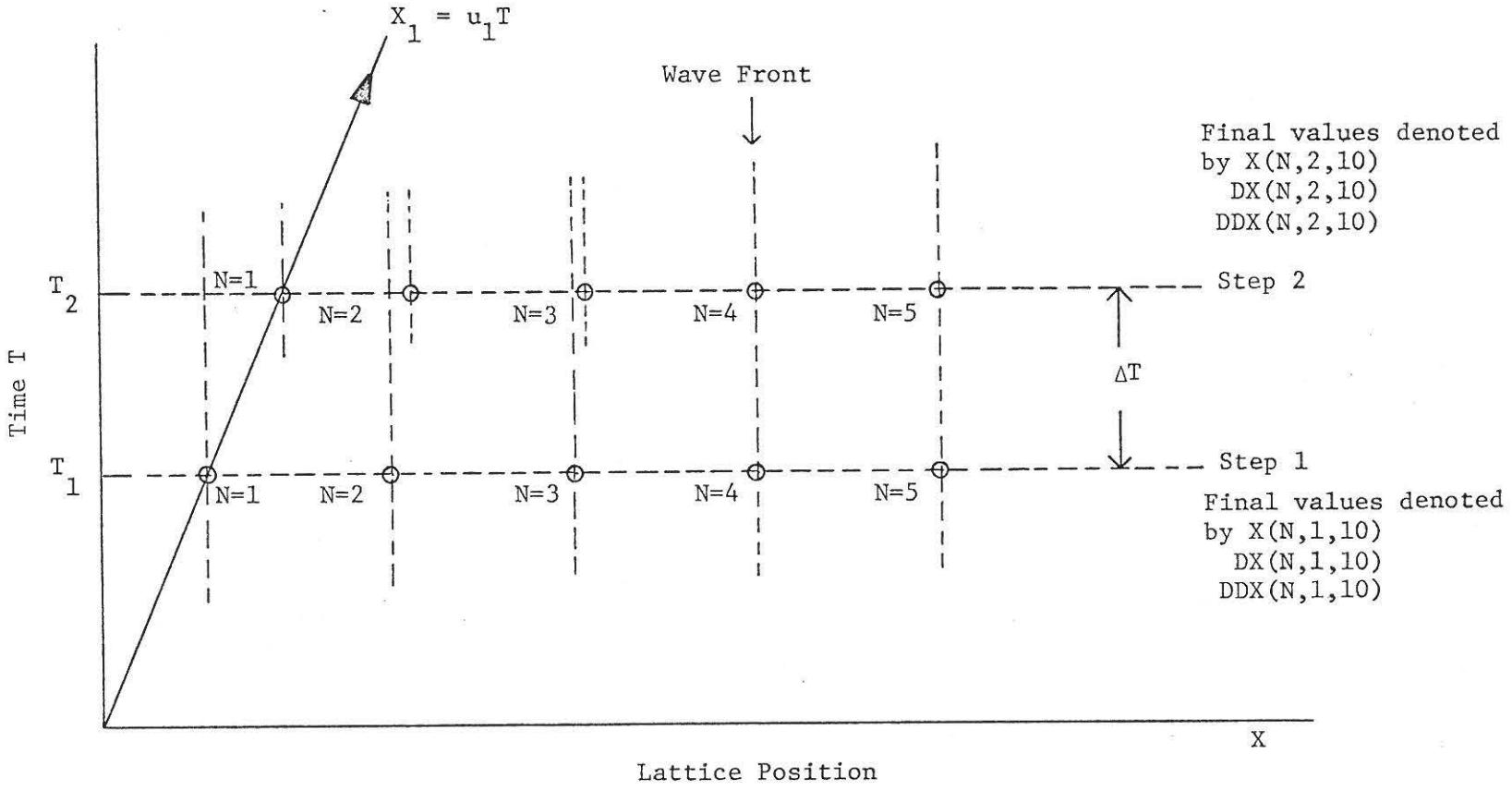

Fig. 4.--Numerical Integration Procedure

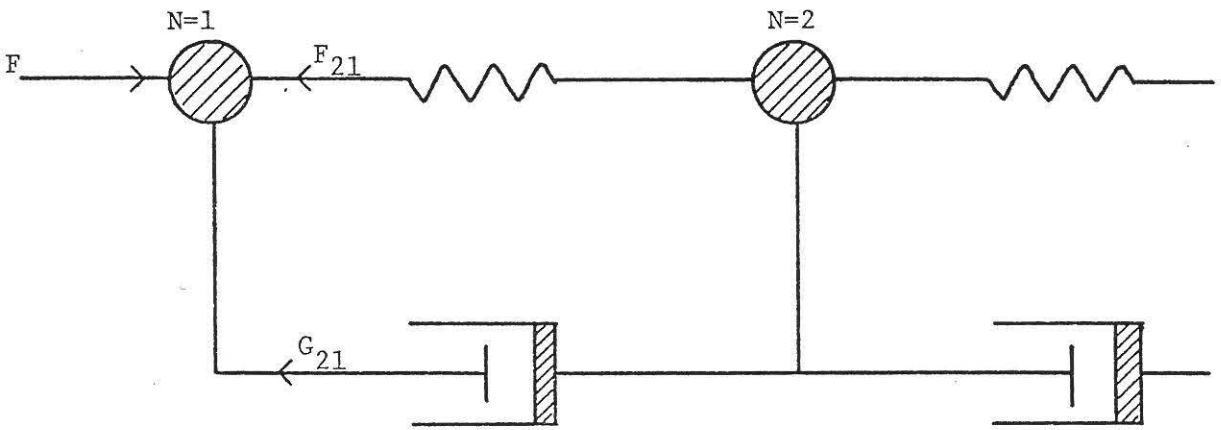

$$F = F_{21} + G_{21}$$

Fig. 5.--Force on the Mass Point N = 1

CHAPTER V

RESULTS OF NUMERICAL INTEGRATION

In this chapter we shall describe the results of numerical integration of the equations appearing in Chapter III. Before proceeding to do so, we will need to know something about the constants appearing in the equations of motion.

Constants in Constitutive Relations

In the present study we have used the physical constants of aluminum in the constitutive relations. Extensive experimental data on shock in aluminum are given in references [2,44]. In Fig. 6 and 7 the experimental Hugoniot points are indicated by a cross mark (X). The longitudinal stress is nondimensionalized by dividing it by $(\rho o D_o^2)$. ρo and D_o are density and sound speed respectively in the unstrained medium. The abscissae in these figures represent the strain in the medium.

The nondimensional equilibrium stress in the lattice model is given by equations (3.40) and (3.53) for parabolic and Morse law interaction respectively. We can rewrite these in a slightly different manner by making use of the definition of strain in the lattice as

$$X_{N+1} - X_N - 1 = (X_{N+1} - X_N - d_1)/d_1$$

$$\equiv \epsilon, \text{ strain in the lattice .} \qquad (5.1)$$

In the present work, for convenience, we have taken $d_1 = 1$ cm. With this definition we obtain from equation (3.40) for the parabolic case

$$P_s(N,T) = - (\text{strain}) + A_P \cdot (\text{strain})^2 . \tag{5.2}$$

Similarly, for the Morse law

$$P_s(N,T) = \frac{1}{A_M} [\exp \{-2A_M \cdot (\text{strain})\} - \exp \{-A_M \cdot (\text{strain})\}] . \tag{5.3}$$

Equation (5.2) is illustrated in Fig. 6 for different values of A_P. The Hugoniot points on this figure are close to the curve for a value of $A_P = 3.0$. Hence, in the computer study we adopt this value. Similarly, in Fig. 7 we have shown equation (5.3) for different values of A_M. For a value of $A_M = 2.0$ the Hugoniot data of aluminum lie close to the curve of equation (5.3); therefore, we use this value in our numerical work. To study the effects of the constants, computer runs with out values of A_P and A_M were also tried, and these are indicated in Tables 2 and 3.

As mentioned earlier in Chapter III, A_P and A_M represent nonlinearity of the lattice and therefore, increasing values of these constants mean that the springs connecting two mass points have a greater stiffness. We observed that for large values of A_P and A_M, i.e., $A_P = 10$ and $A_M = 7$, a large number of iterations (> 10) are needed for convergence.

We list below the relevant physical constants of aluminum for calculating various nondimensional quantities used in the program.

TABLE 1

PHYSICAL CONSTANTS USED IN THE PRESENT STUDY

Property	Value
Material	24 ST aluminum
Density ρ_o	2.78 g/cm^3
Bulk sound speed D_o	0.528 cm/μsec
Lattice equilibrium-separation d_1	1.00 cm
Frequency ω_1	0.528 μsec^{-1}
$\rho_o D_o^2$	780 K bars

The equilibrium lattice spacing d_1 is arbitrary. For convenience, we have taken it to be equal to 1 cm. We have yet to define sound speed in a lattice. This will be done in the next chapter. For the present we take it as $D_o = \omega_1 d_1$. If d_1 is fixed arbitrarily as 1 cm, then $\omega_1 = D_o/d_1$ sec^{-1} = D_o sec^{-1}.

To study the effect of dissipation, the nondimensional viscosity of parameter η was allowed to assume different values. To compare the effects of different amounts of damping, we need a reference quantity. This is taken in our work to be the critical damping η^*, at which oscillations in the particle velocity versus time plot vanish. We determined critical damping approximately by allowing the computer program to run for short times for cases with different amounts of damping, increased in steps of $\Delta\eta = 0.05$. Some of these cases were allowed to run for longer times and are listed in Tables 2 and 3.

In Appendix C, we have used the value of η^* for one particular case to compute the viscosity of aluminum, and we compare this value with the experimentally-determined viscosity of aluminum obtained by Russian workers [45].

Summary of Computer Runs

For reasons of economy, most of the computer runs in the present study were usually terminated when the shock front reached some 120 lattice spacings from the free surface. For the same reasons, momentum and energy checks were performed only for some of the cases; and these are indicated in the case number column of the tables below. Practically all of the runs converged for a value of QD = 2×10^{-5} [see equation (4.12)]. The cases in which this value had to be increased are indicated by a (+) plus sign in the remarks column along with the increased value. In the tables (JJJ) denotes the number of iterations required for values to converge for any time step.

Table 2 lists the various cases studied with parabolic interaction, and Table 3 the cases for Morse-law interaction. Program execution time on the IBM 360/67 machine was between 1 and 2 minutes depending on the printout. The parabolic cases are numbered serially as P1, P2, etc., and the Morse-law cases as M1, M2, etc., to facilitate later discussions.

Results and Discussion

At any given instant, the computer calculations give us the position, velocity, and acceleration of a lattice point. The nondimensional stress defined by equations (3.40) to (3.43) and (3.53) is then easily computed by determining the values for two neighboring mass points. In the present study we call the velocity profile the "shock profile."

In the figures of this section we have adopted a convention that curves in a graph represent variations of a particular lattice point with time, whereas points joined by straight lines in a graph represent a profile pertaining to a number of mass points at fixed time.

TABLE 2

SUMMARY OF COMPUTER RUNS WITH PARABOLIC INTERACTION

Case No.	A_p	u_1	Eta, η	ΔT Time Step	$(JJJ)^b$	Comments
P- 1	1.00	0.10	0.10	0.10	3	Rapid convergence due to small time step.
P-2	0.00	0.10	0.00	0.20	4	Linear lattice.
P-3	1.00	0.10	0.00	0.20	4	Oscillatory shock (velocity) profile.
P-4	1.00	0.10	0.10	0.20	4	Steady shock (velocity) profile.
P-5	1.00	0.10	0.20*	0.20	4	Steady shock profile. Critical damping. No oscillations in profile.
P-6[a]	1.00	0.10	0.00	0.60	7	Poor rate of convergence due to large time step. Compare with Case P-3. H CHECK = $- 3.07 \times 10^{-4}$, E CHECK = $- 7.47 \times 10^{-4}$.
P-7[a]	1.00	0.20	0.00	0.229	5	H CHECK = $- 1.5 \times 10^{-4}$, E CHECK = $- 1.5 \times 10^{-4}$. Oscillatory shock profile.
P-8[a]	1.00	0.20	0.60	0.229	5	Non-oscillatory steady shock profile. H CHECK = 2.65×10^{-2}, E CHECK = 2.50×10^{-2}.
P-9[a]	1.00	0.15	0.10	0.20	5	H CHECK = $- 3.65 \times 10^{-3}$, E CHECK = 3.61×10^{-3}.
P-10	3.00	0.10	0.00	0.20	5	Constant $A_p = 3$ is for aluminum. Oscillatory shcok (velocity) profile.

TABLE 2--Continued

Case No.	A_P	u_1	Eta, η	ΔT Time Step	(JJJ)[b]	Comments
P-11	3.00	0.10	0.25*	0.20	5	Steady shock profile. No oscillations. Critical damping.
P-12	3.00	0.10	0.50	0.20	5	Steady shock profile. Overdamped.
P-13	3.00	0.20	0.00	0.20	6	Oscillatory shock (velocity) profile.
P-14	3.00	0.30	0.00	0.20	6	Heavy oscillations due to increased amplitude of u_1.
P-15	5.00	0.10	0.00	0.20	6	Heavy oscillations due to increased nonlinearity of the springs.
P-16	10.00	0.10	0.00	0.20	7	Poor convergence of iterations due to large nonlinearity. QD = 3×10^{-5}.
					7	QD = 4×10^{-5}. + [c]
					7	QD = 5×10^{-5}. + [c]
P-17	3.00	0.10	0.00	0.05	3	Rapid convergence due to small time step.

[a]Cases for which energy and momentum checks were performed.

[b]Number of iterations required for convergence.

[c]Addition signs indicate cases where value of QD had to be increased.

*Critical damping.

TABLE 3

SUMMARY OF COMPUTER RUNS WITH MORSE-LAW INTERACTION

Case No.	A_M	u_1	Eta, η	ΔT Time Step	$(JJJ)^b$	Comments
M-1[a]	2.00 (Γ = 1.334)	0.10	0.00	0.20	5	A_M = 2.0 is the constant for aluminum. Oscillatory shock (velocity) profile. H CHECK = 2.38 x 10^{-4}, E CHECK = 2.90 x 10^{-4}.
M-2[n]	2.00 (Γ = 1.334)	0.10	0.25*	0.20	5	Steady shock profile. Critical damping. H CHECK = 1.672 x 10^{-3}, E CHECK = 1.59 x 10^{-3}.
M-3[a]	2.00 (Γ = 1.334)	0.20	0.00	0.20	5	Heavy oscillations due to increased amplitude of u_1. H CHECK = 6.73 x 10^{-4}, E CHECK = 9.16 x 10^{-4}.
M-4[a]	2.00 (Γ = 1.334)	0.30	0.00	0.20	6	Frequency of oscillations increased due to increase in amplitude of u_1. H CHECK = 2.97 x 10^{-4}, E CHECK = 6.6 x 10^{1-4}.
M-5[a]	2.00 (Γ = 1.334)	0.15	0.40	0.20	5	Non-oscillatory shock (velocity) profile. Overdamped case. H CHECK = 2.03 x 10^{-3}, E CHECK = 1.98 x 10^{-3}.
M-6	3.434 (Γ = 2.05)	0.10	0.00	0.20	5	Heavy oscillations due to increased nonlinearity of the springs. Γ = 2.05.
M-7	3.434 (Γ = 2.05)	0.10	0.10	0.20	5	Few oscillations in the shock (velocity) profile due to damping.
M-8	3.434 (Γ = 2.05)	0.10	0.20	0.20	5	Overshooting at the head of the wave and no oscillations behind. Close to critical damping.

TABLE 3--Continued

Case No.	A_M	u_1	Eta, η	ΔT Time Step	(JJJ)[b]	Comments
M-9	3.434 (Γ = 2.05)	0.10	0.30*	0.20	5	Steady shock profile without any oscillations. Critical damping.
M-10[a]	2.00 (Γ = 1.334)	0.10	0.00	0.10	4	Oscillatory shock profile. Smaller number of iterations required due to a small time step. Compare with M-1. H CHECK = -4.19×10^{-4}, E CHECK = -2.78×10^{-4}.
M-11[a]	2.00 (Γ = 1.334)	0.10	0.00	0.50	7 7 7	Poor convergence due to a large time step; QD = 3×10^{-5}, QD = 4×10^{-5}, QD = 5×10^{-5}. +[c] Results not reliable.

[a]Cases for which energy and momentum checks were performed.

[b]Number of iterations required for convergence.

[c]Addition signs indicate cases where value of QD had to be increased.

*Critical damping.

Typical particle paths (X versus T) are illustrated in Fig. 8-10 for two separate cases. Figures 8 and 9 are for two different lattices without dissipation, whereas Fig. 10 is for the lattice of Fig. 9 with dissipation close to critical damping.

We observe the following with reference to these figures, valid for all the cases studied. Any mass point N remains at its initial equilibrium position until the arrival of a disturbance at some time T, denoted by T_N. Subsequently, the mass point shows an oscillatory motion in the absence of dissipation, as shown in Fig. 8 and 9. As T increases, the particle performs oscillations of decreasing amplitude and period about a mean position represented by a line of slope $\frac{dx}{dT} = u_1$ in the X-T plane, u_1 being the amplitude of the input velocity step. This is shown in Fig. 9 for N = 47. For large times the position-time plot approaches a uniform slope u_1.

In the presence of a small amount of dissipation, i.e., $\eta < \eta^*$, the particle still shows an oscillatory X-T plot with a more rapid damping. Close to values of $\eta = \eta^*$, the oscillations completely vanish. This is shown in Fig. 10. The particle N remains at its initial equilibrium position until T_N, then accelerates smoothly to velocity u_1. We observed slight changes in T_N for a mass point under identical shock conditions and with slightly different amounts of damping. The effect of large damping ($\eta >> \eta^*$) is to make T_N decrease with increase in damping because of diffusion in the lattice.

In Fig. 8-10 we have shown the motion of a mass point N and its two neighbors. For all the cases studied, it was observed that for N sufficiently far from the free surface, the motion is similar to that of its neighbor. This is apparent from Fig. 8-10. One important result follows from this similarity. If we make the time of arrival of the disturbance coincident for two neighboring mass points, then the particle paths lie on one curve (plotting

accuracy .005). Specifically with reference to Fig. 8, if we shift the curve for N= 57 to the right so that points a and a' coincide, followed by a shift in time, $\theta_{N,N+1}$, such that b and b' coincide, then the points for N = 57 and N = 58 fall on the same smooth curve (plotting accuracy .005).

The characteristic time shift $\theta_{N,N+1}$ is the difference in times of arrival of the disturbance, i.e., $\theta_{N,N+1} = T_{N+1} - T_N$, and hence, is a property of the nonlinear lattice as well as the amplitude of the disturbance. We shall discuss this in greater detail later. For the present we put the above-discussed observation in a mathematical form as

$$X_{N+1}(T) = X_N (T - \theta_{N,N+1}) + 1$$

and

$$X_{N-1}(T) = X_N (T + \theta_{N-1,N}) - 1 . \tag{5.4}$$

The above yield for the displacement

$$S_{N+1}(T) = S_N (T - \theta_{N,N+1})$$

and

$$S_{N-1}(T) = S_N (T + \theta_{N-1,N}) . \tag{5.5}$$

Equations (5.4) and (5.5) are very important recurrence relations, found to be valid in the present study within the errors of computation and plotting.

For a nonlinear lattice without dissipation, we observed that $\theta_{N,N+1}$ was not the same as $\theta_{N-1,N}$ even for large N. This suggests that the disturbance in such a lattice does not propagate at a constant velocity even after large distances of propagation. We believe that the propagation

velocity of a disturbance in a nonlinear lattice to be time dependent. This will be taken up later in this section.

In equations (5.4) and (5.5), if $\theta_{N,N+1}$, $\theta_{N-1,N}$, etc., are constant and equal to θ, then the disturbance propagates at a constant velocity U_s. This was found to be true when critical damping was exceeded, i.e., $\eta > \eta^*$. For such a case equations (5.4) and (5.5) are statements of steady state conditions [18] and are rewritten as

$$X_{N+1}(T) = X_N\ (T - \theta) + 1\ ,$$

and

$$X_{N-1}(T) = X_N\ (T + \theta) - 1\ . \tag{5.4a}$$

$$S_{N+1}(T) = S_N\ (T - \theta)\ ,$$

and

$$S_{N-1}(T) = S_N\ (T + \theta)\ . \tag{5.5a}$$

If U_s is the constant shock velocity, then it follows that

$$\theta \equiv 1/U_s,\ (< 1)\ . \tag{5.6}$$

Figure 11 shows a typical plot of velocity versus time of a mass point in a non-dissipating lattice. The point rapidly accelerates from rest to a velocity u_P^* greater than u_1 and subsequently performs irregular oscillations about the mean drift velocity u_1. The overshooting $(u_P^* - u_1)$ is dependent on the amplitude of disturbance and lattice nonlinearity. It increases with nonlinearity and increasing amplitudes.

The amplitude of the oscillations decreases with time as shown in Fig. 11, and for large times the particle approaches a uniform drift velocity u_1. This is in accord with slope of curves in Fig. 8 and 9 becoming constant for very large times. The effect of dissipation is to reduce or totally eliminate these irregular oscillations. The behavior demonstrated in Fig. 11 was also observed for other cases and under different conditions. Hence, we believe that this kind of behavior is due to the dynamics of the nonlinear lattice and not to computational errors.

Figures 12 and 13 show, for two different times, shock profiles in which particle velocity u_p is plotted against lattice point N. The ordinate gives the mass point velocity $u_p(N)$. We describe the main features of this typical profile below.

For anharmonic forces and the cases studied, our results differ from those of Tsai and Beckett [17]. In their work the shock front DE (see Fig. 12 and 13) is reported to become steady in time and propagation velocity by the time DE reaches 40 to 50 lattice spacings from the free surface. In the present study DE was found to propagate at a velocity dependent on time, and the slope of DE was also changing slightly as a function of time. Only the average velocity of propagation became essentially constant.

In our work we have calculated the velocity at which the disturbance propagates by computing the position X_s at which the profile has the value $1/2\ u_1$ (see Fig. 12) for various times. Table 4 summarizes such computations for three cases.

Columns 3, 5, and 7 of Table 4 show the local velocity of propagation of the disturbance. We shall call this the shock velocity. It is evident that shock velocity is not a constant but an almost periodic function of time. To make sure that this observed behavior was not due to the choice of time

TABLE 4

SUMMARY OF SHOCK VELOCITY COMPUTATIONS

Time	Case M-1, u_1=0.1		Case M-3, u_1=0.2		Case M-4, u_1=0.3	
	X_s	$\Delta X_s/\Delta T$	X_s	$\Delta X_s/\Delta T$	X_s	$\Delta X_s/\Delta T$
1	2	3	4	5	6	7
43.0	49.130		56.004		62.633	
		1.244		1.505		1.318
44.0	50.374		57.509		63.951	
		1.189		1.288		1.650
45.0	51.563		58.797		65.601	
		1.150		1.206		1.332
46.0	52.713		60.003		66.933	
		1.126		1.506		1.576
47.0	53.839		61.509		68.569	
		1.114		1.289		1.347
48.0	54.953		62.798		69.916	
		1.183		1.206		1.618
49.0	56.136		64.004		71.534	
		1.247		1.508		1.365
50.0	57.383		65.512		72.899	
		1.189		1.288		1.589
51.0	58.572		66.800		74.498	
		1.150		1.206		1.385
52.0	59.722		68.006		75.883	
		1.126		1.510		1.576
53.0	60.848		69.517		77.459	
		1.114		1.287		1.407
54.0	61.962		70.804		78.866	
		1.199		1.206		1.553
55.0	63.161		72.010		80.419	
		1.244		1.519		1.431
56.0	64.405		73.529		81.850	
		1.186		1.279		1.526
57.0	65.591		74.808		83.376	
		1.148		1.206		1.459
58.0	66.739		76.014		84.835	
		1.124		1.519		1.496
59.0	67.863		77.533		86.331	
		1.115		1.280		1.488
60.0	68.978		78.813		87.819	
Average $\frac{\Delta X_s}{\Delta T} = \overline{U}_s =$		1.1690	$\overline{U}_s$ =	1.3416	$\overline{U}_s$ =	1.4774

step, we halved the time step and found the same result. If the behavior were due to the computational scheme, then varying the amplitude should not affect the periodicity. But columns 3, 5, and 7 show definite effects of amplitude on the periodicity of the shock velocity.

This behavior illustrated in Table 4 seems to be a property of the nonlinear lattice under study. Further, we observed that the period of oscillations in the position-time plot is essentially the same as the recurrence period of shock velocity. For clarifying this statement, we refer the reader to column 5 of Table 4 and Fig. 8, both for Case M-3.

Oscillations in the shock position versus time plot can be explained in the following way. A particle immediately behind the shock front acts like a piston. An oscillating piston will produce an oscillatory disturbance or vice-versa, i.e., an oscillating shock imparts oscillating velocity to the particles behind it. The initial oscillatory behavior of a mass point in our lattice is due to this sort of behavior. These oscillations are discussed in more detail in Chapter VII.

For the present we are concerned only with the shock path. From results of Table 4, columns 3 and 5, it appears that the period of oscillation of the shock front remains essentially constant. We have shown the oscillatory and averaged paths of the shock in Fig. 8 and 14. The oscillations are of very small amplitude and are not appreciable unless viewed on an expanded scale. These oscillations vanish in the presence of critical damping; then the shock path coincides with the averaged path shown in Fig. 14. Shock velocity in this case is $\overline{U}_s$. The averaged shock velocity $\overline{U}_s$ increases with u_1 in an approximately linear manner.

As the nonlinear coefficients A_M and A_P are increased for fixed u_1, $\overline{U}_s$ increases. The oscillations in the shock path-time also increase in

amplitude and frequency. The reason for this will be explained in the next chapter.

Returning now to Fig. 12 and 13, we see that three regions, AB, BC, and CD, may be distinguished behind the front DE [17]. In the region CD immediately behind the shock front, there exist a few regular oscillations having the appearance of a damped since wave with frequency gradually increasing from D to C. At C the regularity is interrupted by superposition of irregular frequency oscillations. Following this, the oscillations become quite complex but appear to resolve themselves again into a few simple vibrations with a definite period. Finally, at B there appears a fairly abrupt decrease in amplitude of the oscillations which are not of appreciable size unless shown on a large scale. The region AB, though oscillatory, is for all practical purposes a uniform region. The existence of this essentially uniform region was reported by Tsai and Beckett [17].

The regions CD and BD both increase in direct proportion to the distance travelled by the shock front, indicating that these groups of oscillations have velocities which are less than the shock wave velocity. This results from frequency dispersion effects which make the propagation velocity of high frequency waves found in the region BC less than that of the low frequency waves in region CD. We discuss this in greater detail in the next chapter.

Our observations regarding the shock profile are essentially the same as reference [17]. However, there is one notable difference, and that is the steadiness of the front DE. It appears from our computations that a steady front and steady shock velocity do not exist in the nonlinear, nondissipating lattice model under study. Only the averaged shock velocity remains constant.

To obtain a steady shock profile, it is necessary to have dissipation in the system. Figure 15 shows the effects of different amounts of damping. In a critically damped nonlinear lattice, we observe the steady state conditions. At a later stage, we use the steady state conditions to derive interesting shock profiles.

In Chapter II (page 11) we mentioned that the jump conditions are useful even for cases where steady state and equilibrium conditions are not fully satisfied. For a nondissipating anharmonic lattice, we have such a case. We next investigate the validity of application of jump conditions for such a lattice. We have essentially a uniform region AB (see Fig. 12 or 13) far behind the front and a constant average shock velocity $\overline{U}_s$ to use in the jump relations.

In terms of nondimensional quantities the conservation relations of mass and momentum for steady state can be written as

$$\rho o/\rho = V^* = 1 - (u_1/\overline{U}_s), \text{ conservation of mass} \qquad (5.7)$$

and

$$P^* = \overline{U}_s \cdot u_1, \text{ conservation of momentum .} \qquad (5.8)$$

The nondimensionalizing parameters are $(\rho o D_o^2)$ for pressure or stress and D_o for velocities.

Combining equations (5.7) and (5.8), we obtain the following expressions for shock and particle velocities;

$$\overline{U}_s = P^*/(1 - V^*) \qquad (5.9)$$

and

$$u_1 = \sqrt{P^* (1 - V^*)} \ . \qquad (5.10)$$

Equilibrium compression of the lattice gives the same P* - V* curve as for the continuum because of the choice of constants in the constitutive relations. In Table 5, we have listed values for pressure and dilatation obtained in the uniform region AB (see Fig. 12 and 13) of the lattice for three cases. We have used these values to compute shock and particle velocities from equations (5.9) and (5.10) to compare with lattice calculations in Table 5.

The last two columns of Table 5 show the percentage error between continuum and lattice model calculations. The magnitudes of these errors suggest that the steady state jump conditions represent a useful approximation even though they do not apply exactly. The agreement between values of particle velocity in the lattice model and continuum is quite satisfactory. However, the shock velocity values differ by a small percentage. Shock velocity in a lattice is always higher than that given by the jump conditions. A particle velocity of u_1 =0.3 corresponds to about 300 kilobar shock in aluminum.

We observed that when the average shock velocity $\overline{U}_s$ of the lattice was used to compute pressure and dilatation from equations (5.7) and (5.8) for cases listed in Table 5, the percentage error between steady state jump conditions and the lattice calculations was of the same order as shown in the table. The calculations confirm our belief that the Rankine-Hugoniot jump conditions give satisfactory results for the uniform region in our lattice model.

TABLE 5

COMPARISON OF JUMP CONDITIONS WITH CALCULATIONS OF THE LATTICE MODEL

Case No.	Lattice Model Calculations				Jump Conditions		Error	
	$(u_1)_L$	$(\bar{U}_s)_L$	$(P^*)_L$	$(V^*)_L$	$(u_1)_C$	$(\bar{U}_s)_C$	$\frac{[(u_1)_C - (u_1)_L]}{(u_1)_C}$	$\frac{[(\bar{U}_s)_C - (\bar{U}_s)_L]}{(\bar{U}_s)_C}$
1	2	3	4	5	6	7	8	9
M-1	0.10	1.1690	0.114	0.912	0.10	1.140	0.0%	- 2.54%
M-2	0.20	1.3416	0.255	0.841	0.201	1.260	- 0.05%	- 6.4%
M-3	0.30	1.4774	0.422	0.782	0.302	1.390	- 0.067%	- 6.25%

*Equilibrium values.

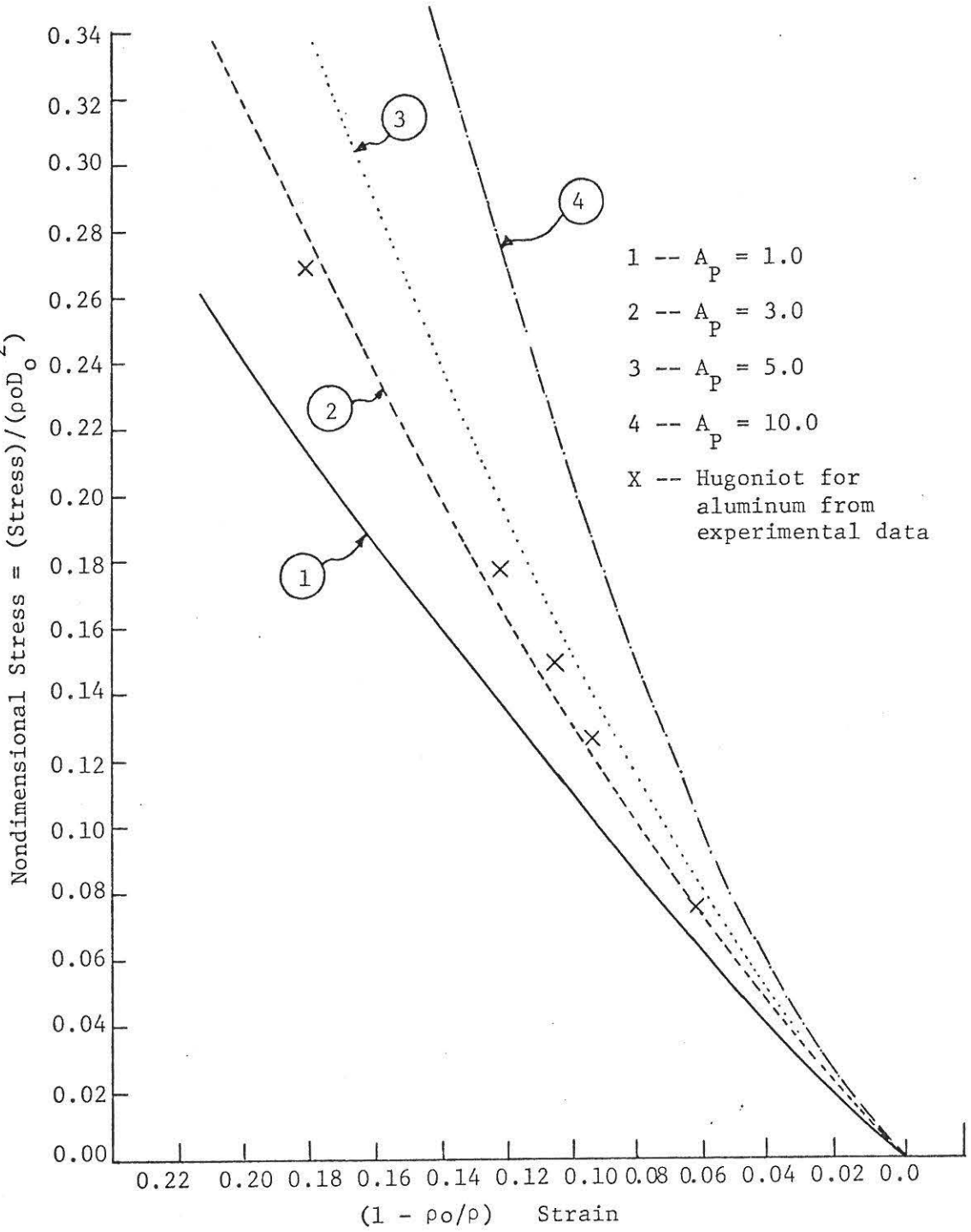

Fig. 6.--Parabolic Constant for Aluminum from Equation (5.2)

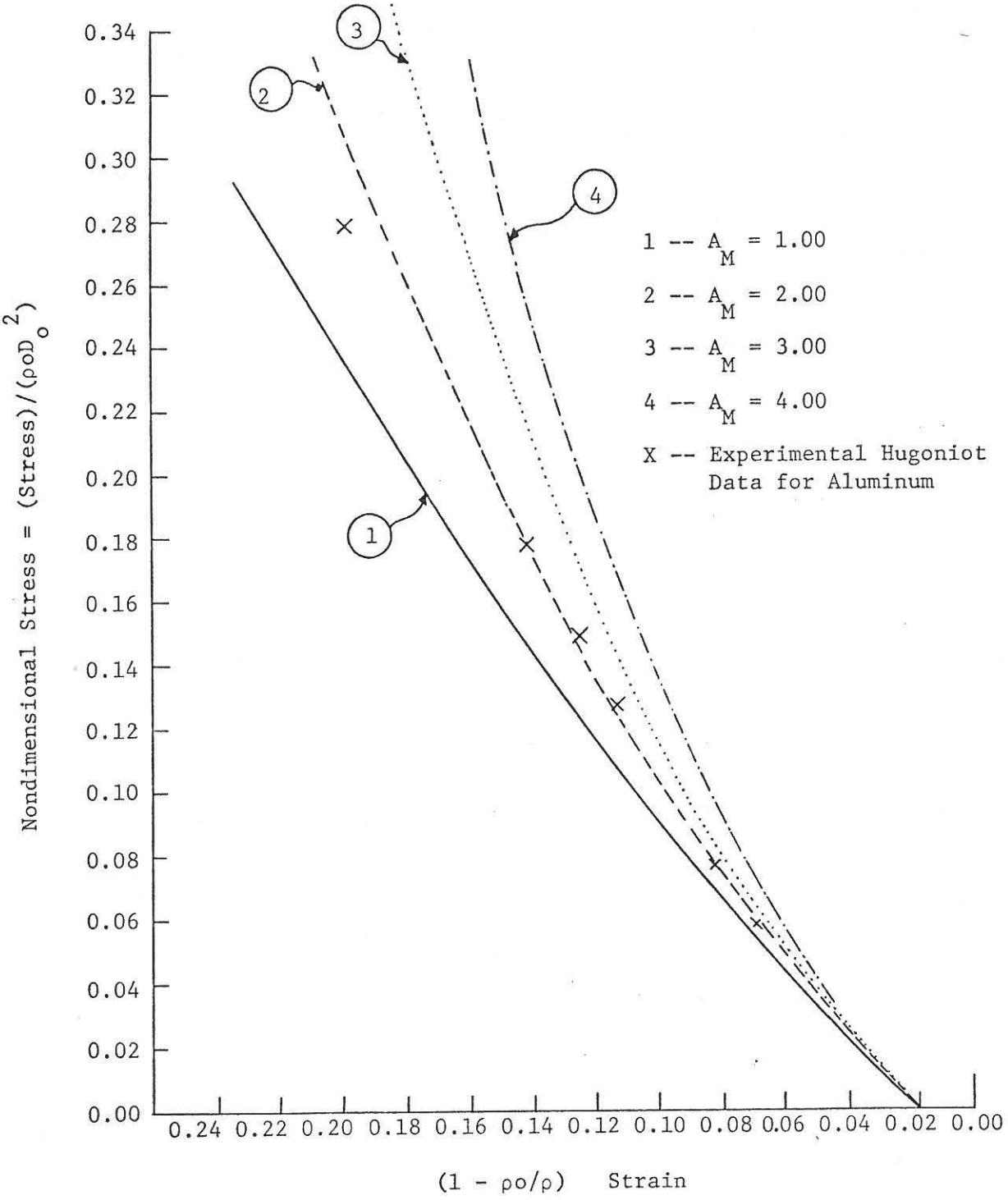

Fig. 7.--Morse Law Constant for Aluminum from Equation (5.3)

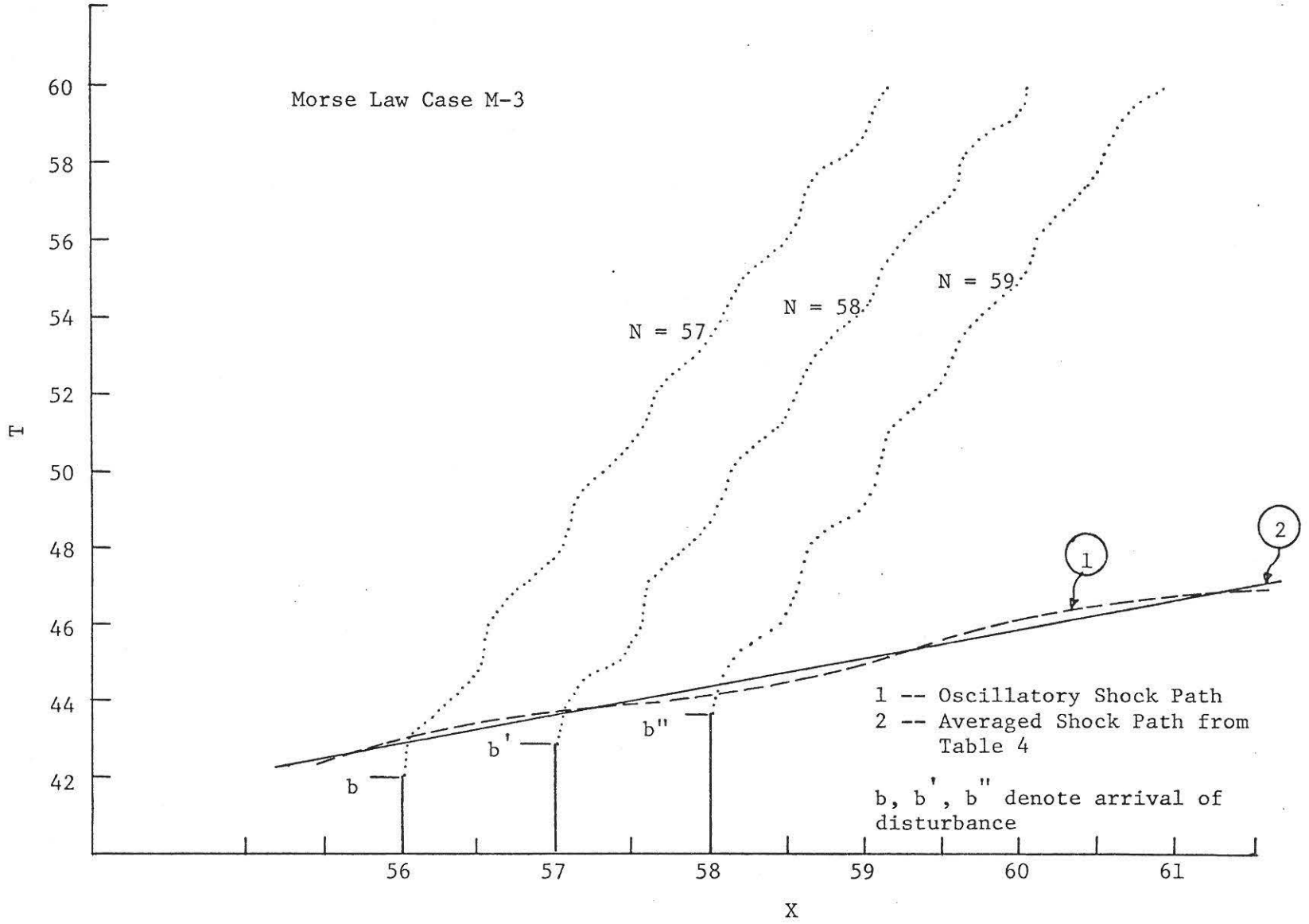

Fig. 8.--Position-Time Plot of Particles, Case M-3

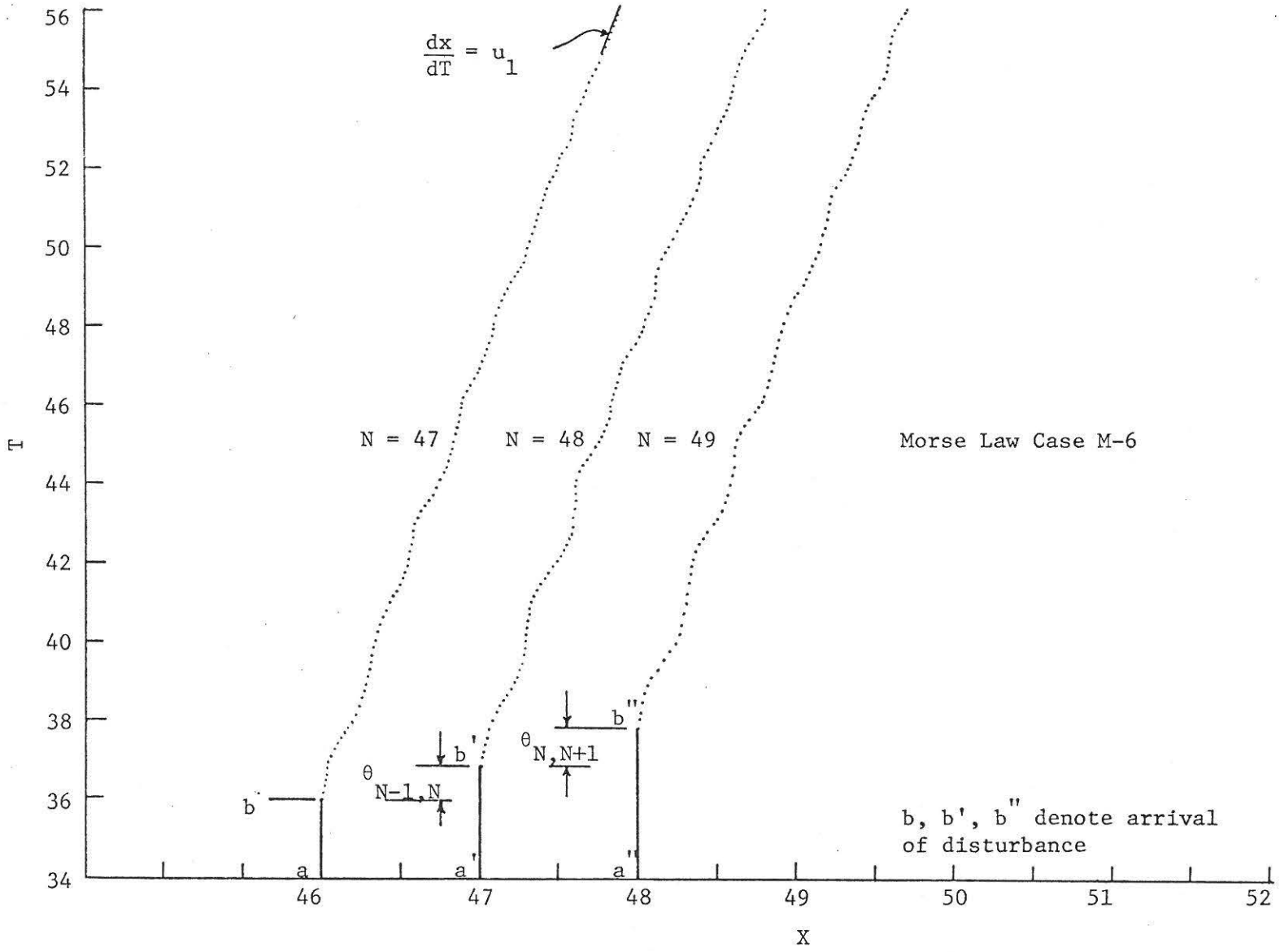

Fig. 9.--Position-Time Plot of Particles, Case M-6

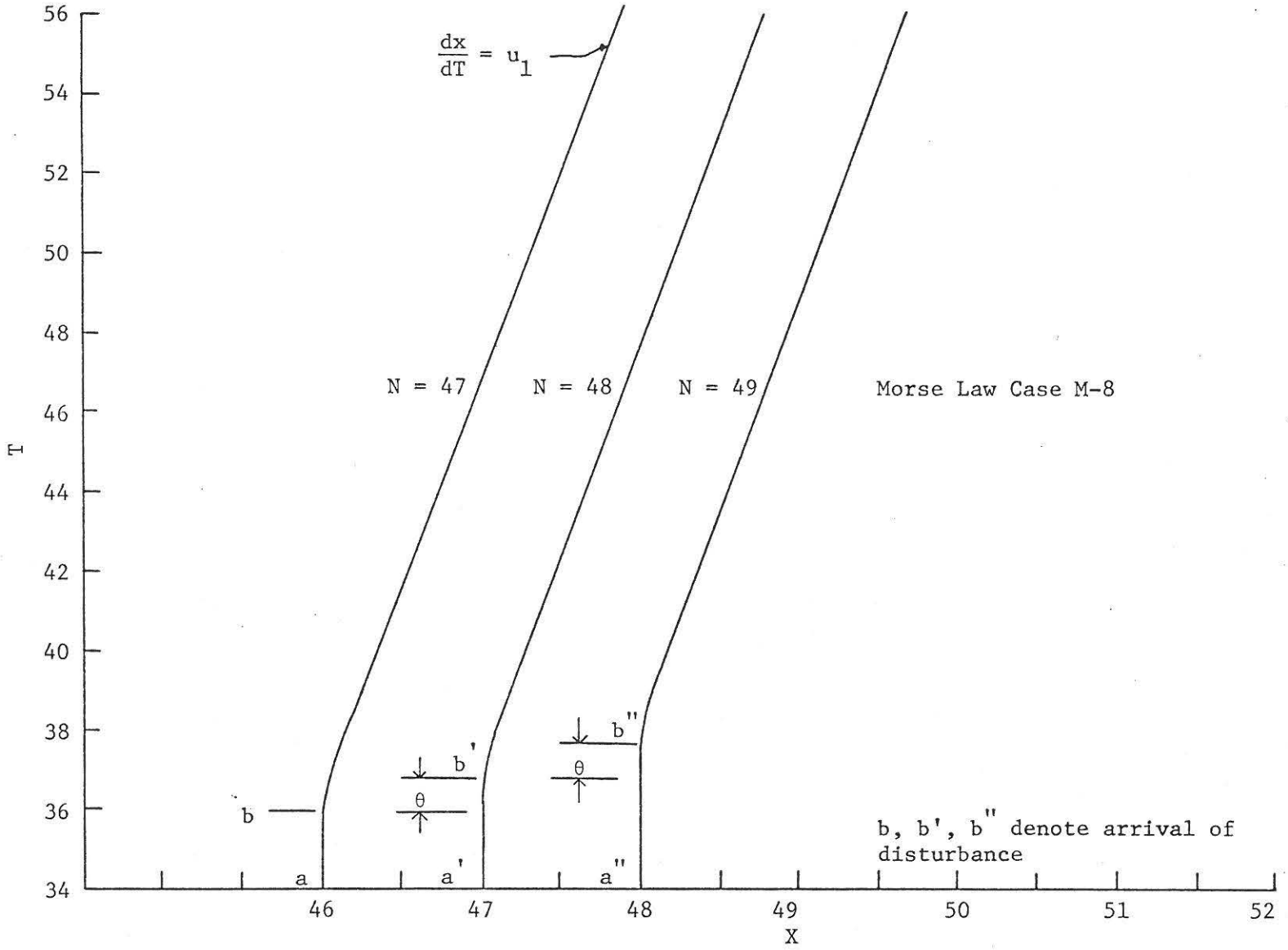

Fig. 10.--Position-Time Plot of Particles, Case M-8 for Steady Shock

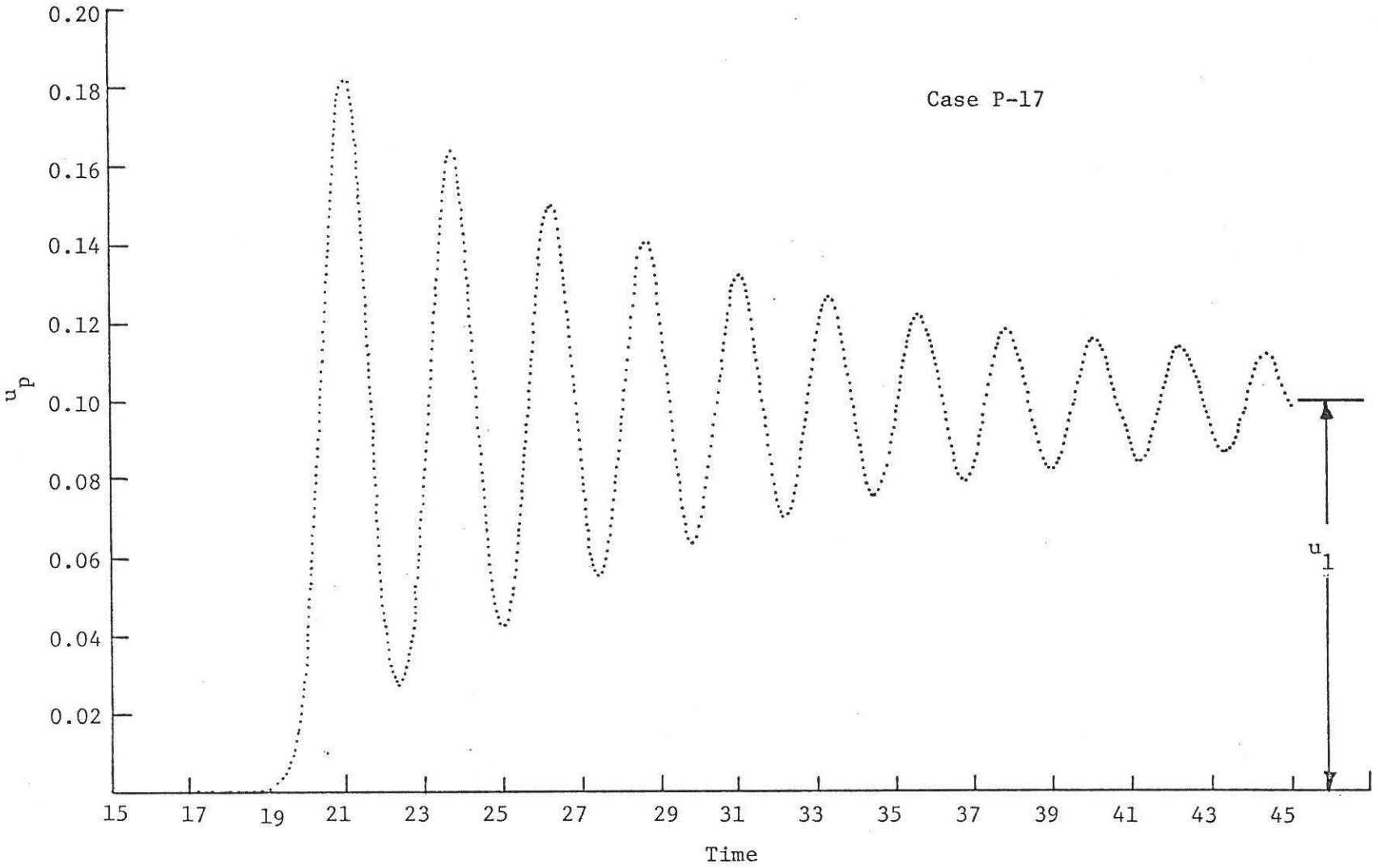

Fig. 11.--Time-Velocity Plot of a Lattice Point, Case P-17

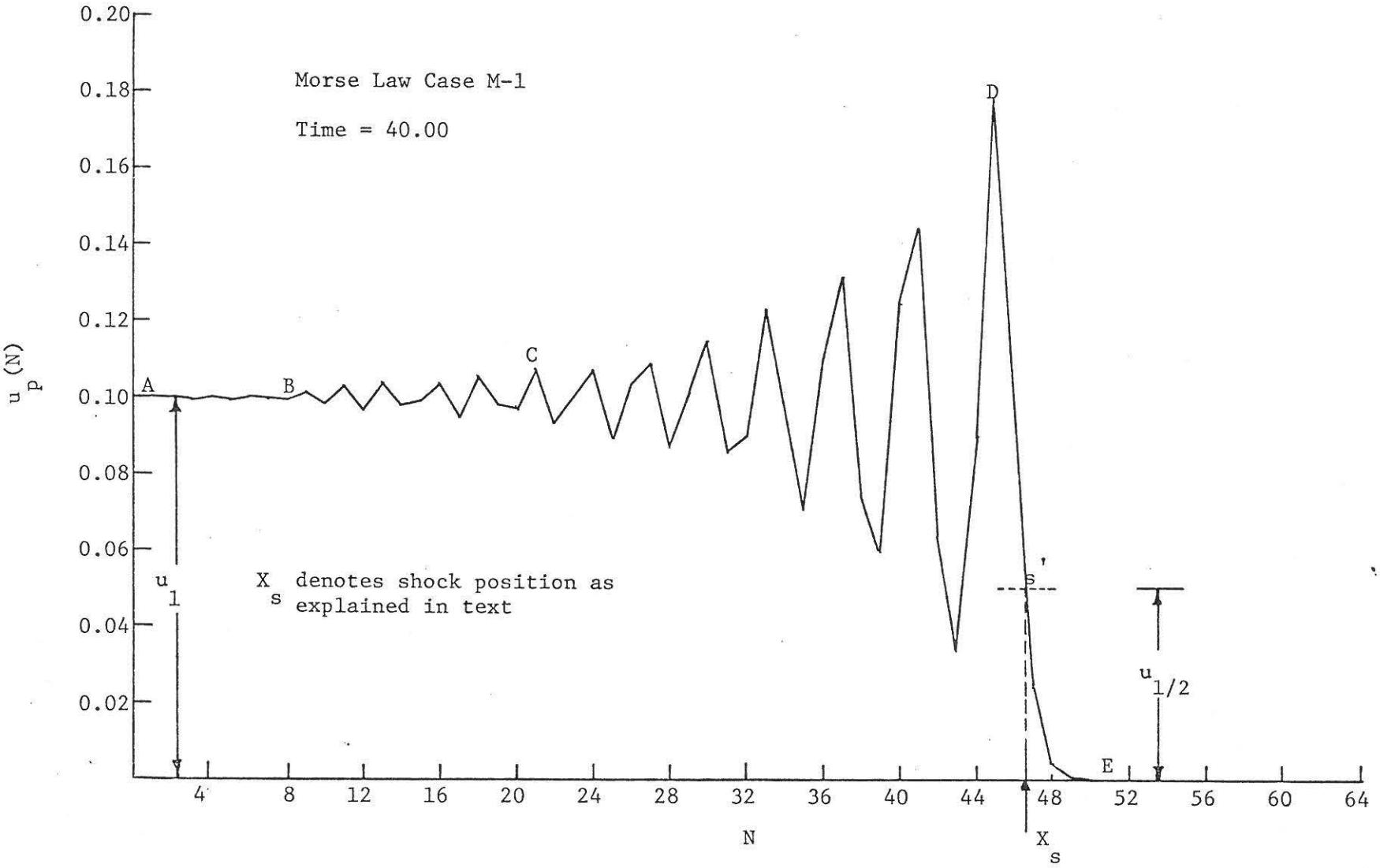

Fig. 12.--Shock (Velocity) Profile, Case M-1, Time = 40.00

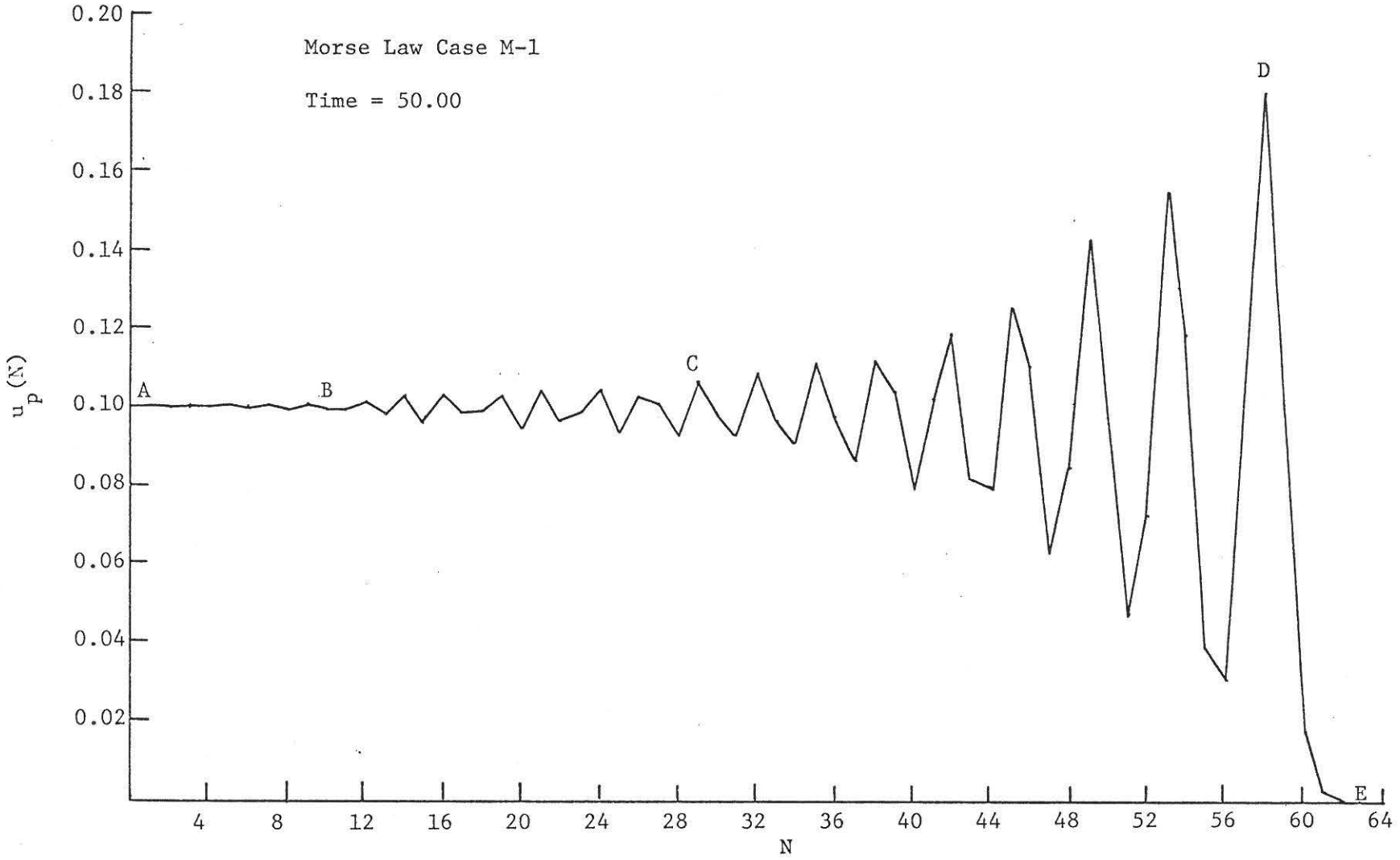

Fig. 13.--Shock (Velocity) Profile, Case M-1, Time = 50.00

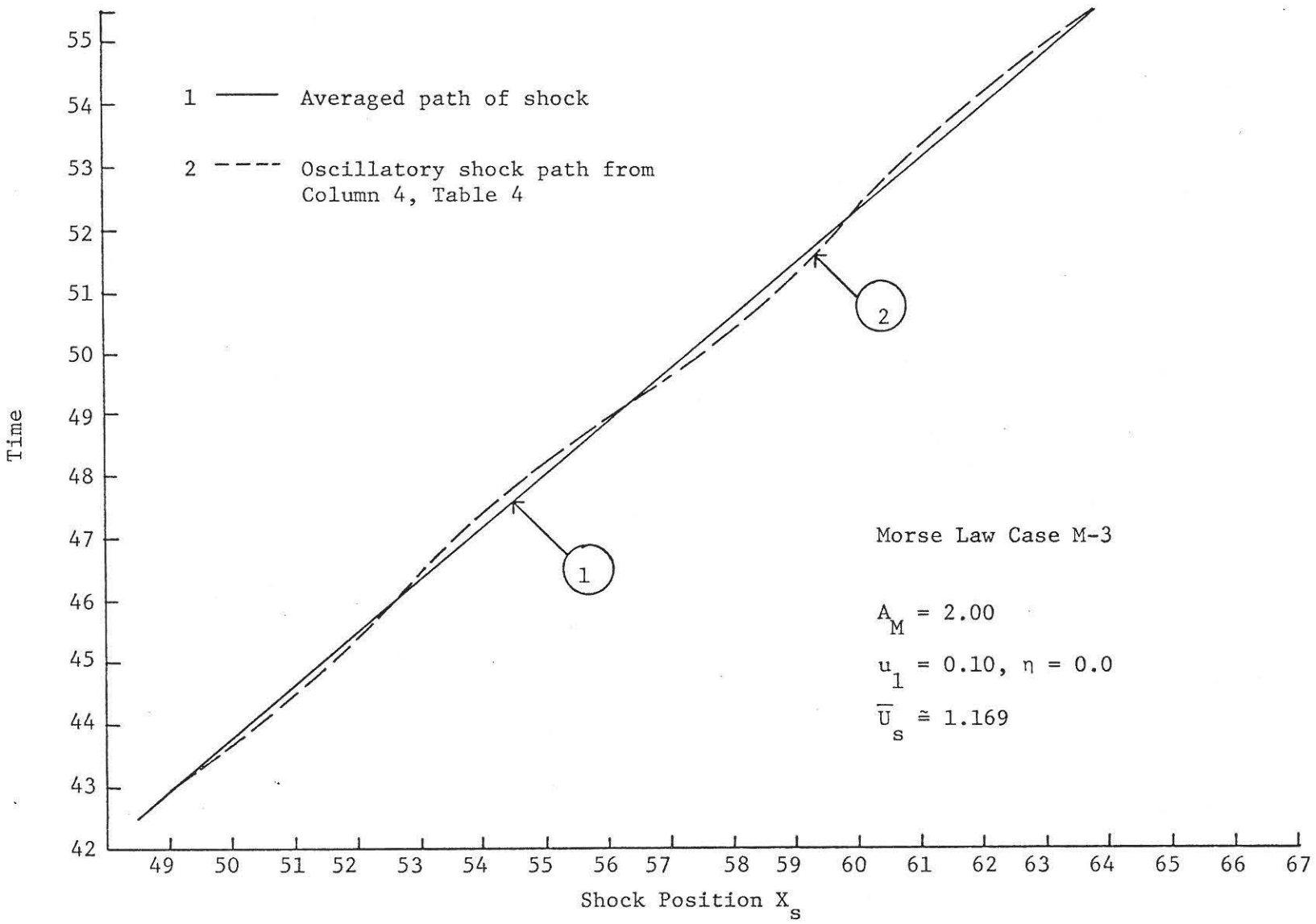

Fig. 14.--Oscillatory and Averaged Shock Path, Case M-3

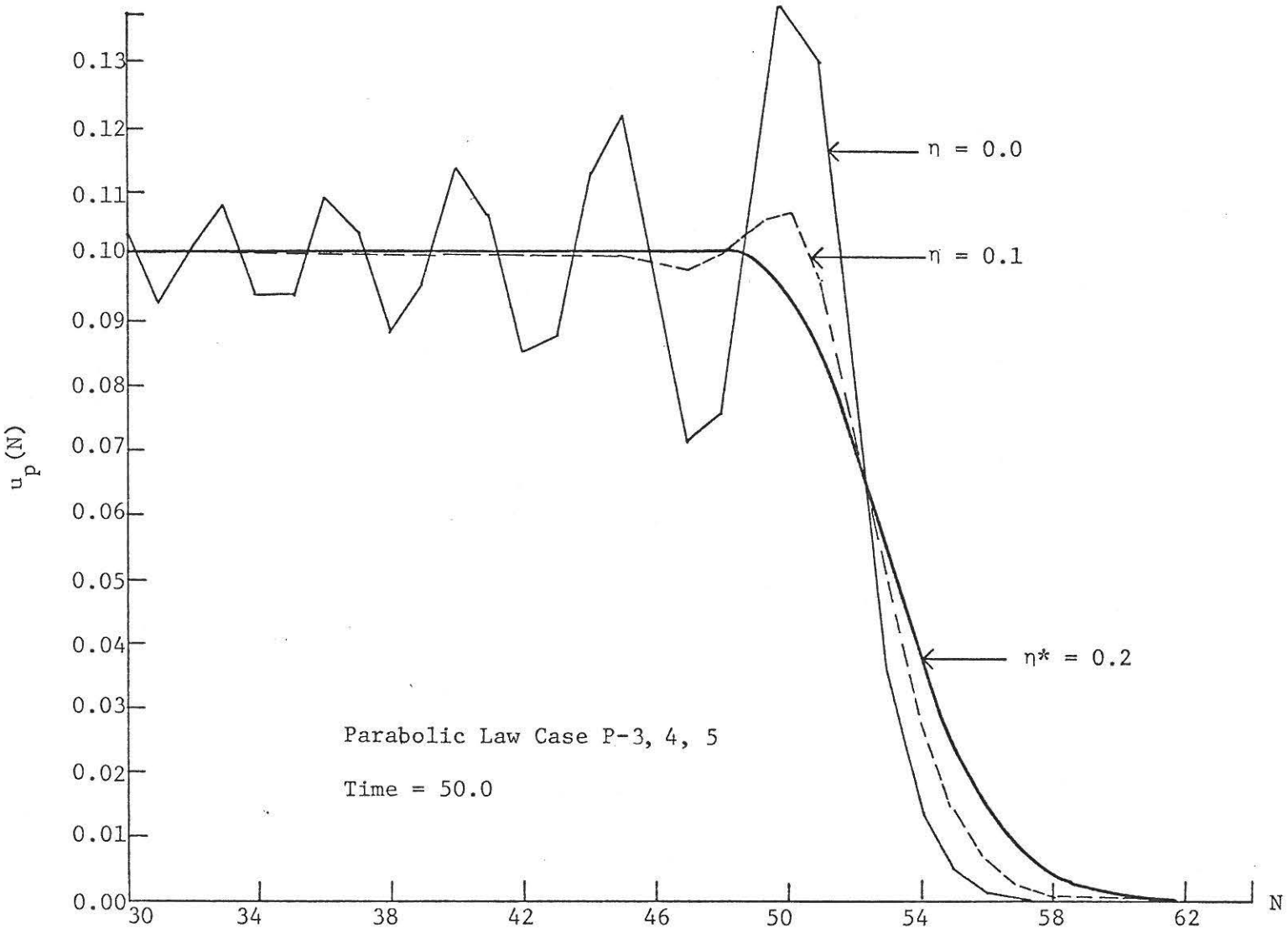

Fig. 15.--Effect of Dissipation on Shock Profile, Cases P-3, 4, 5

CHAPTER VI

DISPERSION IN A CHAIN OF PARTICLES

While discussing our results in the previous chapter, we mentioned frequency dispersion. In this chapter we shall briefly discuss the theory of lattice dynamics to explain frequency dispersion in linear chains and amplitude dispersion in nonlinear chains. With these ideas we hope to gain a better understanding of some of our computer results.

Frequency Dispersion in a Linear Chain

The early successes of Newtonian mechanics encouraged the interpretation of almost all physical phenomena by the use of mechanical models [46]. One of the most popular of these models was that of a linear lattice of material particles interconnected by harmonic springs. Newton was the first to consider such a chain of mass points coupled by linear springs of constant K. In an attempt to calculate the speed of sound in air with such a model, he found the speed to be

$$D_o = d_1\sqrt{K/m} = \omega_1 d_1 \ , \qquad (6.1)$$

where d_1 is the interparticle separation where $m = \rho d_1$.

When the isothermal bulk modulus of air was used to find K, the above equation gave too low a value. Laplace pointed out in 1822 that the adiabatic rather than the isothermal bulk modulus should be used, and good agreement with experimental values of sound speed in air was obtained.

The one-dimensional, single-component harmonic lattice with nearest neighbor interactions has for its equation of motion the following:

$$m \ddot{s}_N(t) = K (s_{N+1} - 2s_N + s_{N-1}) , \tag{6.2}$$

where s_N represents displacements of the N-th particle from its equilibrium position, m is the mass of each particle, and K is the nearest neighbor spring constant.

We shall discuss the motion of an infinite chain, from which it is possible to obtain solutions for a chain of a finite number of particles by superposition and the application of suitable restrictive boundary conditions. We seek solutions to equation (6.2) in the form of travelling waves. It is important to note here that we do not have a continuous medium in which the waves move, but only a set of discrete particles. These waves have no direct physical significance except at the positions of particles, and are known as "mathematical" or "descriptive" waves [47].

A harmonic plane wave of frequency ω and wave number q propagating on the lattice can be represented by a function of the form

$$s_N(t) = A \cdot \exp \{-i(qNd_1 - \omega t)\} . \tag{6.3}$$

Substitution of this solution into equation (6.2) leads to

$$\omega^2 = 4 \omega_1^2 \sin^2 \frac{qd_1}{2} , \tag{6.4}$$

where $\omega_1 = \sqrt{K/m}$. The phase speed D is given by

$$D^2 = \frac{\omega^2}{q^2} = \{(\omega_1 d_1)^2 \cdot \sin \frac{qd_1}{2} \} / \left|\frac{qd_1}{2}\right|^2 . \tag{6.5}$$

We transform the above equation with the use of Newtonian sound speed from equation (6.1) and the identity $q = 2\pi/\lambda$ into

$$D^2 = \{D_o^2 \cdot \sin^2 \frac{\pi d_1}{\lambda} \}/\left(\frac{\pi d_1}{\lambda}\right)^2 \tag{6.6}$$

or

$$D = \{D_o \cdot \left|\sin \frac{\pi d_1}{\lambda}\right| \}/\left(\frac{\pi d_1}{\lambda}\right) . \tag{6.7}$$

The above relation was derived by Baden-Powell in 1841 [19]. We see that $D_o = (\omega_1 d_1)$ is the propagation speed of infinitely long waves or when the interparticle distance d_1 approaches zero; i.e.,

$$D \to D_o \text{ as } \lambda \to \infty \text{ or } d_1 \to 0 .$$

Equation (6.3) shows that if we replace q by

$$q_R = q + \frac{2R\pi}{d_1} , \tag{6.8}$$

where R is any positive or negative integer, the same motion of particle results for a given frequency. Hence, ω is a periodic function of q with a period $\frac{2\pi}{d_1}$ in q. The dispersion relation for a harmonic lattice from equation (6.4) is rewritten as

$$\omega = 2\omega_1 \cdot \left|\sin \frac{qd_1}{2}\right| . \tag{6.9}$$

The multiplicity of wave numbers q associated with a given frequency can be removed by restricting the value of q to $|q| \leq \pi/d_1$. With this restriction there are just two values of q, differing only in sign, for which we have a general solution for a given value of ω;

$$s_N = [A \cdot \exp\{-i(qNd_1 - \omega t)\} + B \cdot \exp\{i(qNd_1 - \omega t)\}] \ . \qquad (6.10)$$

To obtain a general motion, we shall have to form linear combinations of equation (6.10) for various values of ω. For a finite lattice only certain discrete values of ω are allowed. The summing in this case is done over these allowed values. We note from equation (6.9) that real values of q are obtained only for values of ω less than ω_c, where

$$\omega_c = 2\,\omega_1 \ . \qquad (6.11)$$

This shows that waves corresponding to frequencies higher than ω_c are not propagated along the lattice. ω_c is called the upper cut-off frequency. Frequencies above ω_c require that q be imaginary. If we write $q' = iq$, equation (6.4) becomes

$$\frac{\omega}{2\omega_1} = \pm\, i \,\text{Sin h}\, \frac{q'd_1}{2} \ , \qquad (6.12)$$

and corresponding solutions are of the form

$$s_N = A \exp\{-(q'Nd_1 - i\omega t)\} \ . \qquad (6.13)$$

These correspond to exponentially-attenuated waves and will have to be included in the general solution.

In the present study we have worked mostly with nondimensional quantities. We rewrite equations (6.9) and (6.7) in nondimensional form by defining

$$\frac{\omega}{\omega_1} \equiv W \ , \qquad (6.14a)$$

$$qd_1 = Q \ , \qquad (6.14b)$$

and

$$\frac{D}{D_o} = U \ . \tag{6.14c}$$

Equation (6.9) becomes

$$W = 2 \cdot \left|\sin\left(\frac{Q}{2}\right)\right| \ . \tag{6.15}$$

Similarly, equation (6.7) in nondimensional form is

$$U = \frac{W}{Q} = \frac{2 \cdot \left|\sin(Q/2)\right|}{Q} \ . \tag{6.16}$$

We see from the above equations that phase speed U is a function of frequency W. The phase speed of lower frequency waves is higher than those of higher frequency waves. This is called frequency dispersion.

Amplitude Dispersion in a Nonlinear Chain

The linear chain exhibits frequency dispersion. According to equation (6.15), for such a chain the nondimensional frequency W is a function of the nondimensional wave number Q. It is interesting to see how the nonlinearity of the chain changes the dispersion relation. Let us consider equation (3.36) without dissipation. With $\eta = 0$, this equation gives

$$S_N''(T) = \left[\left(S_{N+1} - 2S_N + S_{N-1}\right)\left\{1 - A_P\left(S_{N+1} - S_{N-1}\right)\right\}\right] \ . \tag{6.17}$$

The above is the equation of motion for a nonlinear chain with parabolic interaction force law given by equation (3.10). Equation (6.17) is completely in nondimensional form. We assume for the present that A_P, denoting the nonlinearity of the chain, is a very small quantity, i.e., $A_P << 1$. This assumption implies that equation (6.17) should have many properties in common with the linear chain of the previous section. Let us look for periodic solutions of the form,

$$S_N(T) = \text{constant} \cdot \exp\{-i(QN - WT)\} . \tag{6.18}$$

Substituting this in equation (6.17), we get

$$S_N''(T) = [(e^{-iQ} - 2 + e^{+iQ}) \cdot S_N \cdot \{1 - A_P \cdot (e^{-iQ} - e^{+iQ}) \cdot S_N\}] \tag{6.19}$$

or

$$S_N''(T) = (e^{-iQ} - 2 + e^{+iQ}) \cdot S_N - A_P \cdot (e^{-iQ} - e^{+iQ}) (e^{-iQ} - 2 + e^{+iQ}) \cdot S_N^2 . \tag{6.20}$$

Let us keep the wave number constant for analysis and study the dependence of frequency upon it. Define two constants as follows:

$$(e^{-iQ} - 2 + e^{+iQ}) = - a = \text{constant} \tag{6.21}$$

and

$$A_P \cdot (e^{-iQ} - e^{+iQ}) (-a) = b = \text{a small constant} . \tag{6.22}$$

With the use of the above relations, equation (6.20) becomes

$$S_N''(T) + a S_N + b S_N^2 = 0 . \tag{6.23}$$

This equation represents an anharmonic oscillator. Let

$$S_N(T) = S_{N,0}(T) + b S_{N,1}(T) + b^2 S_{N,2}(T) + - - - \tag{6.24}$$

and

$$a = W^2 + b W_1^2 + b^2 W_2^2 + - - - . \tag{6.25}$$

In equation (6.24) $S_{N,0}$, $S_{N,1}$, etc. represent perturbed values [48]. The value of b is small. If b = 0, then equation (6.23) is the motion of a harmonic oscillator of frequency W. This explains the motivation for expanding a as in equation (6.25). In reference [48] a nonlinear oscillator problem represented by equation (6.23) is solved by a perturbation technique using equations analogous to equations (6.24) and (6.25) and with initial conditions for S_N of the form $S_N(0) = A$ and $S_N'(0) = 0$. We quote below the results appropriate for our work. The perturbed S_N to the second order in b are given by

$$S_{N,0}(T) = A \cos(WT) \ ,$$

$$S_{N,1}(T) = \frac{A^2}{W^2} [- 1/2 + 1/3 \cos(WT) + 1/6 \cos(2WT)] \ ,$$

$$S_{N,2}(T) = \frac{A^3}{3W^4} [- 1 + \frac{29}{48} \cos(WT) +$$

$$1/3 \cos(2WT) + 1/16 \cos(3WT)] \ . \qquad (6.26)$$

Similarly, the perturbed frequencies up to second order in b are

$$W_1 = 0 \ ,$$

$$W_2 = \frac{5A^2}{6W^2} \ . \qquad (6.27)$$

The solution for $S_N(T)$ to second order in b for the prescribed initial condition is obtained by substitution of equations (6.26) into (6.24). From equation (6.25) and equation (6.27) we get, to second order in b, the relation

$$W^2 = a - \frac{5A^2b^2}{6W^2} \ . \qquad (6.28)$$

If $a >> \frac{5b^2A^2}{6W^2}$, we obtain from the above

$$W \simeq \sqrt{a}\ [1 - \frac{5b^2A^2}{12a^2}] \ . \tag{6.29}$$

Substituting the expressions for a and b into equation (6.29) from equations (6.21) and (6.22) yields

$$W \simeq 2 \cdot |\sin(Q/2)| \cdot [1 + 5/12 \cdot A^2 \cdot (4A_p^2 \sin^2 Q)] \ . \tag{6.30}$$

If there is no nonlinearity in the chain, then $A_p = 0$ and the above equation reduces to the nondimensional frequency dispersion equation of a linear chain given by equation (6.15). From equation (6.30) we see that in a nonlinear chain, the frequency depends on both the wave number and the wave amplitude. It further follows that frequency increases with increase in either amplitude of the wave or nonlinearity of the chain. This is a very interesting result. The increase in frequency of oscillations with increase in amplitude is just the opposite of a single nonlinear oscillator described by equation (6.23). In such a single oscillator the frequency decreases with increase in amplitude [48].

In a nonlinear chain we are concerned with the frequency dispersion, given by the first part of equation (6.30) and, secondly, with the dispersion due to variation in amplitude of the wave denoted as "amplitude dispersion" [49]. In a nonlinear dispersive system, there is the influence of both "frequency dispersion" and "amplitude dispersion."

Equation (6.30) explains the reasons for our observing higher frequency oscillations in the computer results of Chapter V when the amplitude of u_1 or nonlinearity of the lattice was increased. Lighthill [49] has shown

that in a nonlinear dispersive dynamic system exhibiting both "frequency" and "amplitude" dispersion, small changes in, for example, wave length are in general propagated through the wave train at different group speeds, so that the region influenced by changes increases linearly with time.

CHAPTER VII

FINITE AMPLITUDE WAVES IN LINEAR AND NONLINEAR CHAINS

In this chapter we shall study finite amplitude wave propagation in linear and nonlinear chains. It is possible to obtain exact analytic solutions for the linear case. We propose to extend the method of this case to the nonlinear lattice model under study and obtain approximate analytic solutions to compare with computer results.

Finite Strain Wave in a Linear Chain

In Chapter VI it was shown that elementary solutions of the equation of motion can represented as travelling waves. For the linear case these can, in principle, be superposed to satisfy any initial and boundary conditions. In practice, however, the superposition of such waves to satisfy arbitrary initial and boundary conditions poses formidable mathematical difficulties. An alternative procedure has been provided by Schrodinger [50], who developed a set of elementary solutions for initial disturbance of a single particle. We reproduce here his basic idea.

Starting from equation (6.2), we set

$$y_{2N} = \sqrt{m}\,\dot{s}_N;\quad y_{2N+1} = \sqrt{K}(s_N - s_{N+1});\quad r = 2\omega_1 t\ . \tag{7.1}$$

Let us rewrite equation (6.2) as

$$2m\omega_1 \frac{d\dot{s}_N}{dr} = -\sqrt{K}\,[\sqrt{K}(s_N - s_{N+1}) - \sqrt{K}(s_{N-1} - s_N)]\ , \tag{7.2}$$

where $\dot{s}_N = ds_N/dt$. Using the relations of equation (7.1) in (7.2), we obtain

$$\frac{dy_{2N}}{dr} = 1/2\ (y_{2N-1} - y_{2N+1}) \ . \tag{7.3}$$

Differentiating the second relation of equation (7.1) with respect to r and using the first relation of the same equation, one obtains

$$\frac{dy_{2N+1}}{dr} = 1/2\ (y_{2N} - y_{2N+2}) \ . \tag{7.4}$$

Hence, for both even and odd subscripts, the y's obey

$$\frac{dy_N}{dr} = 1/2\ (y_{N-1} - y_{N+1}) \ . \tag{7.5}$$

This is precisely one of the recursion formulae satisfied by cylindrical functions [51]. The solution must remain finite for all real values of r, so we choose Bessel functions of the first kind $J_L(r)$. The general solutions of equation (7.5) will then be given by

$$y_N(r) = \sum_{L=-\infty}^{L=+\infty} J_{N-L}(r)\ y_L^{\circ} \ , \tag{7.6}$$

where y_L° is the initial value of y_L; this follows from the relation $J_{N-L}(o) = \delta_{NL}$.

Transforming back to the original variables [46], the solution for the motion of the N-th particle is

$$s_N(t) = \sum_{L=-\infty}^{L=+\infty} [s_L(o)\ J_{2N-2L}\ (2\omega_1 t) + \dot{s}_L(o) \int_o^t J_{2N-2L}\ (2\omega_1 t)dt] \ . \tag{7.7}$$

Next, we shall study an interesting case where all particles initially zero velocities, $\dot{s}_L(o) = 0$, then from equation (7.7) we get

$$s_N(t) = \sum_{L=-\infty}^{L=+\infty} s_L(o)\, J_{2N-2L}(2\omega_1 t) \; . \tag{7.8}$$

We rewrite the above equation in a nondimensional form for use in our work by defining

$$\frac{s_N}{d_1} \equiv S_N, \text{ and } \omega_1 t \equiv T \; ; \tag{7.9}$$

then

$$S_N(T) = \sum_{L=-\infty}^{L=+\infty} S_L(o)\, J_{2N-2L}(2T) \; . \tag{7.10}$$

Now let us imagine a purely artificial case wherein the infinite chain the particles from $L = -\infty$ to $L = 0$ are displaced initially as shown in Fig. 16. This corresponds to uniform strain conditions on the left-hand side of the chain following the definition of strain from equation (5.1). At nondimensional time $T = 0$ the particles are released. This is analogous to the physical case of a shock tube in which the diaphragm is broken at zero time.

We require

$$S_{L-1}(o) - S_L(o) = \varepsilon, \text{ for } L = -\infty \text{ to } L = 0$$

$$S_L(o) = 0, \text{ for } L = 0 \text{ to } L = +\infty \; . \tag{7.11}$$

Therefore, we get from above

$$S_L(o) = (-L) \cdot \varepsilon \text{ for } L = -\infty \text{ to } L = 0 \ . \qquad (7.11a)$$

With the use of the above initial condition equation (7.10) becomes

$$S_N(T) = \sum_{L=-\infty}^{L=0} (-L) \cdot \varepsilon \cdot J_{2N-2L}(2T)$$

$$= \varepsilon \cdot \sum_{M=0}^{\infty} (M)\, J_{2(M+N)}(2T) \ . \qquad (7.12)$$

To study the behavior of the above solution, let us check the strain in the link $(0 \leftrightarrow 1)$ connecting N = 0 and N = +1. From equation (7.12) we have

$$S_o(T) = \varepsilon \cdot \sum_{M=0}^{\infty} (M)\, J_{2M}(2T) \qquad (7.13)$$

and

$$S_1(T) = \varepsilon \cdot \sum_{M=0}^{\infty} (M)\, J_{2M+2}(2T) \ . \qquad (7.14)$$

The strain in the link $(0 \leftrightarrow 1)$ is

$$S_o(T) - S_1(T) = \varepsilon \cdot \left[\sum_{M=0}^{\infty} M \cdot J_{2M}(2T) - \sum_{M=0}^{\infty} M \cdot J_{2M+2}(2T)\right] \ . \qquad (7.15)$$

Putting P = M + 1 in the second sum on the right-hand side, we get

$$S_o(T) - S_1(T) = \varepsilon \cdot \left[\sum_{M=0}^{\infty} M \cdot J_{2M}(2T) - \sum_{P=1}^{\infty} (P-1) \cdot J_{2P}(2T)\right] \ . \qquad (7.16)$$

Simplifying the sum on the right-hand side, we get

$$S_o(T) - S_1(T) = \varepsilon/2 \cdot [2 \cdot \sum_{P=1}^{\infty} J_{2P}(2T)] \ . \qquad (7.17)$$

The generating function of unity in terms of Bessel's function is given by [52] as

$$1 = J_o(2T) + 2 \cdot \sum_{P=1}^{\infty} J_{2P}(2T) \ . \qquad (7.18)$$

Using this in equation (7.17), we get

$$S_o(T) - S_1(T) = \varepsilon/2 \cdot [1 - J_o(2T)] \ . \qquad (7.19)$$

This equation shows that the strain in the link $(0 \leftrightarrow 1)$ is initially zero since $J_o(0) = 1$, and from the asymptotic behavior of Bessel functions, it can be seen that ultimately this strain oscillates about a mean value $\varepsilon/2$ sinusoidally with an amplitude that decreases as $1/\sqrt{T}$. Hence, as $T \to \infty$,

$$S_o(T) - S_1(T) \to \varepsilon/2 = \text{constant} \ . \qquad (7.20)$$

This value is half the initial strain on the left-hand side of the chain. Hence, a forward facing wave propagates in the right-hand side of the chain creating a strain of $\varepsilon/2$.

Let us determine the strain in the link $(-1 \leftrightarrow 0)$ joining $N = -1$ and $N = 0$. From equation (7.10) we obtain

$$S_{-1}(T) - S_o(T) = \varepsilon \cdot [\sum_{M=0}^{\infty} M \cdot J_{2M-2}(2T) - \sum_{M=0}^{\infty} M \cdot J_{2M}(2T)] \ . \qquad (7.21)$$

Simplifying the above equation along the lines previously outlined and using

once more the identity of equation (7.18), we get

$$S_{-1}(T) - S_o(T) = \varepsilon/2 \cdot [1 + J_o(2T)] \ . \qquad (7.22)$$

Initially at T = 0, the strain in the link ($-1 \leftrightarrow 0$) is ε, and for large times the strain approaches asymptotically $\varepsilon/2$. Hence, in the left-hand side of the chain we have a backward facing rarefaction wave relieving the strain from ε to $\varepsilon/2$. The analogy with the shock tube [53] is apparent.

For this infinite linear lattice we have seen that, starting from a uniform state, the subsequent motion was oscillatory; but for theoretically infinite times, again an essentially uniform state resulted. We did not have any dissipation in the system to achieve this. The dynamics of the lattice is responsible for decay of the amplitude of oscillations with time.

Shock in a Linear Lattice with No Dissipation

The solution obtained in the previous section for an infinite lattice for a finite amplitude strain wave showed that the dynamics of the linear lattice is responsible for decay of oscillations with time in spite of absence of dissipation. However, our lattice model is semi-infinite and has a special boundary condition of velocity step u_1 applied to the free surface. In this section we shall obtain an exact solution for such a model with linear forces and no dissipation.

The nondimensional equation of motion for a nondissipating linear lattice is obtained by setting A_P and η both equal to zero in equation (3.36). Hence, we have

$$S_N''(T) = S_{N+1} - 2S_N + S_{N-1} \text{ for } N \geq 2 \ . \qquad (7.23)$$

We seek a solution to the above equation with the initial conditions

$$S_N(0) = 0 \text{ and } S_N'(0) = 0 \text{ for all } N \geq 2 . \tag{7.24}$$

The boundary condition for N = 1 is

$$S_1'(T) = u_1 \cdot H(T) , \tag{7.25}$$

where H(T) is the Heaviside function,

$$H(T) = 0, \; T < 0$$

$$= 1, \; T > 0 . \tag{7.26}$$

The velocity step applied at the mass point N = 1 produces a compressive wave which we shall call a shock even though the wave front does not exhibit the stability expected of a real shock wave.

In the previous section we saw that a travelling wave solution of equation (7.23) can be obtained in terms of Bessel functions of the first kind. It can be easily shown that an elementary solution of the form

$$S_N(T) = \text{constant} \cdot J_{2(N-1)+L}(2T) = \text{constant} \cdot J_M(2T) , \tag{7.27}$$

satisfies equation (7.23). The following recursion relations are required [51,52]:

$$2J_M'(x) = J_{M-1}(x) - J_{M+1}(x) \tag{7.28}$$

and

$$4J_M''(x) = J_{M+2}(x) - 2J_M(x) + J_{M-2}(x) . \tag{7.29}$$

To satisfy the boundary and initial conditions, constants have to be fixed and solutions superposed. This is allowed for the linear problem. A superposed solution of the type given in equation (7.31) satisfies equation (7.23) and the particular boundary condition under consideration; i.e.,

$$S_1(T) = u_1 \cdot T \text{ for } T \geq 0 \ . \tag{7.30}$$

The solution is

$$S_N(T) = u_1 \cdot \sum_{K=0}^{\infty} (2K + 1)\ J_{2(N-1)+2K+1}(2T)$$

$$\text{for } N \geq 1 \text{ and } T \geq 0 \ . \tag{7.31}$$

To check if the boundary condition (7.30) is satisfied, we substitute $N = 1$ in the above to get

$$S_1(T) = u_1 \cdot \sum_{K=0}^{\infty} (2K + 1)\ J_{2K+1}(2T) = 1/2\ (2T) \cdot u_1 = u_1 T \ . \tag{7.32}$$

In the above equation we have made use of the identity [54],

$$\sum_{K=0}^{\infty} (2K + 1)\ J_{2K+1}(x) = (1/2)\, x \ . \tag{7.33}$$

The solution (7.31) also satisfies the initial conditions of equation (7.24) because, for $N \geq 2$ and $K \geq 0$, we have

$$2(N - 1) + 2K + 1 \geq 3,\ 2N + 2K - 2 \geq 2,\ 2N + 2K \geq 4 \ ;$$

and equations (7.31) and its derivative are zero at $T = 0$ since

$$J_L(0) = 0 \text{ for } L > 0 \ . \tag{7.34}$$

It is shown in Appendix A, equation (A4), that solution (7.31) when substituted in equation (7.23) leads to the form

$$S_N''(T) = 2u_1 \cdot (N - 1)/T \cdot J_{2(N-1)}(2T) \text{ for } N \geq 2 \ . \tag{7.35}$$

Therefore, the velocity profile is given by

$$S_N'(T) = u_{NP}(T) = 2u_1 \cdot (N - 1) \cdot \int_0^T 1/y \cdot J_{2(N-1)}(2y) \cdot dy \ . \tag{7.36}$$

Displacement from equilibrium is obtained from another integration of the above equation.

Equation (7.35) is illustrated in Fig. 17 along with the values obtained from numerical integration of equation (7.23) for the specified boundary and initial conditions. We note the following two effects:

1. Peak amplitude of acceleration decreases with travel distance.
2. Acceleration of each particle decreases with time after first peak. This follows from the asymptotic behavior of Bessel functions, $| J_{2(N-1)}(2T) | < 1/\sqrt{2T}$ for large times T and hence, the acceleration of the N-th mass point

$$| S_N''(T) | < (\text{constant})/T^{3/2} \text{ for large times} \ . \tag{7.37}$$

Theoretically, the mass point has a zero acceleration for $T \to \infty$. Hence, even in this case we have demonstrated that the dynamics of the lattice is responsible for the decay of oscillations with time, in spite of the absence of dissipation.

We mentioned before in Chapter IV that there are two questions of concern in the numerical integration scheme: (1) convergence of the process to correct, i.e., analytic, values; and (2) stability of the procedure for the selected time step T. The close agreement of the numerical and analytic solutions shown in Fig. 17 satisfies us that both of these questions are answered favorably.

For large order L, the Bessel functions $J_L(x)$ will be zero essentially until the argument equals the order [54]. From equation (7.37) we see that

$$S_N''(T) \tilde{} 0 \text{ until } 2T \tilde{} 2\,(N - 1)\ . \qquad (7.38)$$

Since the nondimensional distance of the N-th mass point from the free surface is (N - 1), the relation in equation (7.38) indicates that the average velocity of propagation of the disturbance is $\bar{U}_s \tilde{} 1$ in the linear lattice. We have nondimensionalized all velocities with respect to the Newtonian sound speed in a lattice, i.e., $(\omega_1 d_1)$. In the previous chapter this was found to be propagation speed for infinitely long waves corresponding to the low frequency limit. The conclusion is that the leading disturbance propagates at an average velocity equal to Newtonian sound speed in a linear lattice no matter what the amplitude of the disturbance.

Shock in a Nonlinear Lattice with No Dissipation

In the previous sections it was found possible to obtain the solution of a general type of motion by superposition of elementary solutions because of the linearity of the differential-difference equation. When the force of interaction is no longer linear, as in equation (6.17), such superposition is no longer possible. By using a special transformation Toda [55] obtained solutions for vibrations of a nonlinear chain for a particular type of

interaction and particular initial conditions. A complete solution satisfying an arbitrary initial and boundary conditions cannot be obtained from his method.

For the present the only possible approaches seem to be numerical integration and approximate analytic techniques such as time averaging [56]. In this section we propose to extend the analysis of the previous section to the nonlinear problem.

Our lattice model, when nonlinear and in the absence of dissipation, can be represented by an equation of the form

$$S_N''(T) = [(S_{N+1} - 2S_N + S_{N-1}) \{1 - \alpha (S_{N+1} - S_{N-1})\}] , \qquad (7.39)$$

where $\alpha = A_P$ is the case of parabolic interaction, i.e., equation (6.17), and $\alpha = \frac{3A_M}{2}$ for approximate Morse-law interaction, equation (3.52), when displacements are assumed to be small. If $\alpha = 0$, equation (7.39) is the linear lattice of the previous section. We are seeking the solution to equation (7.39) for the initial conditions of equation (7.24) and the boundary condition of equation (7.25) or (7.30).

We rewrite equation (7.39) as

$$\frac{S_N''(T)}{(S_{N+1} - 2S_N + S_{N-1})} = 1 - \alpha (S_{N+1} - S_{N-1}) . \qquad (7.40)$$

If α is very small, then the behavior of the above equation is expected to be analogous to that of equation (7.23), as illustrated in equation (7.31). The expression on the right-hand side of equation (7.40) is a function of mass point N and time T. We define

$$\sigma (N, T) \equiv 1 - \alpha (S_{N+1} - S_{N-1}) , \qquad (7.41)$$

and illustrate this function in Fig. 18 for a particular case. Until the arrival of the disturbance at the (N-1)-th mass point, both the displacements S_{N+1} and S_{N-1} are zero and hence, the value of σ (N, T) equals unity.

Our numerical results in Chapter V showed that the disturbance or shock propagates at a uniform average velocity denoted as $\overline{U}_s$. For times greater than the time of arrival of the disturbance at the (N-1)-th mass point, the value of σ (N, T) oscillates about a mean value greater than unity since

$$\sigma\ (N,\ T) = 1 - \alpha\ (S_{N+1} - S_N)$$

$$= 1 - \alpha\ [(S_{N+1} - S_N) + (S_N - S_{N-1})]\ . \qquad (7.42)$$

$(S_{N+1} - S_N)$ and $(S_N - S_{N-1})$ represent strain in the lattice. At equilibrium $S_{N-1} > S_N > S_{N+1}$. Hence, for the shock σ (N, T) > 1. In the present study numerical results show this to be true.

From the previous chapters, we have seen that essentially equilibrium states are attained in the lattice after a long time and far behind the shock front. To get an approximate solution to equation (7.40), we take advantage of this state of equilibrium by writing the following for the asumptotic value of σ(N, T):

$$\sigma^*(N) \cong 1 + 2\,\alpha \cdot (\text{final equilibrium strain}),\ T \to \infty\ . \qquad (7.43)$$

In Chapter V we saw that the application of Rankine-Hugoniot jump conditions (see Table 5) gave the equilibrium values in the lattice model with a small percentage error. The shock speed to be used is the average shock speed $\overline{U}_s$. From equations (5.1) and (5.7) we get

$$\text{final equilibrium strain} = 1 - (\rho o/\rho) = \frac{u_1}{\overline{U}_s}\ . \qquad (7.44)$$

Therefore,

$$\sigma^*(N) \cong 1 + 2\alpha \cdot \frac{u_1}{U_s} = B^2 = \text{constant} . \tag{7.45}$$

Next we assume that instead of a time dependent function, $\sigma(N, T)$, we can substitute the asymptotic value $\sigma^*(N)$ from equation (7.45) in equation (7.40) to obtain an approximate analytic solution. The assumption is

$$\sigma(N, T) = 1, \text{ for } T < T_N$$

$$= \sigma^*(N) = B^2, \text{ for } T > T_N ,$$

$$\text{where } T_N = (N - 1)/\overline{U}_s . \tag{7.46}$$

Figure 18 explains the assumption. Until time $T = T_N$, the value of $\sigma(N, T)$ is unity and at $T = T_N$ it jumps to $\sigma^*(N)$ = constant. We are, therefore, led to replace equation (7.40) with two approximate linear equations;

$$\frac{S_N''(T)}{(S_{N+1} - 2S_N + S_{N-1})} = 1, \text{ for } T < T_N \tag{7.47}$$

and

$$\frac{S_N''(T)}{(S_{N+1} - 2S_N + S_{N-1})} = \sigma^*(N) = B^2, \text{ for } T > T_N . \tag{7.48}$$

The initial and boundary conditions, i.e., equations (7.24) and (7.30), remain the same for the differential-difference equation (7.47), whereas the initial conditions for equation (7.48) are provided by the solution of equation (7.47) at time $T = T_N$. The boundary condition (7.30) remains the same. We denote the solution of equation (7.47) by $S_{N,1}(T)$ and that of equation (7.48)

by $S_{N,2}(T)$. The continuity of displacement and velocity at T_N implies

$$S_{N,1}(T_N) = S_{N,2}(T_N) \tag{7.49}$$

and

$$S'_{N,1}(T_N) = S'_{N,2}(T_N) \ . \tag{7.50}$$

We note that the situation represented by equation (7.48) is that of replacing the spring in equation (7.47) with a stiffer spring of stiffness B^2 times the original.

The solution of equation (7.47) was obtained in the previous section; and for time $T \leq T_N$ the analytic solution is equation (7.31). From equation (7.48) we have

$$\frac{d^2S_N}{dT^2} / (S_{N+1} - 2S_N + S_{N-1}) = B^2 \ . \tag{7.48a}$$

Let us define a new variable;

$$Z = BT \ . \tag{7.51}$$

Using the new variable, equation (7.48a) becomes

$$\frac{d^2S_N}{dZ^2} = S_{N+1} - 2S_N + S_{N-1} \ . \tag{7.52}$$

We can write the general solution of equation (7.52) in terms of Bessel functions. This follows from our previous work. The solution for $T \geq T_N$ is

$$S_{N,2}(T) = \sum_{K=0}^{\infty} A_K J_{2(N-1)+2K+1}(2BT) + \sum_{K=0}^{\infty} B_K Y_{2(N-1)+2K+1}(2BT) , \quad (7.53)$$

where A_K and B_K are constants dependent upon the summation index K and Y_N is the Bessel function of second kind [54]. Constants A_K and B_K are to be evaluated with the use of continuity requirements of equations (7.49), (7.50), and the solution (7.31) at $T = T_N$. However, there is a simpler way to obtain these constants by studying the behavior of Bessel functions at $T = T_N$.

From equation (7.46) T_N is of the order of $(N - 1)$ and B is of order 1. Hence, $(2BT_N) < 2(N - 1) + 2K + 1$ for $K \geq 0$. The Bessel functions $Y_L(x)$ are very large when the argument is less than the order [52]. Therefore, to satisfy our requirement that for all N the displacement be finite, the constant B_K should be zero for all $K \geq 0$. In addition, the solution (7.53) is required to satisfy the boundary condition (7.30) which fixes the constant A_K as

$$A_K = u_1 (2K + 1)/B . \quad (7.54)$$

Hence, the solution to equation (7.48) is obtained as

$$S_{N,2}(T) = (u_1/B) \cdot \sum_{K=0}^{\infty} (2K+1) J_{2(N-1)+2K+1}(2BT) \text{ for } N \geq 1, T \geq T_N . \quad (7.55)$$

Because of the choice of constants B_K equal to zero, we need only use one continuity condition; i.e., equation (7.49) for displacement at $T = T_N$. Hence, from equations (7.31), (7.49), and (7.55), we require

$$u_1 \cdot \sum_{K=0}^{\infty} (2K + 1)\, J_{2(N-1)+2K+1}(2T_N) = (u_1/B) \cdot \sum_{K=0}^{\infty} (2K + 1) \cdot J_{2(N-1)+2K+1}(2BT_N) ,$$

$$\text{for } N \geq 1 . \qquad (7.56)$$

Equation (7.56) is an interesting identity to determine T_N as a function of B. The necessary mathematics is quite complicated. In the present study we have used the average shock velocity $\bar{U}_s$ to compute B from equation (7.45) and T_N from equation (7.46). With such a procedure we have checked the identity in equation (7.56) for N = 1 and N = 2, and are satisfied that equation (7.56) is the solution to equation (7.48).

From equation (7.55) we obtain

$$S''_{N,2}(T) = \frac{2u_1(N - 1)}{T} \cdot J_{2(N-1}(2BT), \text{ for } N \geq 2,\ T \geq T_N . \qquad (7.57)$$

The velocity profile is, therefore, given by

$$S'_N(T) = 2u_1(N - 1) \cdot \int_{T_N}^{T} 1/y \cdot J_{2(N-1)}(2By)\, dy . \qquad (7.58)$$

By one more integration we obtain the displacement from equilibrium of the N-th mass point.

The average shock velocity $\bar{U}_s$, appearing in equation (7.45) for computing the constant B, is obtained from equations (5.7) and (5.8) as

$$\bar{U}_s \approx \sqrt{1 + \alpha\, (u_1/\bar{U}_s)} . \qquad (7.59)$$

We have used the approximate identity in the above equation because of the presence of a small percentage error (2-6%) between the lattice model and jump condition calculations as shown in Table 5.

Equation (7.57) is illustrated in Fig. 19 for parabolic interaction where $\alpha = 1$ and $u_1 = 0.1$, along with the numerical solution of equation (7.40) for the condition $u_1 = 0.1$ which corresponds to a 100-kilobar shock in aluminum.

We have to note that at $T = T_N$ there will be a jump in acceleration of the mass point because of the jump in σ (N, T). The continuity requirements of equations (7.49) and (7.50) were for displacement and velocity only.

We have also shown the solution (7.35) in Fig. 19 valid for time $T < T_N$. The dotted line is for the jump in the solution at $T = T_N$. From Fig. 19 we see that the assumptions made to obtain the approximate solution are reasonable. The approximate analytic solution shows a behavior analogous to the numerical solution. It yields a solution which has about the same period as the numerical solution, but which is of different amplitude; the most important result is the decay of oscillations in Fig. 19.

From the asymptotic behavior of Bessel functions and equation (7.55) we see that the approximate analytic solution predicts that the mass point N will have an acceleration which is oscillatory, but the amplitude of these oscillations decrease as in the linear case; i.e.,

$$|S_N''(T)| < \frac{\text{constant}}{T^{3/2}}, \quad T \to \infty . \tag{7.37}$$

In view of the similarity of numerical solution and approximate analytic solution, we are led to believe that the decay of oscillations found from numerical integration of equation (7.40) is the result of dispersion and is not due to any externally introduced pseudo-viscosity of the integration scheme.

Shock in a Dissipating Nonlinear Lattice "Steady Profile"

In the presence of dissipation our lattice model has for its equation of motion

$$S_N''(T) = [(S_{N+1} - 2S_N + S_{N-1}) \{1 - \alpha (S_{N+1} - S_{N-1})\}] + \eta (S'_{N+1} - 2S'_N + S'_{N-1}) . \quad (7.60)$$

The numerical results of Chapter V suggested the set of recurrence relations;

$$S_{N+1}(T) = S_N(T - \theta)$$

and

$$S_{N-1}(T) = S_N(T + \theta) . \quad (5.5a)$$

The parameter θ for steady state conditions was defined in equation (5.6).

Expanding the expressions in equation (5.5a) in Taylor series [18] and retaining terms only up to third order in θ, we get

$$S_N(T - \theta) \cong S_N(T) - \theta \cdot S'_N(T) + \theta^2/2 \cdot S''_N(T) - 1/6 \cdot \theta^3 \cdot S'''_N(T) + - - - \quad (7.61)$$

and

$$S_N(T + \theta) \cong S_N(T) + \theta \cdot S'_N(T) + \theta^2/2 \cdot S''_N(T) + 1/6 \cdot \theta^3 \cdot S'''_N(T) + - - - . \quad (7.62)$$

It is assumed in the above expansions that the higher derivatives of $S_N(T)$ are negligible. Since $\theta < 1$, this implies rapid convergence. With these expansions we get

$$S_{N+1} - 2S_N + S_{N-1} \cong \theta^2 \cdot S_N''(T) \ , \tag{7.62}$$

$$\{1 - \alpha(S_{N+1} - S_{N-1})\} \cong \{1 + 2 \cdot \alpha \cdot \theta[S_N'(T) + 1/6 \cdot \theta^2 \cdot S_N'''(T)]\} \ , \tag{7.63}$$

and

$$\eta \cdot d/dT \ (S_{N+1} - 2S_N + S_{N-1}) \cong \eta \cdot \theta^2 \cdot S_N'''(T) \ . \tag{7.64}$$

Substitution of equations (7.62), (7.63), and (7.64) into the equation of motion (7.60) gives

$$S_N''(T) \cong [\theta^2 \cdot S_N''(T) \{1 + 2\alpha\theta [S_N'(T) + 1/6 \cdot \theta^2 \cdot S_N'''(T)\}] + \eta \cdot \theta^2 \cdot S_N'''(T) \ . \tag{7.65}$$

Rearranging, we get

$$S_N''(T) \cong [\theta^2 \cdot S_N''(T) + 2\alpha\theta^3 \cdot S_N'(T) \cdot S_N''(T) + \eta \cdot \theta^2 \cdot S_N'''(T)] + 1/3 \cdot \alpha \cdot \theta^5 \cdot S_N''(T) \cdot S_N'''(T) \ . \tag{7.66}$$

Since derivatives of $S_N(T)$ are assumed to be small, the last term on the right-hand side of the above equation is of higher order than the rest and is henceforth neglected. Equation (7.66) becomes, after rearrangement of terms,

$$\eta \cdot \theta^2 \cdot S_N'''(T) + 2 \cdot \alpha \cdot \theta^3 \cdot S_N'(T) \cdot S_N''(T) - (1 - \theta^2) \cdot S_N''(T) = 0 \ . \tag{7.67}$$

We define the following:

$$\eta \cdot \theta^2 \equiv a$$

$$2 \cdot \alpha \cdot \theta^3 \equiv b$$

$$(1 - \theta^2) \equiv g \tag{7.68}$$

and

$$S_N'(T) \equiv u(T) \ . \tag{7.69}$$

With the use of the above relations equation (7.67) becomes

$$a \frac{d^2u}{dT^2} + b\, u \frac{du}{dT} - g \frac{du}{dT} = 0 \ . \tag{7.70}$$

Integrating once with respect to T, the above gives

$$a \frac{du}{dT} + \frac{b}{2} u^2 - gu = d \ , \tag{7.71}$$

where d is an integration constant. At time $T = -\infty$ the mass points are all at rest; hence, $u = 0$ and $\frac{du}{dT} = 0$. Substitution of these conditions into equation (7.71) gives $d = 0$. Hence, from equation (7.71)

$$a \frac{du}{dT} + \frac{b}{2} u^2 - gu = 0 \ . \tag{7.72}$$

The boundary conditions for this equation are

$$u = 0, \text{ at } T = -\infty$$

$$u = u_1, \text{ at } T = +\infty \ . \tag{7.73}$$

Let us, for convenience, denote by T_N the time at which the N-th mass point attains half the final equilibrium velocity, i.e., $u = u_1/2$ at $T = T_N$

for mass point N. This is illustrated in Fig. 20. We assume that the shock arrives at the N-th mass point at this time $T = T_N$. The same convention is adopted for all the mass points. If U_s denotes the steady shock velocity, then

$$T_N \equiv (N - 1)/U_s \ , \tag{7.74}$$

where (N - 1) is the nondimensional initial equilibrium position of the N-th mass point.

Equation (7.72) is integrated between $T = T_N$ and T to obtain the velocity profile as

$$u = \frac{u_1 g \cdot \exp\{g/a \cdot (T - T_N)\}}{[2c - b/2 \cdot u_1 \cdot (1 - \exp\{g/a\ (T - T_N)\})]} \ . \tag{7.75}$$

We can simplify the above expression by noting that as $T \to \infty$, we require $u = u_1$. Hence, from the above at $T = \infty$,

$$u_1 = \frac{u_1 g}{b/2 \cdot u_1} = \frac{2g}{b} \ . \tag{7.76}$$

With the use of this relation equation (7.75) simplifies to

$$u = u_1 \cdot [1 + \exp\{- g/a \cdot (T - T_N)\}]^{-1} \ ,$$

$$= u_1/2 \cdot [1 - \tanh\{- g/2a \cdot (T - T_N)\}] \ . \tag{7.77}$$

Solution (7.77) satisfies the requirements that at $T = + \infty$, $u = u_1$, and at $T = - \infty$, $u = 0$. At $T = T_N$, $u = u_1/2$. Substitution of T_N from equation (7.74) into (7.77) gives

$$u = \frac{u_1}{2} \cdot [1 - \tanh \{\frac{g}{2a\ U_s} \cdot \left| (N - 1) - U_s T \right| \}] \ . \qquad (7.78)$$

If we consider the initial position (N - 1) of the N-th mass point as the Lagrangian coordinate h, then from the above,

$$u = \frac{u_1}{2} \cdot [1 - \tanh \{\frac{g}{2a\ U_s} \cdot (h - U_s\ T)\}] \ . \qquad (7.79)$$

This is the steady state profile.

It is interesting to compare the above equation with equation (2.43) in Chapter II. Equation (2.43) gives the velocity profile in a continuum described by the constitutive relation of equation (2.26). Equation (7.79) is nondimensional whereas equation (2.43) is not. When equation (7.79) is put in the units of equation (2.43) by the use of equations (2.46) and (6.1), the following relation is obtained, if the two profiles are assumed to be identical:

$$\left[\frac{Cu_1}{2Ru^2}\right]_{\text{Continuum}} = \left[\frac{g \cdot \omega_1}{2a\ U}\right]_{\text{Lattice Model}} \ . \qquad (7.80)$$

If shock velocity in the continuum is equal to that in the lattice model, we obtain from the above

$$R\big|_{\text{Continuum}} = \text{viscosity}\big|_{\text{Continuum}} = (C \cdot u_1/U)_{\text{Continuum}} \cdot (a/g\ \omega_1)_{\text{Lattice Model}} \ . \qquad (7.81)$$

Equation (7.81) will be employed in Appendix B to calculate the viscosity of aluminum. For the present we point out the units of parameters appearing in equation (7.81); the units are:

R in poises (dyne-sec/cm^2), C in dynes/cm^2, u_1 and U in cm/μsec, ω_1 in sec^{-1}, and a and g are nondimensional quantities described in equation (7.68).

From equations (7.76) and (7.68) we get

$$u_1 = \frac{2g}{b} = \frac{2(1 - \theta^2)}{2\alpha\ \theta^3} = \frac{(1 - \theta^2)}{\alpha\theta^3} \tag{7.82}$$

or

$$\theta^2(u_1\ \alpha\ \theta + 1) = 1\ . \tag{7.83}$$

From the above relation and equation (5.6) we get

$$U_s^2 = 1 + \frac{u_1 \cdot \alpha}{U_s}\ , \tag{7.84}$$

a relation obtainable by direct application of the jump conditions for determining the shock velocity [equation (7.59)]. In the presence of damping the average shock velocity $\overline{U}_s$ becomes the steady state shock velocity U_s as previously noted (Chapter V).

By comparison of equation (7.83) and equation (2.47) we see that in a steady state, equation (7.83) is the lattice analog of equation (2.47) for the continuum.

We have illustrated equation (7.77) for two cases in Fig. 20 and 21. The agreement between the derived analytic solution of the profile and the numerical solution of Chapter V is quite satisfactory for values of $\eta > \eta^*$.

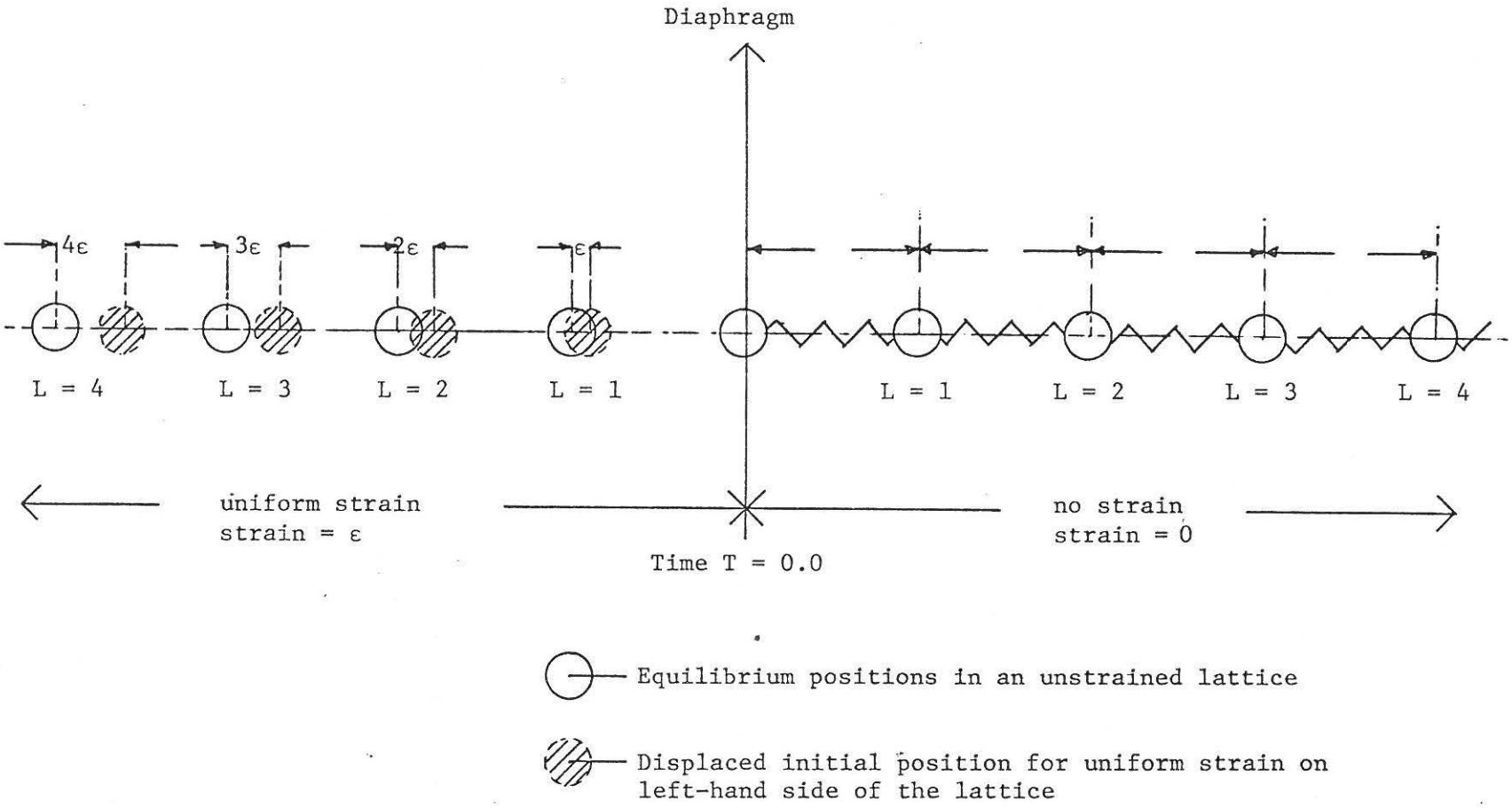

Fig. 16.--Strain in a Linear Lattice

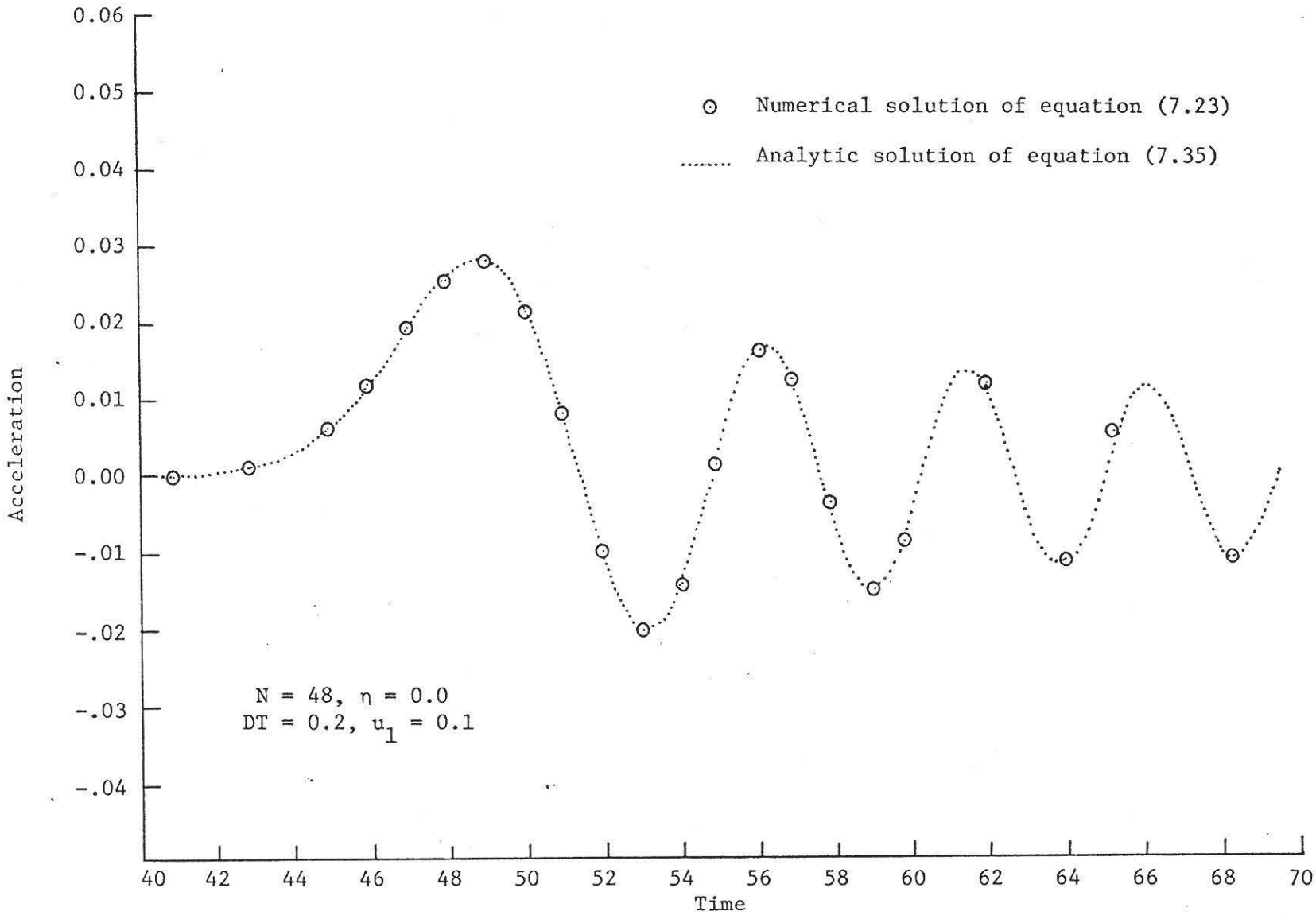

Fig. 17.--Acceleration of a Mass Point in a Linear Lattice, Case P-2

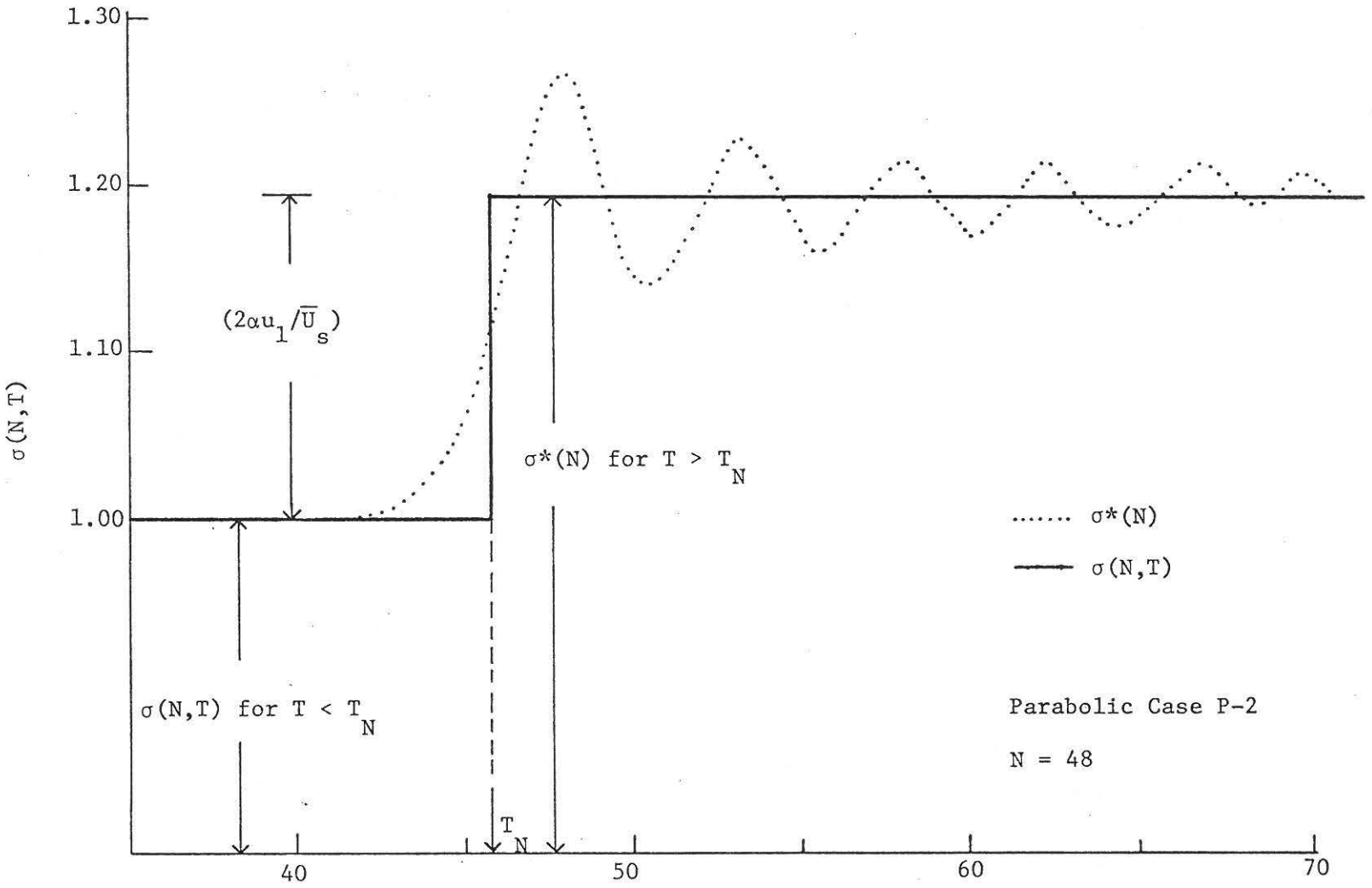

Fig. 18.--σ(N,T) as Defined in Equation (7.41) for Case P-2

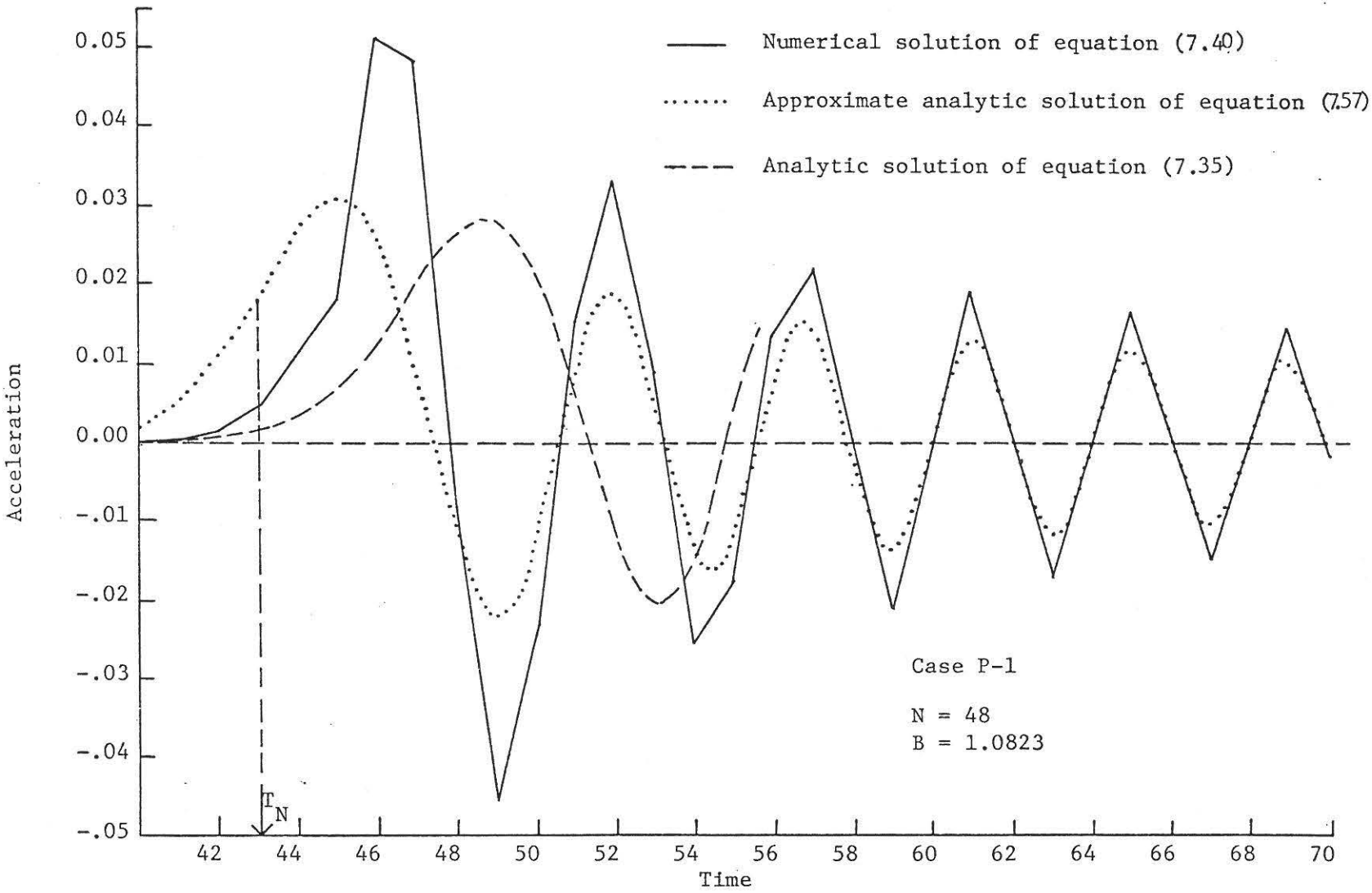

Fig. 19.--Acceleration of a Mass Point in a Nonlinear Lattice, Case P-1

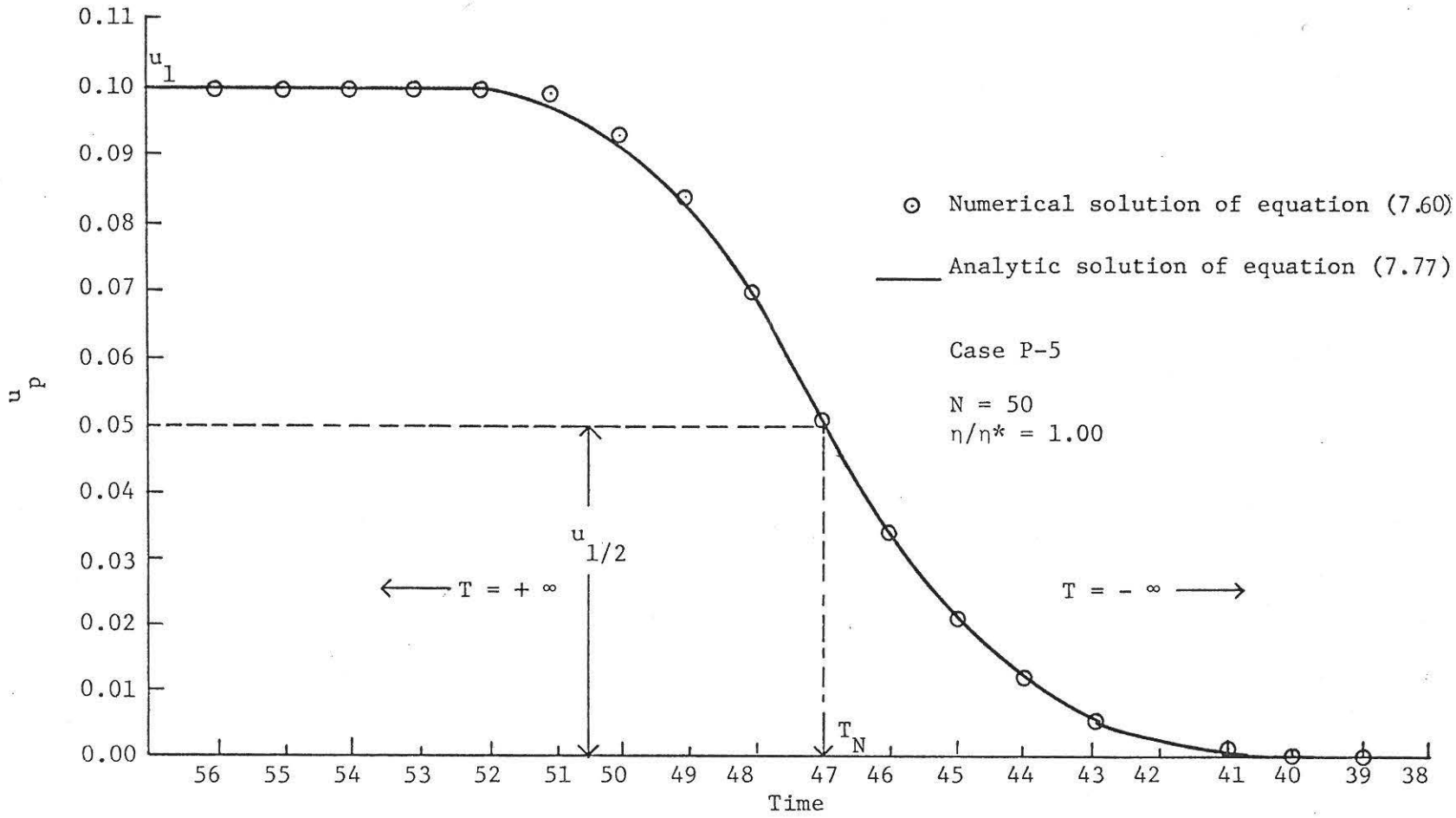

Fig. 20.--Steady Shock Profile in a Nonlinear Lattice, Case P-5

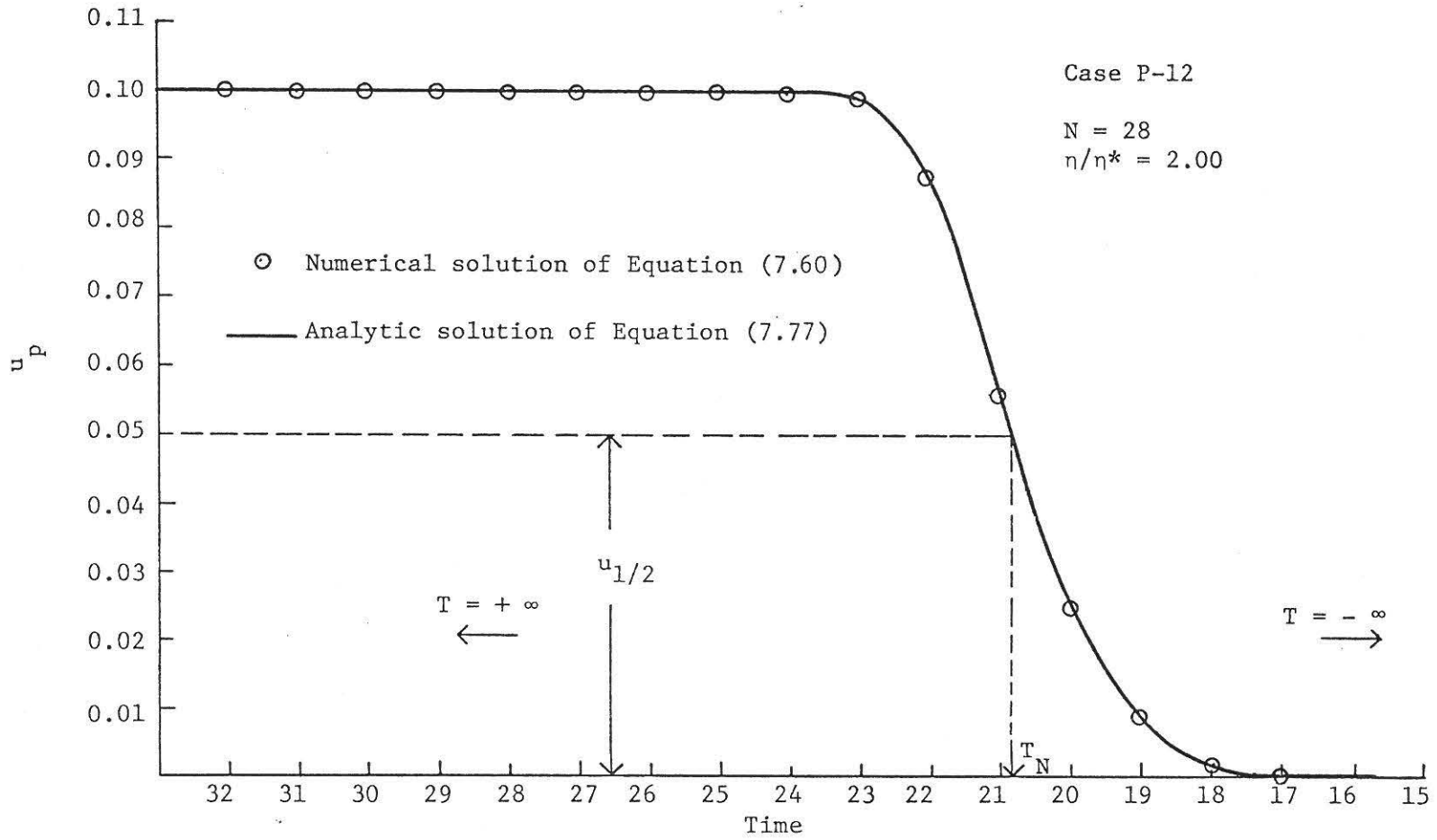

Fig. 21.--Steady Shock Profile in a Nonlinear Lattice, Case P-12

CHAPTER VIII

CONCLUSIONS AND RECOMMENDATIONS

Conclusions

We have studied the propagation of finite amplitude waves in one-dimensional linear and nonlinear chains. Disturbance in the semi-infinite chains was created by application of a velocity step to the mass point in the free surface. Only nearest neighbor interactions were considered. Two types of nonlinear interactions were studied, and the effects of dissipation were investigated.

The solution of the nonlinear differential-difference equations of motion on the IBM 360/67 computer produced the following results:

1. In the absence of dissipation the N-th mass point in the chain has an oscillatory path in the X-T plane. For all the cases studied, it was observed that a recurrence relation for displacements resulted. This was

$$S_{N+1}(T) = S_N(T - \theta_{N,N+1}); \; S_{N-1}(T) = S_N(T + \theta_{N-1,N}) \; ,$$

where $\theta_{N-1,N} = T_N - T_{N-1}$, $\theta_{N,N+1} = T_{N+1} - T_N$, etc. T_N is the time of arrival of the disturbance at the N-th mass point.

2. In the presence of dissipation--i.e., when the damping coefficient η is greater than η^*--oscillations in the X-T plot disappear and all the characteristic times $\theta_{N-1,N}$, $\theta_{N,N+1}$, etc. become equal to a constant, θ. The following relations become the expressions of steady

state conditions:

$$S_{N+1}(T) = S_N(T - \theta); \; S_{N-1}(T) = S_N(T + \theta) \; .$$

3. The typical shock profile of particle velocity, $U_p(N)$, in the absence of dissipation, consists of a rapidly rising front, behind which U_p oscillates about a new equilibrium position. Far behind the front, an essentially uniform state exists. The decay of oscillations even in the absence of dissipation is due to amplitude and frequency dispersion. In the present study we observed that the shock front does not propagate at a constant velocity as reported by Tsai and Beckett [17] for cubic lattices. Only the average speed is constant. The period of oscillations of the shock path was observed to be directly connected with that of particle path or vice versa.
4. The increase in frequency of oscillations with increase in amplitude and nonlinearity of the lattice is the result of amplitude dispersion. This result is of opposite sign than for a single nonlinear oscillator governed by the same force of interaction. In the oscillator, frequency decreases with increase in amplitude or nonlinearity.
5. In spite of an oscillatory shock profile, the stresses and the relative volume in the essentially uniform region far behind the shock front agree satisfactorily with those obtained by application of the Rankine-Hugoniot jump conditions. The shock velocity used was the average shock speed in the lattice.
6. The explicit, approximate analytic solutions for the finite amplitude wave in the linear lattice, when extended to the nonlinear lattice, confirmed our belief that decay of oscillations in the shock profile, even in the absence of dissipation, was the result of dispersion and

not due to any diffusion terms introduced in the numerical integration scheme.

7. The effect of dissipation is to decrease the amplitude of oscillations behind the shock front. For a critically damped lattice the shock profile is nonoscillatory and propagates without changing shape. For this case the recurrence relations in 1 can be used to derive a steady shock profile. The agreement between the approximate analytic solution and the numerical solution for the shock profile is good when damping $\eta > \eta^*$ (plotting accuracy .001).
8. In the presence of dissipation ($\eta > \eta^*$) and for a particular constitutive relation, the shock profile in a continuum is of the same form as that obtained with a lattice model. The conclusion is that a steady shock in a damped nonlinear lattice is analogous to a steady shock in a continuum when the interaction in the lattice is analogous to the constitutive relation of the continuum. In view of this, we believe that a continuum approach is adequate for arriving at a shock profile in a solid.
9. The lattice model under study was stable for finite amplitude wave propagation. The present study describes a procedure for converting constants in the constitutive relation of a continuum solid model to constants of the lattice model.

Recommendations

With minor changes in the computer program the following problems can be studied:

1. Extend the present study to cover the case of more than nearest neighbor interaction and to check the validity of present conclusions in that case.

LITERATURE CITED

[1] G. E. Duvall. "Shock Waves in the Study of Solids," Applied Mechanics Surveys. Edited by H. N. Abramson, H. Liebowitz, J. H. Crowley, and S. Juhass. Washington, D. C.: Spartan Books, 1966.

[2] M. H. Rice, R. G. McQueen, and J. M. Walsh. "Compression of Solids by Strong Shock Waves," Solid State Physics, vol. 6. Edited by F. Seitz and D. Turnbull. New York: Academic Press, 1958.

[3] G. E. Duvall. "Properties and Applications of Shock Waves," Response of Metals to High Velocity Deformation, vol. 9. Edited by P. G. Shewmon and V. F. Zackay. London: Interscience Publishers, 1961.

[4] W. Band and G. E. Duvall. "Physical Nature of Shock Propagation," American Journal of Physics, vol. 29 (1961), pp. 780-785.

[5] W. Band. Introduction to Mathematical Physics. New York: D. Van Nostrand Company, Inc., 1959.

[6] M. J. Lighthill. "Viscosity Effects in Sound Waves of Finite Amplitude," Surveys in Mechanics. Edited by G. K. Batchelor and R. M. Davies. Cambridge: Cambridge University Press, 1956.

[7] B. Riemann. "Gesselschaft der Wissenschaften Zu Gottingen," Mathematisch Physicalische Klasse, vol. 8 (1860), p. 43.

[8] I. M. Gelfand. "Some Problems in the Theory of Quasi-Linear Equations," American Mathematical Society Translations, vol. 29 (1963), p. 298.

[9] W. Band. "Studies in the Theory of Shock Propagation in Solids," Journal of Geophysical Research, vol. 65 (1960), pp. 695-719.

[10] I. C. Skidmore. "An Introduction to Shock Waves in Solids," Applied Material Research, vol. 4 (1965), pp. 131-147.

[11] J. O. Hirschfelder, C. F. Curtiss, and R. B. Bird. Molecular Theory of Gases and Liquids. New York: John Wiley and Sons, 1954.

[12] H. Kolsky. Stress Wave in Solids. New York: Dover Publications, Inc., 1963.

[13] D. Gilbarg and D. Paolucci. "The Structure of Shock Waves in Continuum Theory of Fluids," Journal of Rational Mechanics and Analysis, vol. 2 (1953), pp. 617-642.

[14] R. Becker. "Stosswelle und Detonation," Zeitschrift fur Physik, vol. 8 (1922), pp. 321-362.

[15] H. Grad. "The Profile of Steady Shock Wave," Communications on Pure and Applied Mathematics, vol. 5 (1952), pp. 257-300.

[16] H. M. Mott-Smith. "The Solution of Boltzmann Equation for a Shock Wave," Physical Review, vol. 82 (1951), pp. 885-892.

[17] D. H. Tsai and C. W. Beckett. "Shock Wave Propagation in Cubic Lattices," Journal of Geophysical Research, vol. 71 (1966), pp. 2601-2608.

[18] G. D. Anderson. "Shock Wave Propagation on a One Dimensional Lattice," Ph.D. Thesis, Washington State University, Pullman, Washington (1964).

[19] L. Brillouin. Wave Propagation in Periodic Structures. New York: Dover Publications, Inc., 1953.

[20] S. C. Lowell. "Non-Linear Dispersive Waves in Crystal Lattices," to be published.

[21] R. D. Richtmyer. Difference Methods for Initial Value Problems. New York: Interscience Publishers, Inc., 1957.

[22] J. Von Neumann. NDRC Applied Math. Report No. 1081, R (1944).

[23] R. Von Mises. Mathematical Theory of Compressible Fluid Flow. New York: Academic Press, Inc., 1958.

[24] G. E. Duvall and W. Band. Shock Waves in Solids. New York: McGraw-Hill Book Company, to be published.

[25] M. L. Wilkins. Methods in Computational Physics, vol. 3. Edited by B. Alder, S. Fernbach, and M. Rotenberg. New York: Academic Press, 1964.

[26] R. Courant and K. O. Friedrichs. Supersonic Flow and Shock Waves. New York: Interscience Publishers, Inc., 1948.

[27] Y. B. Zeldovich and Y. B. Raizer. Shock Waves and High Temperature Hydrodynamic Phenomena, vol. 1. New York: Academic Press, 1966.

[28] B. J. Lazan. "Damping Mechanisms and Phenomenology in Materials," Applied Mechanics. Edited by H. Gortler. Berlin: Springer Verlag, 1966.

[29] A. S. Nowick. "Anelastic Phenomena in Metals and Non-Metallics," Internal Friction, Damping, and Cyclic Plasticity, ASTM STP 378, 1964.

[30] L. M. Barker. "Fine Structure of Compressive and Release Wave Shapes in Aluminum, Measured by the Velocity Interferometer Technique," Sandia Corporation Report No. SC-DC-66-2447 (1966).

[31] B. J. Lazan. "Damping Studies in Material Science and Material Engineering," ASTM STP 378 (1964).

[32] C. H. Zener. Elasticity and Anelasticity of Metals. Chicago: The University of Chicago Press, 1948.

[33] E. H. Lee and T. Wierzbicki. "Analysis of the Propagation of Plane Elastic-Plastic Waves at Finite Strain," Technical Report No. 164, Division of Engineering Mechanics, Stanford University (1967).

[34] D. R. Bland. "On the Shock Structure in a Solid," Journal of Institute of Mathematics and its Applications, vol. 1 (1965), pp. 56-75.

[35] G. I. Taylor. "The Conditions Necessary for Discontinuous Motion in Gases," Proceedings of the Royal Society, A84 (1910), pp. 371-377.

[36] Y. Kogure. "Energy Transfer in Gas Atomic Collision with One Dimensional Lattice," Progress of Theoretical Physics, Supplement, vol. 36 (1966), pp. 138-153.

[37] J. C. Slater. Introduction to Chemical Physics. New York: McGraw-Hill Book Company, 1939.

[38] L. A. Girifalco and V. G. Weizer. "Application of Morse Potential Function to Cubic Metals," Physical Review, vol. 114 (1959) pp. 687-690.

[39] M. Born and K. Huang. Dynamical Theory of Crystal Lattices. Oxford: Clarendon Press, 1954.

[40] W. H. Anderson. "Evaluation of Gruneisen Parameter for Compressed Substances--Part I. Metals," The Fourth Symposium on Detonation, U. S. Naval Ordnance Lab. (1965).

[41] G. B. Benedek. "Deduction of the Volume Dependence of the Cohesive Energy of Solids from Shock Wave Compression Measurements," Physical Review, vol. 114 (1959), pp. 467-475.

[42] A. E. H. Love. A Treatise on the Mathematical Theory of Elasticity. New York: Dover Publications, Inc., 1944.

[43] A. N. Tickhnov and A. A. Samaraski. Equations of Mathematical Physics. New York: The Macmillan Company, 1963.

[44] S. Katz, D. G. Doran, and D. R. Curran. "Hugoniot Equation of State of Aluminum and Steel from Oblique Shock Measurement," Journal of Applied Physics, vol. 30 (1959), p. 568.

[45] A. D. Sakharov, R. M. Zeidel, V. N. Mineev, and A. G. Oleinik. "Experimental Investigation of the Stability of Shock Waves and the Mechanical Properties of Substances at High Pressures and Temperatures," Soviet Physics--DOKLADY, vol. 9 (1965), p. 1091.

APPENDIX A

SIMPLIFIED EQUATION (7.23)

SIMPLIFIED EQUATION (7.23)

Substitution of solution of equation (7.31) into equation (7.23) gives

$$S_N''(T) = u_1 \cdot \sum_{K=0}^{\infty} (2K+1)\ J_{2N+2K-3}(2T) - 2 \cdot \sum_{K=0}^{\infty} (2K+1)\ J_{2N+2K-1}(2T)$$

$$+ \sum_{K=0}^{\infty} (2K+1)\ J_{2N+2K+1}(2T) \quad . \tag{7.23a}$$

By defining a dummy variable of summation, M, such that $2M + 1 = 2N + 2K - 3$ for the first sum on the right, $2M + 1 = 2N + 2K - 1$ for the second sum on the right, and $2M + 1 = 2N + 2K + 1$ for the third sum on the right, equation (7.23a) becomes

$$S_N''(T) = u_1 \cdot \sum_{M=N-2}^{\infty} \{(2M-2N+5)\ J_{2M+1}(2T)\} - 2 \cdot \sum_{M=N-1}^{\infty} \{(2M-2N+3) \cdot$$

$$J_{2M+1}(2T)\} + \sum_{M=N}^{\infty} \{(2M-2N+1)\ J_{2M+1}(2T)\} \quad . \tag{A.1}$$

Simplifying,

$$= u_1 \cdot 5 \sum_{M=N-2}^{\infty} J_{2M+1}(2T) - 6 \sum_{M=N-1}^{\infty} J_{2M+1}(2T) + \sum_{M=N}^{\infty} J_{2M+1}(2T)$$

$$- 4\ J_{2N-3}(2T) + 2\ J_{2N-1}(2T) \quad .$$

APPENDIX B

VISCOSITY OF ALUMINUM IN SHOCK

VISCOSITY OF ALUMINUM IN SHOCK

When shock pressures are very much larger than material rigidity, solids behave in many respects as fluids [2]. The dissipative mechanism may then be taken to be due to viscosity. Russian experimenters [45] introduced sinusoidal perturbations on the shock front and studied the attenuation of such perturbations as the front propagates into the material. Then, using concepts of simply hydrodynamics and experimental observations, they calculated the viscosity of an aluminum alloy, brand AL-9 (90% AL), to be 2×10^4 to 1×10^5 poise. This viscosity, as reported by the Russians, remains essentially constant over a wide range of shock pressures (100 K-bar to 1000 K-bar).

In our lattice model, we have used the physical constants of aluminum (see Table 1). For a parabolic force law interaction, and in the presence of dissipation ($\eta > \eta^*$), the continuum equations and lattice dynamical approach yield the same shock profile, as discussed in Chapter VII. Hence, equation (7.81) should relate the nondimensional viscosity of the lattice model to the viscosity of the continuum. To get an order or magnitude of this viscosity, we arbitrarily use the critical damping, η^*, of the lattice model. The calculations are outlined below.

For $u_1 = 0.1$, corresponding to a ~ 100 K-bar shock in aluminum, we required a critical damping of $\eta^* = 0.25$ (Case P-11 in Table 2). From equation (7.81) we have

$$R\Big|_{\text{Continuum}} = [C \cdot (u_1/U)]_{\text{Continuum}} \cdot [a/(g\omega_1)]_{\text{Lattice}} \quad . \qquad (7.81)$$

From equation (2.46) and Table 1, for aluminum,

$$C = A_P \cdot (\rho_o D_o^2) = 3 \times (780) \text{ K-bars}$$

$$= 2.340 \times 10^{12} \text{ dynes/cm}^2 \quad . \qquad (B.1)$$

For a shock of ~ 100 K-bar in aluminum, the ratio (u_1/U) from Table 5 (Case M-1) is

$$(u_1/\overline{U}_s)_{\text{aluminum}} \simeq 0.0854 \quad . \qquad (B.2)$$

From Table 4 we have for Case M-1

$$\overline{U}_s = 1.1690, \text{ from which } \theta = 1/\overline{U}_s = 0.854 \quad . \qquad (B.3)$$

Substitution of this value of θ and $\eta = \eta^* = 0.25$ in equation (7.67) gives

$$a = \eta^* \cdot \theta^2 = 0.25 \ (0.736) = 0.184$$

$$g = (1 - \theta^2) = (1 - 0.736) = 0.264 \quad . \qquad (B.4)$$

For aluminum, $\omega_1 = 0.528 \ \mu\text{sec}^{-1}$. Hence, equation (7.81), along with equations (B.1) to (B.4) yields

$$R\Big|_{\text{aluminum}} = [2.340 \times 10^{12} \text{ dynes/cm}^2 \cdot (0.0854)] \cdot$$

$$[(0.184)/(0.264) \cdot 1/(0.528 \times 10^6 \text{ sec}^{-1})] \ ;$$

$$R\Big|_{\text{aluminum}} = \frac{2.340 \times 0.0854 \times 0.184}{0.264 \times 0.528} \times 10^{6} \text{ dynes sec/cm}^2$$

$$= 2.60 \times 10^{5} \text{ poise .}$$

This value of viscosity for aluminum is higher than that found by the Russian experimenters [45]. To our knowledge, no other experimental data is available for viscosity of aluminum. It is difficult, therefore, to comment on the disparity of the values. However, it is encouraging that with realistic interaction constants in a lattice model and with appropriate interaction law, it is possible to get a rough idea of the magnitude of dissipative forces tending to establish steady state conditions.

APPENDIX C

FORTRAN PROGRAM

FORTRAN PROGRAM

The program was assembled to solve the equations of motion of Chapter III. The numerical integration procedure was outlined in Chapter IV. Information is printed out at specified cycles, i.e., interval of time. The computations are terminated by any one of these means:

1. Maximum cycle (MAC).
2. Maximum mass point to which wave advanced, NN = 150.
3. Momentum conservation not satisfied.
4. Energy conservation not satisfied.
5. Excessive number of iterations required, J > 10.
6. End of input data, KK < 3.

Below we describe the program nomenclature and list the parameters. Input data are marked in the following list of symbols by an asterisk (*). The output variables are marked by a plus (+) sign. All the computations are done with nondimensional quantities.

Program Nomenclature and Parameters

Input or Output	Program Symbol	Description and Definition
*	A	A_M, A_P. Chapter III.
+	X	Position of a mass point.
+	DX	Velocity of a mass point.
+	DDX	Acceleration of a mass point.
+	C	Dilatation ρ_o/ρ.
*	DTAU	Nondimensional time increment.

	E INPUT	Input energy.
	E TOTAL	Energy of the system.
+	E CHECK	(E INPUT - E TOTAL)/E INPUT.
*	ETA	Viscosity η.
	H INPUT	Input momentum.
	H TOTAL	Momentum of the system.
+	H CHECK	(H INPUT - H TOTAL)/H INPUT.
*	KK	A parameter in data cards.
+	F	$P_s(N,T)$, nondimensional stress due to spring forces.
+	G	$P_V(N,T)$, dimensionless stress due to viscous forces.
	J	Iteration number.
	L	Cycle count.
+	T	$P_s(N,T) + P_V(N,T)$.
*	MA	A parameter controlling the cyclic time interval at which information is printed in the initial stage of computation.
+	MB	A parameter controlling the cyclic time interval at which information is printed in later stages of computation.
*	MAC	Maximum number of time steps for which computations are carried out.
*	MAD	A parameter controlling time at which the print-out interval is changed from MA to MB.
	NN	Last lattice point to which wave has advanced.
	QB	Difference in successive iterated positions.
*	QC	Equation (4.11).

*	QD	Equation (4.12).
*	QP	Increment in QD.
*	QQ	Maximum allowable QD.
	QX	Difference in successive iterations of position.
*	QQP	A parameter controlling the momentum check. If H CHECK > QQP, program stops.
*	QQR	A parameter controlling the energy check. If E CHECK > QQR, program is terminated.
*	RHO	ρ_o.
*	W1 (OMEGA 1)	ω_1. Equation (3.15) or (3.16).
*	W2 (OMEGA 2)	Gruneisen parameter for Morse law. For parabolic law we require A_P = W2/W1.
*	U1	u_1.

Computer Program

The computer program listed below is for Morse law interaction. The program for parabolic interaction is essentially the same. We have divided the program into several blocks and identified the blocks by a block number and type of interaction.

The program for parabolic interaction is assembled by retaining blocks marked "common" and replacing every block marked "Morse" by the identically-numbered block marked "parabolic." These appear at the end of listing.

The flow chart following the listing is the same for both types of interaction.

```
C       SHOCK WAVE STUDIES ON A ONE DIMENSIONAL DISSIPATING LATTICE
C*************************************BLOCK. 1***COMMON****START*******
        DIMENSION X(150,2,10), F(150,2,10), DX(150,2,10), DDX(150,2,10),
       1QB(150), G(150,2,10), T(150,2,10), C(150,2,10), C(150,2,10)
        READ(5,350), MA,MB,MAC,MAD,QQP,QQR
  350   FORMAT (416,2F20.6)
  505   READ(5,400) W1,W2,ETA,RHO,U1,DTAU,A,KK
  400   FORMAT(7F10.6,12)
        IF (KK-3)501,502,502
  502   QD=1.00E-05
        QP=1.00E-05
        QC=1.00E-07
        QQ=1.00E-04
        WRITE (6,300)
  300   FORMAT (1H1,5X,24H INITIAL VALUES AT TAU=0,11X,2H N, 10X,2HX,10X,
       13H DX,10X,4H DDX//)
        DO 10 N=1, 150
        X(N,1,10)=(N-1)*1.
        DX(N,1,10)=0.
        DDX(N,1,10)=0.
        WRITE (6,302)N,X(N,1,10),DX(N,1,10),DDX(N,1,10)
  302   FORMAT (39X,13,F12.1,F13.3,F14.3)
   10   CONTINUE
        L=0
   90   J=0
        L=L+1
        IF(MAC-L)505,106,106
  106   IF(L.GT.MAD) GO TO 107
        LL=MA
        LLL=LL*(L/LL)
        TIME=L*DTAU
        GO TO 102
  107   LL=MB
        LLL=LL*(L/LL)
        TIME=L*DTAU
  102   J=J+1
        IF(7-J)600,600,601
  601   DO 11 M=1,10
        X(1,2,M)=U1
        DX(1,2,M)=U1
        DDX(1,2,M)=0.
        X(150,2,M)=X(150,1,10)
        DX(150,2,M)=0.
        DDX(150,2,M)=0.
   11   CONTINUE
        DO 12 N=2,149
        X(N,2,1)=X(N,1,10)
        DX(N,2,1)=DX(N,1,10)
        DDX(N,2,1)=DDX(N,1,10)
   12   CONTINUE
```

```
   50   N=2
   40   DDX(N,2,J+1)=(FORCE1(X,N,2,J,A)+FORCE2(DX,N,2,J,ETA))
        DX(N,2,J+1)=DX(N,2,1)+(1./2.)*DTAU*(DDX(N,2,1)+DDX(N,2,J+1))
        X(N,2,J+1)=X(N,2,1)+(1./2.)*DTAU*(DX(N,2,1)+DX(N,2,J+1))
        JJJ=J+1
        J=JJJ-1
  206   QX=(X(N,2,J+1)-X(N,2,1))/X(N,2,1)
        IF (ABS(QX)-QC)110,110,101
  101   N=N+1
        IF(N-149)40,40,180
  110   NN=N+1
        DO 18 MM=NN,149
        X(MM,2,J+1)=X(MM,2,J)
        DX(MM,2,J+1)=DX(MM,2,J)
        DDX(MM,2,J+1)=DDX(MM,2,J)
   18   CONTINUE
  100   DO 13 N=2,NN
        QB(N)=X(N,2,J+1)-X(N,2,J)
        IF(QB(N).EQ.0.OR.ABS(QB(N)).LE.QD)GO TO 103
        GO TO 102
  103   CONTINUE
   13   CONTINUE
        IF(L.EQ.LLL) GO TO 330
        GO TO 104
  330   WRITE (6,506)W1,W2,ETA,RHO,U1,DTAU,QD
  506   FORMAT(1H1,3X,9H OMEGA1= , F6.4,3X,9H GAMMA= ,F6.4,3X,6H ETA= ,
       IF8.4,3X,6H RHO= , F6.4,3X,5H U1= ,F6.4,3X,7H DTAU= ,F6.4,3X,
       15H QD= ,E10.2//)
        WRITE (6,520)
  520   FORMAT(1HO,8X,2H N,15X,5H TIME,13X,7H X(N,T),12X,8H UP(N,T),12X,
       18H TP(N,T),12X,8H CP(N,T),3X,7H ITR NO//)
  104   DO 14 N=2,149
        X(N,2,10)=X(N,2,J+1)
        DX(N,2,10)=DX(N,2,J+1)
        DDX(N,2,10)=DDX(N,2,J+1)
   14   CONTINUE
C************************************BLOCK.1***COMMON****END*********
C************************************BLOCK.2***MORSE*****START*******
        DO 16 N=2,NN
        F(N,2,10)=0.5*(1./A)*(EXP(-2.*A*(X(N,2,10)-X(N-1,2,10)-1.))-
       1EXP(-1.*A*(X(N,2,10)-X(N-1,2,10)-1.))+EXP(-2.*A*(X(N+1,2,10)-
       2X(N,2,10)-1.))-EXP(-1.*A*(X(N+1,2,10)-X(N,2,10)-1.)))
        G(N,2,10)=(1./2.)*ETA*(DX(N-1,2,10)-DX(N+1,2,10))
        T(N,2,10)=F(N,2,10)+G(N,2,10)
        C(N,2,10)=X(N,2,10)-X(N-1,2,10)
        IF(L.EQ.LLL)WRITE(6,800)N, TIME,X(N,2,10),DX(N,2,10),T(N,2,10),
       1C(N,2,10),JJJ
  800   FORMAT(5X,15,5E20.6,8X,12)
   16   CONTINUE
C       MOMENTUM CHECK BEGINS HERE FOR MORSE LAW CASE
        HINPUT=(1./A)*(EXP(-2.*A*(C(2,2,10)-1.))-
       1EXP(-1.*A*(C(2,2,10)-1.)))
        TMOM=0.
```

```
      DO 36 N=1,NN
      TMOM=TMOM+DDX(N,2,10)
   36 CONTINUE
      HTOTAL=TMOM
      HCHECK=(HINPUT-HTOTAL)/HINPUT
      IF(ABS(HCHECK).GT.QQP)GO TO 182
C     ENERGY CHECK BEGINS HERE FOR MORSE LAW CASE
      EINPUT=HINPUT*U1
      SUMA=0.
      DO 37 N=1,NN
      SUMA=SUMA+DX(N,2,10)*DDX(N,2,10)
   37 CONTINUE
      SUM1=SUMA
      SUMB=0.
      DO 38 N=2,NN
      SUMB=SUMB+(1./A)*(EXP(-2.*A*(C(N,2,10)-1.))-
     1EXP(-1.*A*(C(N,2,10)-1.)))*(DX(N-1,2,10)-DX(N,2,10))
   38 CONTINUE
      SUM2=SUMB
      SUMC=0.
      DO 39 N=2,NN
      SUMC=SUMC+ETA*(DX(N,2,10)-DX(N-1,2,10))**2
   39 CONTINUE
      SUM3=SUMC
      ETOTAL=SUM1+SUM2+SUM3
      ECHECK=(EINPUT-ETOTAL)/EINPUT
      IF(ABS(ECHECK).GT.QQR)GO TO 184
      IF(L.EQ.LLL)WRITE(6,85)HCHECK,ECHECK
   85 FORMAT(//5X,17H MOMENTUM CHECK= ,E20.6),5X,
     115H ENERGY CHECK= ,E2-.6)
C**************************************BLOCK.2***MORSE*****END*********
C**************************************BLOCK.3***COMMON****START*******
      DO 15 N=2,149
      X(N,1,10)=X(N,2,10)
      DX(N,1,10)=DX(N,2,10)
      DDX(N,1,10)=DDX(N,2,10)
      F(N,1,10)=F(N,2,10)
      G(N,1,10)=G(N,2,10)
      T(N,1,10)=T(N,2,10)
      C(N,1,10)=C(N,2,10)
   15 CONTINUE
      GO TO 90
  600 WRITE(6,700)QD
  700 FORMAT(//48H EXCESSIVE NUMBER OF ITERATIONS ARE REQUIRED, 2X,
     19H FOR QD= ,E10.2/)
      QD=QD+QP
      WRITE(6,524)QD
  524 FORMAT(/16H WE SET NEW QD= ,E10.2)
      L=L-1
      IF(QD.LE.QQ)GO TO 90
      GO TO 501
  180 WRITE(6,181)TIME
```

```
  181   FORMAT(//42H LATTICE DIMENSIONS NOT CORRECT FOR TIME= ,E20.6)
        GO TO 501
  182   WRITE(6,183)TIME
  183   FORMAT(//40H MOMENTUM CHECK NOT SATISFIED FOR TIME= ,E20.6)
        GO TO 501
  184   WRITE(6,185)TIME
  185   FORMAT(//38H ENERGY CHECK NOT SATISFIED FOR TIME= ,E20.6)
  501   RETURN
        END
C*************************************BLOCK.3***COMMON****END*********
C*************************************BLOCK.4***MORSE*****START*******
        FUNCTION FORCE1 (X,NN,MM,JJ,A)
C       CALCULATION OF SPRING FORCES (MORSE LAW)
        DIMENSION X(150,2,10)
        FORCE1=(1./A)*EXP(-2.*A*(X(NN,MM,JJ)-X(NN-1,MM,JJ+1)-1.))-
       1EXP(-1.*A*(X(NN,MM,JJ)-X(NN-1,MM,JJ+1)-1.))-EXP(-2.*A*( X(NN+1),
       2MM,JJ)-X(NN,MM,JJ)-1.))+EXP(-1.*A*(X(NN+1,MM,JJ)-X(NN,MM,JJ)-
       31.)))
        RETURN
        END
        FUNCTION FORCE2(DX,NN,MM,JJ,ETA)
C       CALCULATION OF VISCOUS FORCES
        DIMENSION DX(150,2,10)
        FORCE2=ETA*(DX(NN+1,MM,JJ)-2.*DX(NN,MM,JJ)+DX(NN-1,MM,JJ+1))
        RETURN
        END
/*
//GO.SYSIN DD *
      5      1     100      90           800.000000           800.000000
000.528000002.050000000.000000002.780000000.100000000.1000000003.4340005
                                                                       02
/*
C*************************************BLOCK.4***MORSE*****END********
C       REPLACEMENT BLOCKS FOR ASSEMBLING PROGRAM FOR PARABOLIC INTERACTION
C*************************************BLOCK.2***PARABOLIC*START******
        DO 16 N=2,NN
        F(N,2,10)=(1./2.)*((X(N+1,2,10)-X(N,2,10)-1.)*(A*(X(N+1,2,10)-
       1X(N,2,10)-1.)-1.)+(X(N,2,10)-X(N-1,2,10)-1.)*(A*(X(N,2,10)-
       1X(N-1,2,10)-1.)-1.))
        G(N,2,10)=(1./2.)*ETA*(DX(N-1,2,10)-DX(N+1,2,10))
        T(N,2,10)=F(N,2,10)+G(N,2,10)
        C(N,2,10)=X(N,2,10)-X(N-1,2,10)
        IF(L.EQ,LLL)WRITE(6,800)N, TIME,X(N,2,10),DX(N,2,10),T(N,2,10),
       IC(N,2,10),JJJ
  800   FORMAT(5X,I5,5E20.6,8X,I2)
   16   CONTINUE
C       MOMENTUM CHECK BEGINS HERE FOR PARABOLIC CASE
        HINPUT=(1.-C(2,2,10))*(1.-A*(C(2,2,10)-1.))
        TMOM=0.
        DO 36 N=1,NN
        TMOM=TMOM+DDX(N,2,10)
   36   CONTINUE
        HTOTAL=TMOM
```

```
      HCHECK=(HINPUT-HTOTAL)/HINPUT
      IF(ABS(HCHECK).GT.QQP)GO TO 182
C     ENERGY CHECK BEGINS HERE FOR PARABOLIC CASE
      EINPUT=HINPUT*U1
      SUMA=0.
      DO 37 N=1,NN
      SUMA=SUMA+DX(N,2,10)*DDX(N,2,10)
   37 CONTINUE
      SUM1=SUMA
      SUMB=0.
      DO 38 N=2,NN
      SUMB=SUMB+(DX(N,2,10)-DX(N-1,2,10))*(C(N,2,10)-1.)*(1.-
     1A*(C(N,2,10)-1.))
   38 CONTINUE
      SUM2=SUMB
      SUMC=0.
      DO 39 N=2,NN
      SUMC=SUMC+ETA*(DX(N,2,10)-DX(N-1,2,10))**2
   39 CONTINUE
      SUM3=SUMC
      ETOTAL=SUM1+SUM2+SUM3
      ECHECK=(EINPUT-ETOTAL)/EINPUT
      IF(ABS(ECHECK).GT.QQR)GO TO 184
   85 FORMAT(//5X,17H MOMENTUM CHECK= ,E20.6,5X,
     115H ENERGY CHECK = ,E20.6)
C*************************************BLOCK.2***PARABOLIC*END*********
C*************************************BLOCK.4***PARABOLIC*START*******
      FUNCTION FORCE1(X,NN,MM,JJ,A)
C     CALCULATION OF SPRING FORCES
      DIMENSION X(150,2,10)
      FORCE1=(X(NN+1,MM,JJ)-2.*X(NN,MM,JJ)+X(NN-1,MM,JJ+1))*(1-A*
     1(X(NN+1,MM,JJ)-X(NN-1,MM,JJ+1)-2.))
      RETURN
      END
      FUNCTION FORCE2(DX,NN,MM,JJ,ETA)
C     CALCULATION OF VISCOUS FORCES
      DIMENSION DX(150,2,10)
      FORCE2=ETA*(DX(NN+1,MM,JJ)-2.*DX(NN,MM,JJ)+DX(NN-1,MM,JJ+1))
      RETURN
      END
C*************************************BLOCK.4***PARABOLIC*END*********
/*
```

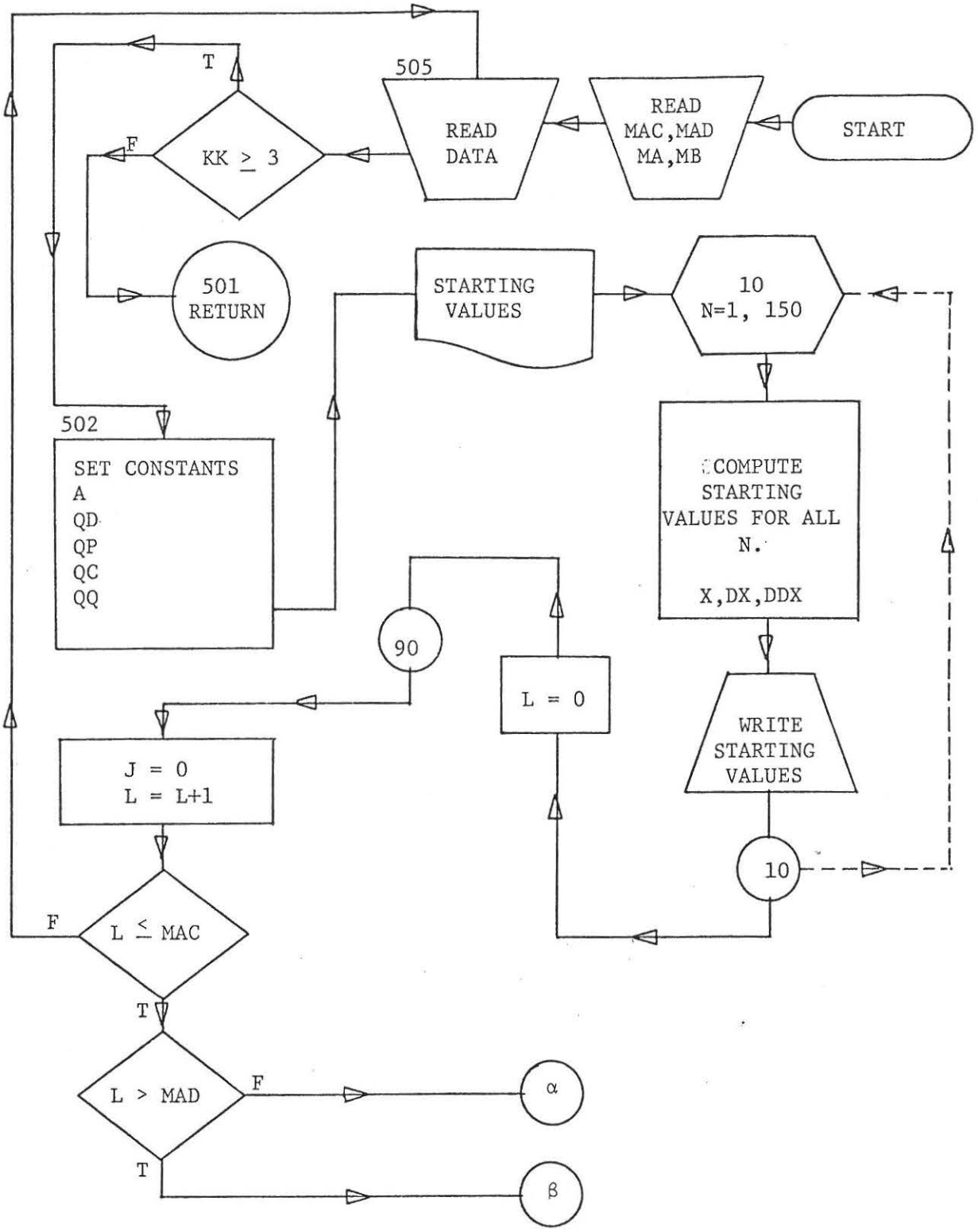

Fig. 22.--Flow Chart for Computer Program

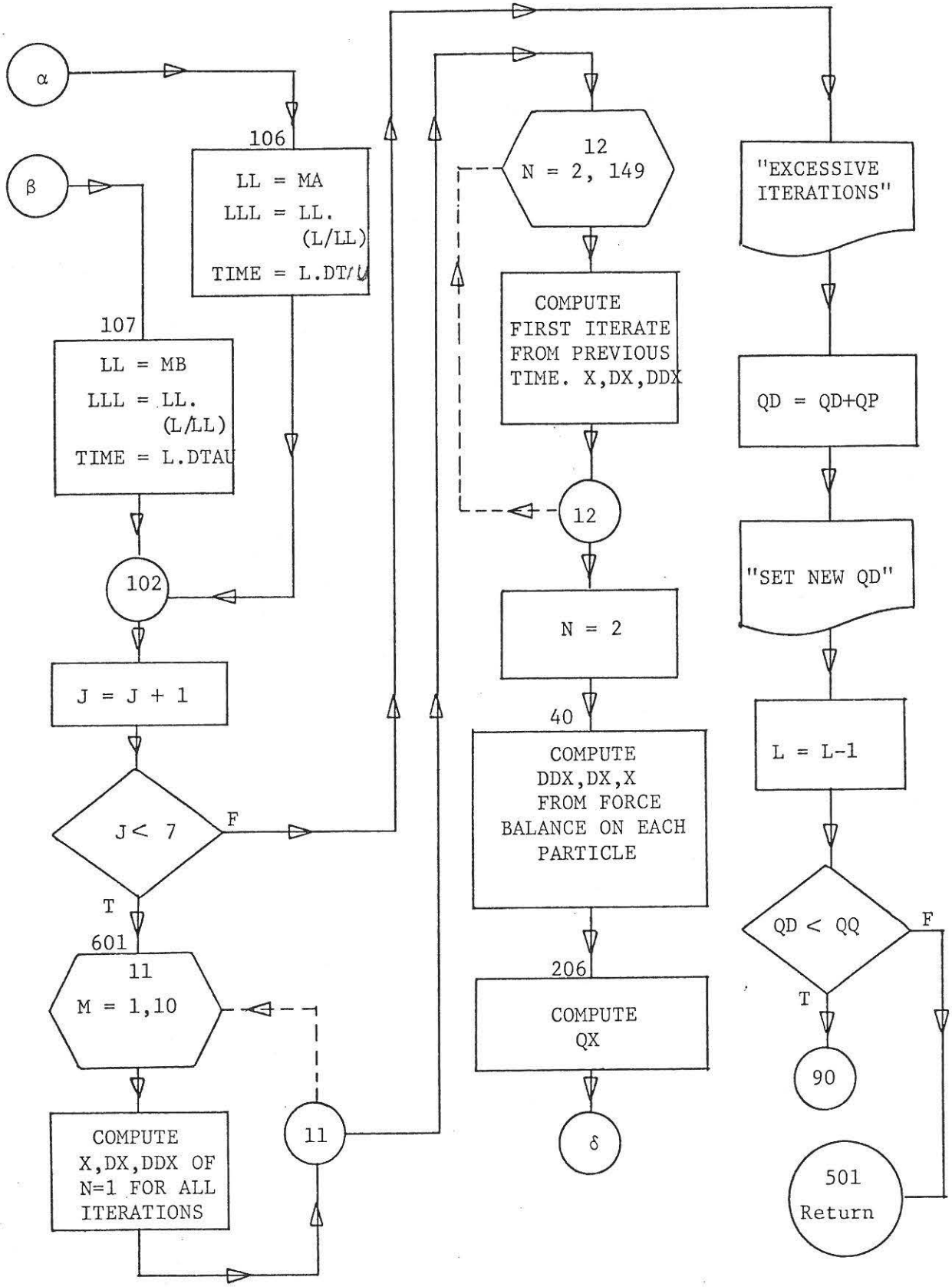

Fig. 22.--Continued

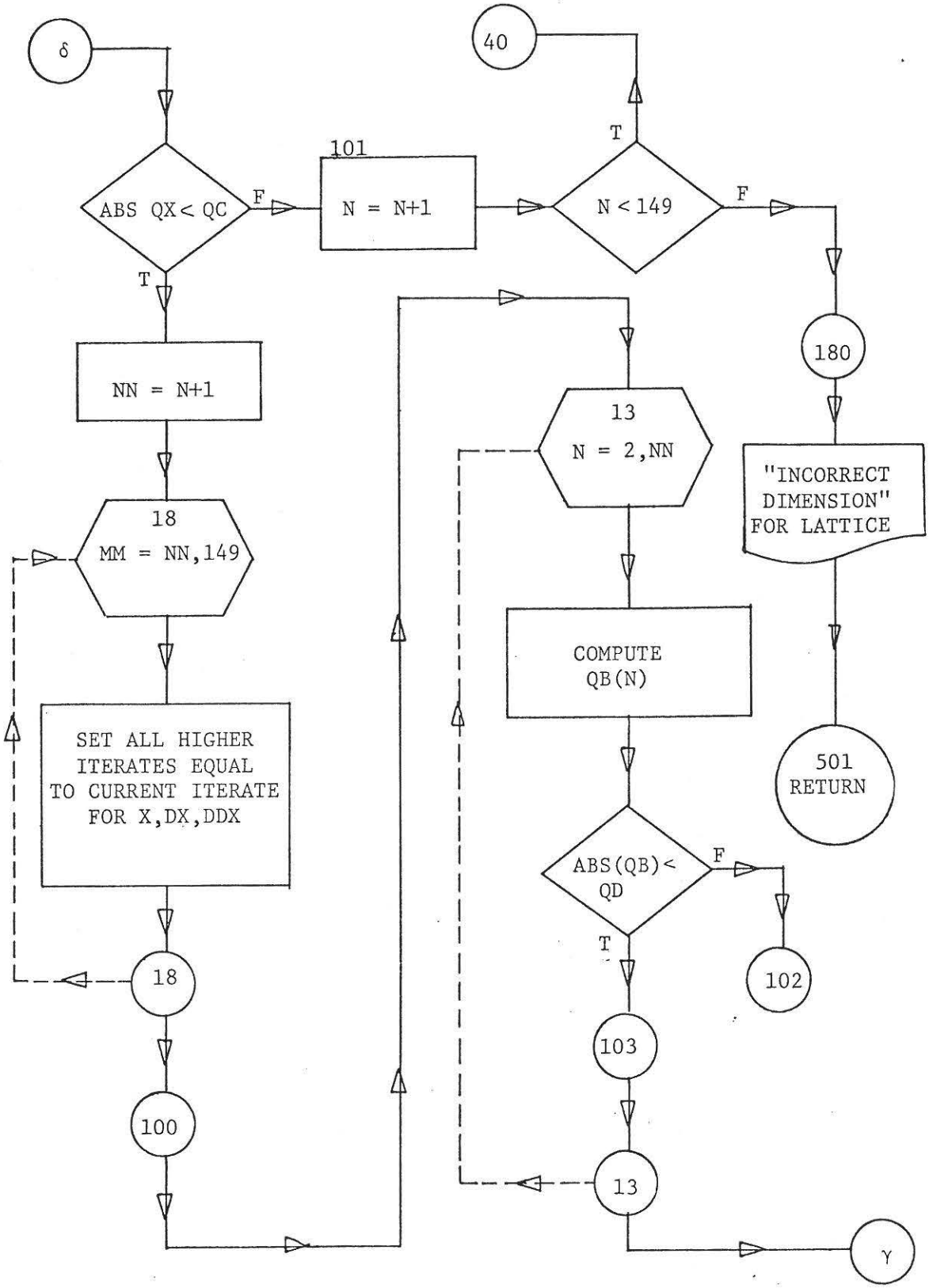

Fig. 22.--Continued

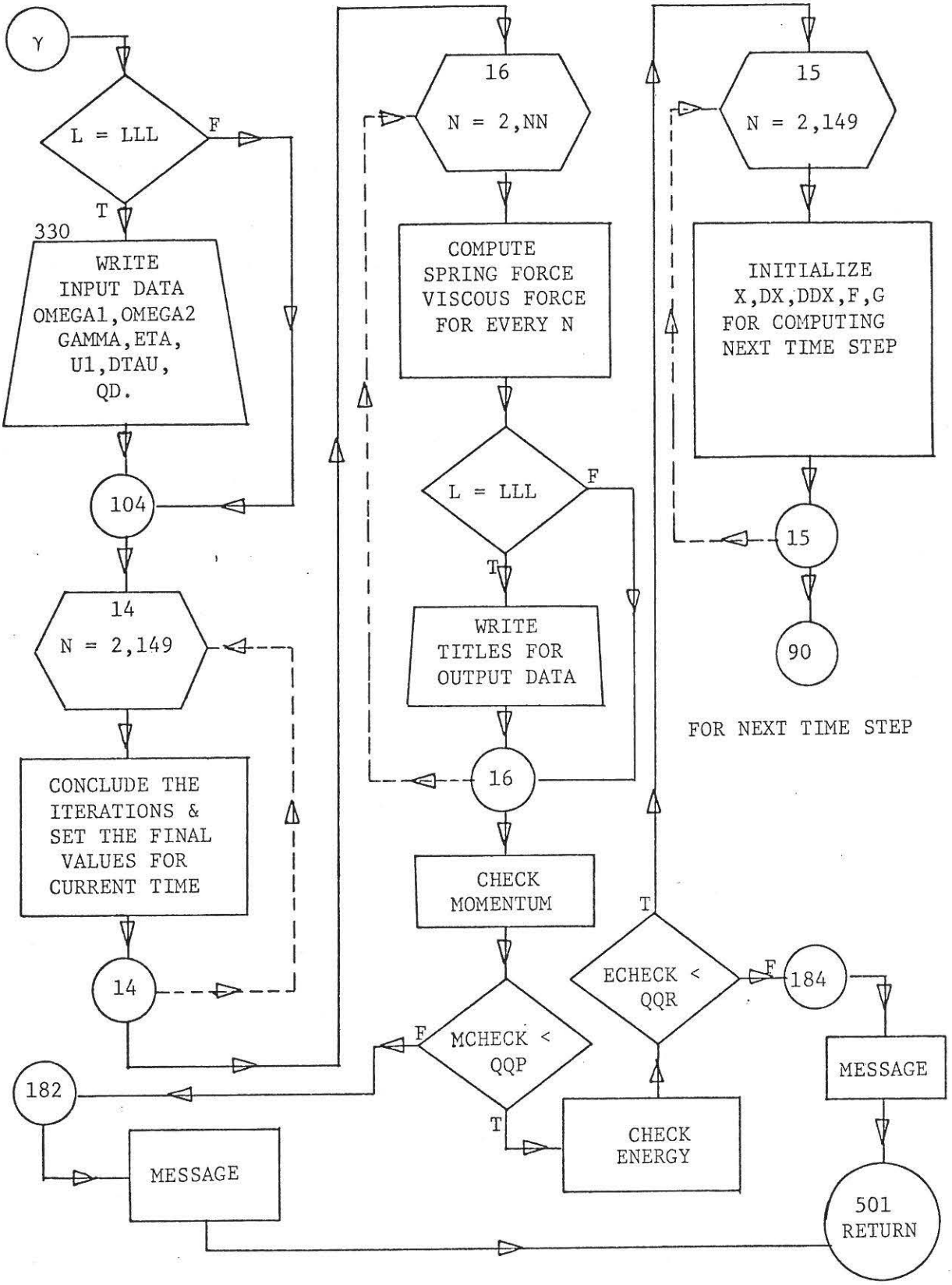

Fig. 22.--Continued